NEURAL MICROTISSUE ENGINEERING FOR HIGH THROUGHPUT SCREENING IN PRE-CLINICAL DRUG DISCOVERY

by

YINZHI LAI

(Under the Direction of William S. Kisaalita)

ABSTRACT

Cells cultured in three dimensional (3D) scaffolds as opposed to traditional two-dimensional (2D) substrates have been considered more physiologically relevant based on their superior ability to emulate the *in vivo* environment. Combined with stem cell technology, 3D cell cultures can provide a promising alternative for use in cell-based assays or biosensors in pre-clinical drug discovery studies. The number of research publications about 3D cell culture *in vitro* models is increasing drastically in the recent decade; however, the adoption of 3D cell culture in industry is slow. The possible reasons include 1) lack of concrete evidence for *in vivo* emulation, 2) absence of measure to ascertain three dimensionality of the culture, and 3) high cost of commercial systems in a climate of great need to reduce cost of screening per compound.

In this study, we aimed at advancing 3D culture application in neuronal cell based assays for pre-clinical drug discovery by attempting to solve the above three problems. First we established the *in vivo* emulating property of 3D cultured neuronal cells by comparing with freshly dissected tissue as *in vivo* surrogate. Intracellular calcium transient in response to high K^+ depolarization was used as a convenient index to access the physiological relevance of 3D cultured cells. Membrane protein caveolin-1, alpha subunit of L-type VGCC and cytoskeletal

protein F-actin were also compared in this study to shed light on the mechanism behind the phenomenon.

The second step is to identify potential three-dimensionality biomarkers for advancing 3D cell culture technology. With this goal in mind, transcriptomic expression comparison among neural progenitor cells cultured on 2D substrates, in 3D porous polystyrene scaffolds, and as 3D neurospheres (*in vivo* surrogate) was conducted. Up-regulation of cytokines as a group in 3D and neurospheres was observed. The commonly up-regulated cytokines were identified and discussed in depth for their promising role as 3D biomarkers.

Last, automation and robotic techniques were utilized to generate a HTS compatible 3D cell culture platform by chemically welding polystyrene scaffolds into standard 2D polystyrene 96-well plates. Automation can minimize the variability of scaffold properties and increase the Z'-factor of the produced 96-well plates. The fabricated 3D cell culture plates were compared with several commercially available 3D cell culture platforms to confirm the suitability in pre-clinical drug discovery applications.

Keywords: 3D cell culture, Cell-based assay, VGCC, Biomarker, HTS, Pre-clinical drug discovery

NEURAL MICROTISSUE ENGINEERING FOR HIGH THROUGHPUT SCREENING IN PRE-CLINICAL DRUG DISCOVERY

by

YINZHI LAI
B.S., Zhejiang University, China, 2004
M.S., The University of Missouri, 2006

A Dissertation Submitted to the Graduate Faculty of The University of Georgia in Partial Fulfillment of the Requirements for the Degree

DOCTOR OF PHILOSOPHY

ATHENS,GA

2011

NEURAL MICROTISSUE ENGINEERING FOR HIGH THROUGHPUT SCREENING IN PRE-CLINICAL DRUG DISCOVERY

by

YINZHI LAI

Major Professor: William S. Kisaalita

Committee: Jaroslava T. Halper
Andrew T. Sornborger
Steven L. Stice

Electronic Version Approved:

Maureen Grasso
Dean of the Graduate School
The University of Georgia
December 2011

ACKNOWLEGEMENTS

First, I want to express my deepest appreciation to my advisor, Dr. William Kisaalita for overwhelming generosity of time, insightful advice and enormous patience throughout my PhD program. His guidance is an essential part in my graduate studies and my professional development. As a dedicated mentor and researcher, he has been a perfect role model that will impact me for my life time.

I would also like to thank my committee members Dr. Steve Stice, Dr. Andrew Sornborger and Dr. Jaroslava Halper for serving in my dissertation committee. Without their support, help, teaching, advice, and guidance, my work would not be possible.

Special thanks to Amish Asthana, Ke Cheng, Lina Wang and all the members in our lab. The collaboration with them was a huge component throughout my graduate studies. I am truly grateful for all the stimulating conversations and discussions over the years.

Finally, I will give my gratitude to my family, my parents, my loving husband Ruohong, and daughter Erinn. Their love and endless supports are very valuable in all aspects of my life.

TABLE OF CONTENTS

Pages

LIST OF FIGURES

Pages

LIST OF TABLES

Pages

CHAPTER 1

INTRODUCTION AND OBJECTIVES

Three-dimensional (3D) cell cultures have been recognized as more complex and physiologically relevant *in vitro* models that have been proposed to bridge the gap between animal model/*in vivo* and the traditional two-dimensional (2D) *in vitro* cell cultures. There are several advantages of 3D cell cultures: First, compared to animal models, 3D cell cultures can reproduce tissue *ex vivo* with human cells, especially with the advance of stem cell research. Second, the added complexity (e.g., the third dimension/ the z-axis and more) can give the cultured cells better *in vivo* emulating properties when compared to the 2D cell cultures. Third, 3D cell culture can maximize the cell number cultured in a limited space, which can scale up the cell production for therapeutic purposes.

Direct or indirect evidences, which are best exemplified in the field of experimental oncology, show that 3D cell cultures have better *in vivo* emulation property when compared to 2D cultures. Researchers have shown that 3D multicellular tumor spheroids (MCTS) mimic the *in vivo* cancer development better than their 2D counterparts [1, 2]. Another cell type receiving much attention in 3D cell culture studies are stem cells, probably due to their potential in regenerative medicine. According to a recent survey conducted in 2010 [3], researchers from all over the world perceived the most important advantages of 3D culture cells to be the *in vivo* mimicking property, which include but not limited to: better recapitulation of the environment experienced by normal cells in the body, complex tissue structures and *in vivo*-like morphology; and better reflection of normal differentiation, polarisation, cell behavior and intercellular

interactions. However, concrete evidence showing the resemblance of 3D cell cultures to *in vivo* system is lacking.

The increasing interest on 3D cell culture platforms can be reflected by the increasing number of research publications in Pubmed database (Figure 1.1). The 2010 3D cell culture survey also revealed that two thirds of the respondents, which came from universities or other research institutes, biotech or pharmaceutical companies, and hospitals and clinics, are planning to change their cell culture from 2D to 3D, with half of them already partially done so [3, 4]. Being so promising and fast growing, there is still no well accepted and concrete definition as to what defines 3D cell cultures. Intuitively, when talking about 3D cell cultures, the added z-axis is usually the focus of eyes. But how high should the z-axis be to qualify 3D? Also, if the ultimate goal of 3D cell culture is to recreate as close as possible what we have in the human body (e.g., create an identical tissue *ex vivo*); there are more aspects we need to consider beside the added spatial dimension, the z-axis. In our lab, we have extended the definition of 3D to a more complex context (Figure 1.2). We suggested that 3D cell culture models should combine spatial/temporal cues, physical/mechanical cues and chemical cues to produce an *in vivo* mimicking environment for cell adhesion, growth and differentiation. We have suggested to use the complex physiological relevance (CPR) for a more comprehensive and precise definition and discrimination of 3D cell cultures, in which CPR refers to "*in vitro* emulation of *in vivo* structure and/or function in 3D that is not possible in 2D cultures" [5].

Other researchers have also developed similar idea to define 3D cell cultures beyond the added z-axis. For instance, the European researchers who developed Alvetex 3D culture platform define 3D cell cultures as follows [6]:

"3D cell culture is about creating suitable surroundings for optimal cell growth, differentiation and function by:

- Allowing individual cells to maintain their normal 3D shape and structure with minimal exogenous support and interference,
- Encouraging cells to form complex interactions with adjacent cells and receive and transmit signals,
- Enabling a more natural environment to foster the creation of native architecture found in tissue structures,
- Reducing stress and artificial responses as a result of cell adaptation to flat, 2D growth surfaces."

Another well-known 3D cell culture company Glycosan defines 3D cell culture to be "encapsulation of cells within a biocompatible natural or synthetic extracellular matrix (as opposed to plating cells on the surface of a petri dish)" [7]. The same definition is used in SigmaAldrich's HyStem Glossary of terms [8]. Besides the fact that different research groups have different perspective on what defines 3D cell culture, the proposed definitions are qualitative and subject to the understanding of different people. A quantitative and concrete definition is desperately needed to regulate and standardize the 3D cell culture field.

There are various methods to achieve 3D cell cultures, most of which are still under development in the research labs. Some of these have found their way into commercialization and are available with HTS format. But few of them have entered the pharmaceutical company and the drug discovery or screening industry. We have summarized the currently available commercialized 3D HTS plates in Chapter 2.2, the cost of which range from $25 to $800 per plate. In modern drug discovery campaigns, with drastically increased number of possible drug

candidates, it is very important to reduce the cost for screening per compound. The high cost of commercially available 3D HTS plates is probably an obstacle for them to enter the drug screening industry.

In summary, while there is a great interest in 3D culture, the adoption by industry has been slow for several reasons including: 1) lack of concrete evidence for *in vivo* emulation, 2) absence of measure to ascertain three dimensionality of scaffold, and 3) high cost of commercial systems in a climate of great need to reduce cost of screening per compound.

In response to the above concerns, the goals of my study were to 1) follow up our previous study to verify *in vivo* emulation property of our polymer 3D cell culture platform with primary neuronal cells and freshly dissected tissue as *in vivo* surrogate; 2) identify a class of compounds with potential for serving as three-dimensionality biomarkers and 3) establish a fabrication process for HTS compatible 3D polystyrene scaffolds.

References:

1. Mueller-Klieser W (1987) Multicellular spheroids. A review on cellular aggregates in cancer research. J Cancer Res Clin Oncol 113: 101-122.

2. Kunz-Schughart LA, Freyer JP, Hofstaedter F, Ebner R (2004) The use of 3-D cultures for high-throughput screening: the multicellular spheroid model. J Biomol Screen 9: 273-285.

3. Comley J (2010) 3D Cell culture easier said than done. Drug Discovery World Summer 2010: 17.

4. 3D cell culture trends 2010. Internet: http://www.marketreports.com/TOC/HTStec/3DCellCultureTrends2010.pdf [Nov. 6th, 2011]

5. Lai Y, Asthana A, Kisaalita WS (2011) Biomarkers for simplifying HTS 3D cell culture platforms for drug discovery: the case for cytokines. Drug Discov Today 16: 293-297.

6. Technology for routine three dimensional (3D) cell culture. Internet: http://www.amsbio.com/brochures/Technology_for_Routine_Three_Dimensional_3D_Cell_Culture_-_AMSBIO.pdf [Nov.6th, 2011]

7. Glossary of common terms. Internet: http://www.glycosan.com/faq/glossary.html [Nov.6th, 2011].

8. HyStem Glossary of Terms. Internet: http://www.sigmaaldrich.com/life-science/stem-cell-biology/3d-stem-cell-culture/learning-center/hystem-glossary-of.html [Nov. 6th, 2011]

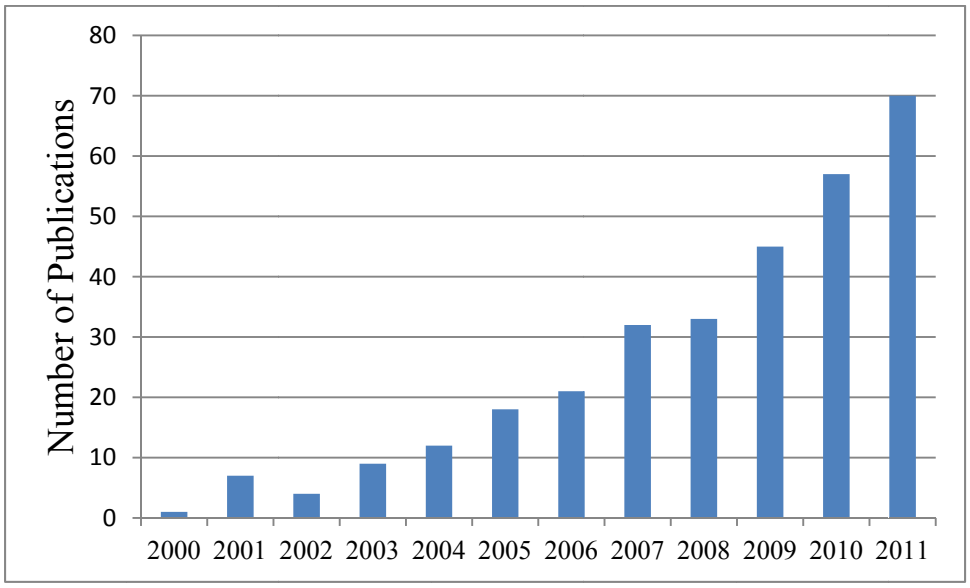

Figure 1. 1 Number of 3D related research publications in Pubmed.
Searching keywords were "3D cell culture *in vitro* model"

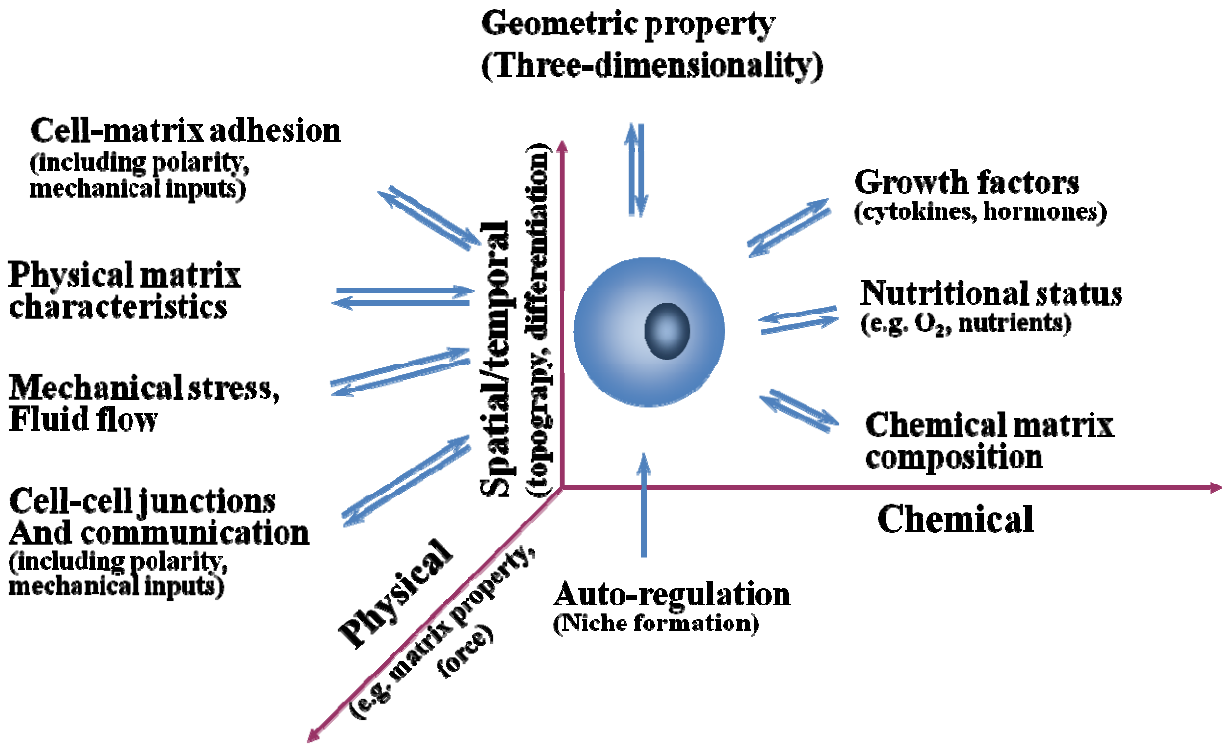

Figure 1. 2 Microenvironmental cues for 3D cell culture definition [4].

CHAPTER 2

LITERATURE REVIEW

2.1 Current 3D cell culture platforms

To date, approaches to culture cells in 3D microenvironment include multicellular aggregates [1, 2], microstructured substrates [3], polymer scaffolds [4, 5, 6], and bioreactors [7, 8]. Multicellular aggregates have become a predominant approach for creating 3D microenvironment for cancerous cells, which offers significant advantages in the research of tumor biology and cancer therapeutics over 2D culture systems [9, 10]. Embryoid body (EB) generated from stem cells are another prime application of multicellular aggreagates. The technique allows easy manipulation of stem cells to mimic the *in vivo* microenvironment, and researchers have shown that the microenvironment (stem cell niche) plays a key role in the maintenance, expansion and differentiation of stem cells. Microfabrication, which can produce a miniaturized, regulated, inexpensive platform for "cell-culture-on-a-chip", offers unique opportunities for engineering a 3D environment for cell culture and other cell-based microdevices [11, 12, 13, 14, 15, 16]. With the development in tissue engineering, polymer scaffolds have become appealing 3D cell culture systems *ex vivo* [17] and promising platform for 3D cell-based biosensor [18, 19, 20].

The polymers used to fabricate scaffolds can be synthetic or natural, producing either structural or biomimicking scaffolds. Natural polymer scaffolds offer the best chemical and physical cues to mimic the *in vivo* environment. Cells can be easily seeded on to those scaffolds with a high rate of attachment. Currently, the popular natural derived polymers for 3D cell

culturing are: collagen, fibrin, fibroin, glycosaminoglycan (GAGs), chitosan, alginates and etc. They can be animal-origin or plant-origin, and usually exhibit good biocompatibility and low toxicity. However, the disadvantages of natural polymers are also notable. Animal-derived polymers may transmit diseases. The chemical and physical properties of naturally derived polymers can differ significantly from batch to batch. The mechanical properties of the natural polymers are generally low, which also limits the formats of the scaffolds they can form. Synthetic polymers have been attracting more and more attention due to their versatility and stable properties.

Synthetic polymers can be divided into two main categories: biodegradable and non-biodegradable. The biodegradability is desired for tissue regeneration and clinical applications. For synthetic polymers, the biodegradation rate usually can be tailored for specific applications, by adjusting polymer composition and polymer molecular weight. For instance, poly (glycolic acid) (PGA) and poly (lactic acid) (PLA), both being poly (alpha-hydroxyacids) polymers, have different degradation rate. The copolymer poly(lactic-co-glycolic acid) (PLGA) generally have lower degradation rate with higher content of glycolic acid moiety and low molecular weight polymers [21], with exceptions. For bioassay applications, such as in pre-clinical drug discovery screening processes, biodegradation is less of concern, unless the rate is such that the assay reproducibility will be affected. Polystyrene, a common polymer that has been widely used in 2D tissue culture vessel fabrication, can be a very good material for 3D cell culture vessel due to its high transparency, good optical property and low cost.

2.2 Commercially available 3D culture platforms

After decades of research, an increasing number of commercially available 3D cell culture platforms are approaching in recent years. Commercially available 3D cell culture products can be found in large laboratory supply outlets such as Invitrogen and Sigma-Aldrich. There are also many new emerging companies who are specializing in 3D cell culture platforms only. A list of commercially available products have been summarized in Table 2.1, which include 3D biotek, BellBrook Labs, BioTek, CellASIC, CELLnTEC Advanced Cell systems, Glycosan BioSystems, Hamilton Company, QGel, RealBio Technology, Reinnervate, and Tissue Growth Technologies.

The majority of commercially available products are based on soft and biomimetic scaffolds (natural or symthetic). Examples of these include BellBrook Labs (ECM proteins such as matrigel), CellASIC (ECM proteins such as matrigel and geltrex), Global Cell Solutions (ECM proteins), Glycosan (hyaluronan, Polyethylene (glycol) diacrylate-based hydrogel and collagen), Hamilton (ECM proteins) and etc. Usually, biomimetic scaffolds takes the form of soft scaffolds or hydrogel and encapsulate the cells inside to achieve 3D. Although claimed to be "ready to use", most if not all of them require mixing reagents (such as adding a cross-linker) and waiting for hydrogel formation. However, since they are in liquid form before solidification, they are flexible to be added into multi-well plates to achieve HTS. However it should be pointed out that the robustness of assays in such platforms are not proven --Z'-factors have not been reported and as such consistence for HTS has to be confirmed prior to use.

Hard scaffolds fabricated from synthetic materials are more promising as far as incorporation into HTS compatible formats (example includes 3D biotek's 3D inserts and Reinnervate's Alvetex) with true "ready to use" formats and more cost competitive. But the

structural formats can vary significantly. 3D biotek has generated a woven type of scaffolds (Figure 2.1 A-D) with PCL (biodegradable) and polystyrene (non-biodegradable) to fulfill different requirements. The generated pores are organized, with determined size and the certainty to be open and interconnected. The spacing between fibers was designed to be about 300 μm for 96 well plate inserts. The large pore size may seem to be helpful for multicellular spheroid formation; however this has not been reported in the literature. The typical fibers used to form the scaffolds are 200 μm in diameter, which is way larger than a typical cell's size. If the cells do manage to attach to the fibers, the relatively large size makes fibers not very different from flat surfaces (Chapter 5, Figure 5.3 I). Reinnervate is a European company which produced polystyrene porous scaffolds in an insert format named Alvetex (Figure 2.1 E-F). Being built in an insert, the scaffolds are immersed in the medium, with both sides contact the medium. Thus, the cells can better migrate to the bottom of the scaffolds. The inserts are designed in a way that it can sit on different height, making it flexible for air-liquid mode culturing. However, up till now, the inserts only works in low throughput format such as 6-well plates or Petri-dish. High-throughput format cell culturing system is still under development.

Micro-patterning and scaffold-free hanging drop methods have also been commercialized for generating multicellular spheroids such as embryoid bodies and tumor models. The examples of the commercialized products are AggreWell™ from STEMCELL technologies and Perfecta^{TM} from 3D Biomatrix. AggreWell^{TM} targets stem cell culturing only and is proposed to generate uniform sized embryoid bodies in large quantity. There are two different size of the microwell in AggreWell, 400 μm and 800 μm (Figure 2.2 A-E). These sizes are sufficiently small for embryoid body formation. Although the company didn't claim 3D cell culturing and only promotes it in stem cell culture field, these plates should be able to generate other multicellular

spheroids from non-stem cells. Since the main function of these plates is to generate large quantities of multicellular spheroids, no HTS formats are available so far. However, the harvested multicellular spheroids can be seeded to HTS format plates for HTS applications. Perfecta^{TM} is a 384-well plates utilizing capillarity force and hanging drop method to generate one multicellular spheroid per well (Figure 2.2 F-H). If the seeding density is controlled well, the plates should be able to provide uniform sized spheroids. However, since the seeding cells are in very small volume (5-10 μl) just as the regular hanging drop method, it's relatively difficult to manipulate manually. But with the more and more advanced automation and robotic method, it should not be a problem. Since the above methods can generate multicellular spheroids only, it limits the applications to other cell types.

2.3 Physiological relevance of 3D cell cultures.

According to a recent survey, researchers perceived that the most important advantages of 3D cell cultures are: better recapitulation of the environment experienced by normal cells in the body, replicates complex tissue structures and *in vivo*-like morphology, better reflection of normal differentiation, polarization, cell behavior and intercellular interactions and more realistic cell biology and function [22]. These four advantages are more or less related to "physiological relevance" which may be the biggest reason why 3D cell cultures gaining popularity.

The most well established applications of 3D cell cultures include but are not limited to 3D tumor models for invasion and drug resistance testing, artificial 3D skin model for wound healing and cosmetic testing, liver toxicity assay with cultured hepatocytes and platforms for enhanced stem cell differentiation, all of which rely on 3D cell cultures' physiological relevancy and are well published. For instance, multicellular spheroids have been able to fully recapitulate the multicellular mediated drug resistance of EMT6 tumors [23], which was inherently induced

in vivo but completely lost when cancer cells were dissociated and cultured on monolayers. Weaver et al. [24] have been able to show the phenotypic transformation of malignant cells in a 3D collagen gel configuration upon treatment with integrin antibodies, while this has never been possible in monolayer cultures. In another study, two tumorigenic cell lines (HT-1080 fibrosarcoma and MDA-MB-231 carcinoma) showed protease-independent amoeboid movement within 3D collagen matrix. This observation challenges the traditional screening for anti-metastatic agents against proteolytic activity with 2D monolayer cultures, and 3D spheroids should become mandatory test systems in cancer therapeutic screening programs. The emergence of artificial skin models can be dated back to 1990s with the development of air-liquid interface culturing method and the utility of ECM proteins as substratum. 3D structured artificial skins achieved similar histology structure as *in vivo* skin where 2D cultures never can. They have shown superior ability to distinguish between corrosive and non-corrosive substances than monolayer cells and the competence to release some of the cytokines under physical or chemical stress which are also found in *in vivo* skins [25]. Fibroblasts grown on cell or tissue derived 3D scaffolds shows complete pattern of adhesion, where complete colocalization of alpha5 integrin, paxillin and fibronectin can be found. The same triple colocalization can be found in transverse cryostate craniofacial mesenchyme sections of an E13.5 mouse embryo, but not in 2D cultured fibroblasts [26].

To date, there is no doubt that 3D cell cultures have superior *in vivo* relevance than 2D cultures. Supportive data has been obtained with many cell types. However, due to the lack of physiological relevance criteria, few supportive data have been provided on how 3D cell cultures technique can improve neuronal cell cultures.

2.4 Cytokines and the their promising role as 3D cell biomarkers [27]

Cytokines are soluble, low molecular weight, extracellular protein mediators that usually act at short range between neighboring cells. They are crucial intercellular regulators and mobilizers of cells engaged in innate and adaptive inflammatory host defenses, cell growth, differentiation, cell death, angiogenesis, and development and repair processes. They have been assigned to various family groups based on the structural homologies of their receptors and can be broadly classified into families such as colony stimulating factors, interleukins, interferons,transforming growth factors (TGF), tumor necrosis factors (TNF), platelet-derived growth factors (PDGF) and chemokines. Although cytokines have been extensively studied in the field of immunology and oncology, they have been overlooked by tissue engineers. However, these same small proteins might have the power to revolutionize the field. Although the evidence for their existence in 3D cultures is compelling, they have not yet been looked at as candidates for potential biomarkers. However, we suggest that they are the ideal family to explore for identification and validation follow-up studies for the following three main reasons.

First, when cells are transitioned from a 2D monolayer to a 3D microenvironment, they become surrounded by homotypic neighbors, forming a loosely bound disorganized aggregate. *In vivo*, such a scenario is encountered only during avascular tumorigenesis or early stages of inflammatory wound healing, which are both similar in nature and regulated by cytokines [28]. Therefore, *in vitro*, the cells growing in 3D relate to any of those two models, depending on their type (malignant or primary, respectively), therefore explaining the upregulation of their cytokine levels.

Second, several 2D–3D comparative transcriptomic studies with cells from the four main tissue types (nerve, muscle, connective and epithelial) cultured on a variety of platforms, have

reported the upregulation of cytokines and their receptors in 3D cultures. For example, Klapperich and Bertozzi [29] reported upregulation of seven cytokines (IL-8, chemokine (C-X-C motif) ligand (CXCL)-1,CXCL2, CXCL3, CXCL5, vascular endothelial growth factor (VEGF) and leukemiainhibitory facto (LIF)) by a human fetal lung fibroblast (IMR-90) cultured in acollagen–glycosaminoglycan (collagen/GAG) 3D mesh. The mesh was prepared by freeze drying and heat enabled cross-linking of the polymer and had an average pore size of 80–100 μm. In addition, Ghosh et al. [30] reported upregulation of six cytokines (CXCL1–3, IL-8, macrophage Inflammatory Protein-3 (MIP-3a) and angiopoetin-like 4) by a melanoma cell line (NA8) cultured on poly-2-hydroxyethyl methacrylate (polyHEMA) plates when compared with 2D surfaces. The polymer coating prevented cells from attaching to the plastic surface leading to the formation of MCTS.

Third, transcriptomic findings such as those in the above examples have been supported by studies at the protein level. For example, Enzerink et al. [31] has shown that clustering of fibroblasts induces chemokine (CCL2-5, CXCL1-3 andCXCL8) secretion in five different fibroblast cell lines cultured in agarose. In addition, Fischbach et al.[32] cultured tumor cells in a 2D and 3D RGD-alginatesystem and reported a dramatic increase in IL-8 levels; however, no significantVEGF differences were reported between 2D and 3D cultures. In the same study, cells grown in alginate gels having RGD peptides (spatial, biophysical and biochemical cues) produced a higher level of IL-8 compared with those lacking the adhesion peptide (only spatial and biophysical cues), although both produced higher levels when compared with 2D (lacking all three cues). This shows that changes in the microenvironment are conveyed directly by the difference in the level of cytokine production. In another study by the same group, the same cells also showed an upregulation of cytokines when grown in Matrigel

(lrBM) compared with their 2D counterparts. This comparison is particularly important as cells grown on Matrigel have already been shown to produce a CPR outcome (formation of mammary gland acinus and milk-like secretions into the lumen) [24], which mean that Matrigel provides the relevant microenvironmental cues. Taken together, these studies suggest that the upregulation of cytokines in 3D compared with 2D cultures is not a random differential response but a potentially ubiquitous biomarker for three-dimensionality. Further studies to establish this view firmly are needed.

Cytokines are particularly attractive as biomarkers for several practical reasons. First, they are secreted in the media, making it easy for their detection to be amenable for HTS readout. Second, they are expressed in a wide range of cells from the four tissue types (muscle, connective, epithelial and nerve), suggesting the potential for their ubiquity as opposed to being cell or tissue specific. Third, their temporal expression suggests the use of profiles as opposed to single-time measurements, which increases their robustness as biomarkers.

2.5 Cell-based assay and HTS in pre-clinical drug discovery

HTS has become a dominant tool in pre-clinical drug discovery for several reasons. One reason relies on the vast number of compounds produced by combinatorial chemistry which need to be tested in a short period of time. Second, cell-based screening is of great interest as a useful tool for lead generation [33]. Cells, as designed and assembled by nature, are precise and complex small factories which still cannot be fully understood or reproduced by current technologies. Unlike biochemical assays in which one or a few mechanisms are investigated, the cell-based assay can test a comprehensive and systematic reaction all at once. It is highly unlikely that any lead will progress without being tested in an appropriate cell model. Since the merit of cell-based assay rely heavily on the fact that cells can better reflect the complex

reactions that happen in the human body after drug administration, how well the model can represent the *in vivo* situation is essential for a successful cell-based assay.

The capability of cells to provide complex response to various stimuli has been configured and adapted to HTS compatible formats. Cell-based assays can be used to test gene transcription, ion flux, transport, proliferation, cytotoxicity, secretion, translocation, redistribution, protein expression and enzyme activity. Most if not all of the above function test cannot be achieved completely by biochemical assays. Famous cell-based assays include promoter-driven luciferase reporter assay, GPCR FLIPR™ Ca2+ response assay and transporter–radioligand uptake assay, which can accommodate more than half million compounds in a single campaign [33].

The current new developments for cell-based assay include automation, high content, label-free, improved physiological relevance and etc. Automation is required for large scale of screening and can increase the reproducibility, precision and reduce errors caused by operators. High content cell-based assay can increase the information gained per run for more efficient lead optimization. High content screening can extract spatial and temporal information from either fixed or living cells. If used with living cells, it is usually achieved with multicolor fluorescent probes [34]. The rationale in using label-free technique in drug screening is to minimize the manmade interference and preserve the native status of the tested substrates as much as possible. Label-free can be applied to biochemical assays and cell-based assays. The most famous example of label-free cell-based assay is the cell adhesion and cell death assay with impedance [35]. As discussed before, physiological relevance is a huge advantage of cell-based assays. To increase the physiological relevance is to increase the ability of the assay to truly reflect what happens in the body. It is now well understood that physiological relevance can be better

achieved by putting cells in an environment that mimics their native environment as much as possible, in other words, 3D cell culturing.

Cell-based assays can be strong tools in drug discovery and screening. However, some of the current development such as label free and high content screening can reduce the robustness of the signal and quality control can become a big issue. It has been discovered that cell lines kept in different labs can be very different. There are cases that publications were based on cell lines which were actually contaminated by other cell lines. Quick and easy quality control for cells' physiological relevance to the tissue they are modeling will be essential for future cell-based assays.

Ion channels have emerged as an attractive drug discovery target class for modern drug discovery [36,37,38]. Ion channels have been discovered to be associated with neuronal signal transduction, muscle contraction, T-cell activation, cell proliferation, apoptosis and other important cellular functions. Recent development of ion channel studies has expanded them from targets for CNS and cardiovascular disorder to targets for other diseases such as cancer [39] and immune disorders [40] . Unlike some enzyme and receptor targets which can be screened with high throughput biochemical assays, ion channels rely heavily on cell-based assay for both primary and secondary screening [41]. Thus the development of efficient, physiologically more relevant, high throughput screening (HTS) compatible cell-based assay is essential for ion channel targeted drug discoveries.

2.6 Neural stem cells in drug discovery

Neurodegenerative disorders, such as Alzheimer's Disease (AD), Parkinson's Disease, Huntington's Diseases, amyotrophic lateral sclerosis (ALS), are among the most devastating illnesses in society. However, currently used drugs for neurodegenerative disorders still have

shortcomings. For example, recent data from patients with severe stages of AD demonstrate the efficacy of the cholinesterase inhibitor donepezil on cognitive and functional measures but not on behaviors [42]. Effective drug discovery against neurodegenerative disorders is in great demand, which calls for novel assays for HTS of available molecular libraries to identify effective small molecules as drug leads.

The development of cell-based biosensor calls for a renewable and unlimited cell source; also these cells should be kept in normal states. The use of these primary cultures is accompanied by excessive animal sacrifice and frequent cell isolation, which cost a lot of time and money. The use of blastoma derived cell lines offers advantages over primary neural cultures due to the easy and unlimited expansion of the tumorigenic cell population. However, results based on blastoma drived cells are always questioned on the grounds of cellular abnormality [43], which makes "physiological relevance" challengeable.

As an alternative to these two cell sources, ES derived neural cells are a good cell source for cell-based drug discovery assays. ES cells before differentiation are proliferative and as easy to maintain as tumor derived cells. ES cell derived neural cells in culture appeared normal morphologically and display normal features of immunoreactivity when tested for neuron-specific elements [44,45]. They are as vulnerable as normal neurons to excitotoxic death [46].

2.7 References

1. Albrecht DR, Underhill GH, Wassermann TB, Sah RL, Bhatia SN (2006) Probing the role of multicellular organization in three-dimensional microenvironments. Nat Methods 3: 369-375.

2. De Bank PA, Hou Q, Warner RM, Wood IV, Ali BE, et al. (2007) Accelerated formation of multicellular 3-D structures by cell-to-cell cross-linking. Biotechnol Bioeng 97: 1617-1625.

3. Wu ZZ, Zhao Y, Kisaalita WS (2006) Interfacing SH-SY5Y human neuroblastoma cells with SU-8 microstructures. Colloids Surf B Biointerfaces 52: 14-21.

4. Drury JL, Mooney DJ (2003) Hydrogels for tissue engineering: scaffold design variables and applications. Biomaterials 24: 4337-4351.

5. Levenberg S, Huang NF, Lavik E, Rogers AB, Itskovitz-Eldor J, et al. (2003) Differentiation of human embryonic stem cells on three-dimensional polymer scaffolds. Proc Natl Acad Sci U S A 100: 12741-12746.

6. Matthews JA, Wnek GE, Simpson DG, Bowlin GL (2002) Electrospinning of collagen nanofibers. Biomacromolecules 3: 232-238.

7. Timmins NE, Scherberich A, Fruh JA, Heberer M, Martin I, et al. (2007) Three-dimensional cell culture and tissue engineering in a T-CUP (tissue culture under perfusion). Tissue Eng 13: 2021-2028.

8. Granet C, Laroche N, Vico L, Alexandre C, Lafage-Proust MH (1998) Rotating-wall vessels, promising bioreactors for osteoblastic cell culture: comparison with other 3D conditions. Med Biol Eng Comput 36: 513-519.

9. Kunz-Schughart LA, Freyer JP, Hofstaedter F, Ebner R (2004) The use of 3-D cultures for high-throughput screening: the multicellular spheroid model. J Biomol Screen 9: 273-285.

10. Birgersdotter A, Sandberg R, Ernberg I (2005) Gene expression perturbation *in vitro*--a growing case for three-dimensional (3D) culture systems. Semin Cancer Biol 15: 405-412.

11. Park TH, Shuler ML (2003) Integration of cell culture and microfabrication technology. Biotechnol Prog 19: 243-253.

12. Li N, Tourovskaia A, Folch A (2003) Biology on a chip: microfabrication for studying the behavior of cultured cells. Crit Rev Biomed Eng 31: 423-488.

13. Tourovskaia A, Figueroa-Masot X, Folch A (2005) Differentiation-on-a-chip: a microfluidic platform for long-term cell culture studies. Lab Chip 5: 14-19.

14. Koh WG, Pishko MV (2006) Fabrication of cell-containing hydrogel microstructures inside microfluidic devices that can be used as cell-based biosensors. Anal Bioanal Chem 385: 1389-1397.

15. Borenstein JT, Weinberg EJ, Orrick BK, Sundback C, Kaazempur-Mofrad MR, et al. (2007) Microfabrication of three-dimensional engineered scaffolds. Tissue Eng 13: 1837-1844.

16. Vickerman V, Blundo J, Chung S, Kamm R (2008) Design, fabrication and implementation of a novel multi-parameter control microfluidic platform for three-dimensional cell culture and real-time imaging. Lab Chip 8: 1468-1477.

17. Cushing MC, Anseth KS (2007) Materials science. Hydrogel cell cultures. Science 316: 1133-1134.

18. O'Connor SM, Andreadis JD, Shaffer KM, Ma W, Pancrazio JJ, et al. (2000) Immobilization of neural cells in three-dimensional matrices for biosensor applications. Biosensors and Bioelectronics 14: 871-881.

19. Mao C, Kisaalita WS (2004) Characterization of 3-D collagen hydrogels for functional cell-based biosensing. Biosens Bioelectron 19: 1075-1088.

20. Gui L, Zhao L, Spencer RW, Burghouwt A, Taylor MS, et al. (2011) Development of novel biodegradable polymer scaffolds for vascular tissue engineering. Tissue Eng Part A 17: 1191-1200.

21. Madhavan Nampoothiri K, Nair NR, John RP (2010) An overview of the recent developments in polylactide (PLA) research. Bioresour Technol 101: 8493-8501.

22. Comley J (2010) 3D Cell culture easier said than done. Drug Discovery World Summer 2010: 17.

23. Graham CH, Kobayashi H, Stankiewicz KS, Man S, Kapitain SJ, et al. (1994) Rapid acquisition of multicellular drug resistance after a single exposure of mammary tumor cells to antitumor alkylating agents. J Natl Cancer Inst 86: 975-982.

24. Weaver VM, Petersen OW, Wang F, Larabell CA, Briand P, et al. (1997) Reversion of the malignant phenotype of human breast cells in three-dimensional culture and *in vivo* by integrin blocking antibodies. J Cell Biol 137: 231-245.

25. Brohem CA, Cardeal LB, Tiago M, Soengas MS, Barros SB, et al. (2011) Artificial skin in perspective: concepts and applications. Pigment Cell Melanoma Res 24: 35-50.

26. Cukierman E, Pankov R, Stevens DR, Yamada KM (2001) Taking cell-matrix adhesions to the third dimension. Science 294: 1708-1712.

27. Lai Y, Asthana A, Kisaalita WS (2011) Biomarkers for simplifying HTS 3D cell culture platforms for drug discovery: the case for cytokines. Drug Discov Today 16: 293-297.

28. Coussens LM, Werb Z (2002) Inflammation and cancer. Nature 420: 860-867.

29. Klapperich CM, Bertozzi CR (2004) Global gene expression of cells attached to a tissue engineering scaffold. Biomaterials 25: 5631-5641.

30. Ghosh S, Spagnoli GC, Martin I, Ploegert S, Demougin P, et al. (2005) Three-dimensional culture of melanoma cells profoundly affects gene expression profile: a high density oligonucleotide array study. J Cell Physiol 204: 522-531.

31. Enzerink A, Salmenpera P, Kankuri E, Vaheri A (2009) Clustering of fibroblasts induces proinflammatory chemokine secretion promoting leukocyte migration. Mol Immunol 46: 1787-1795.

32. Fischbach C, Kong HJ, Hsiong SX, Evangelista MB, Yuen W, et al. (2009) Cancer cell angiogenic capability is regulated by 3D culture and integrin engagement. Proc Natl Acad Sci U S A 106: 399-404.

33. Johnston PA (2002) Cellular platforms for HTS: three case studies. Drug Discov Today 7: 353-363.

34. Zanella F, Lorens JB, Link W (2010) High content screening: seeing is believing. Trends Biotechnol 28: 237-245.

35. Verdonk E, Johnson K, McGuinness R, Leung G, Chen YW, et al. (2006) Cellular dielectric spectroscopy: a label-free comprehensive platform for functional evaluation of endogenous receptors. Assay Drug Dev Technol 4: 609-619.

36. Mathie A (2010) Ion channels as novel therapeutic targets in the treatment of pain. J Pharm Pharmacol 62: 1089-1095.

37. Macphee C (2004) New advances in drug discovery. Expert Opin Investig Drugs 13: 1213-1215.

38. Molokanova E, Savchenko A (2008) Bright future of optical assays for ion channel drug discovery. Drug Discov Today 13: 14-22.

39. Arcangeli A, Crociani O, Lastraioli E, Masi A, Pillozzi S, et al. (2009) Targeting ion channels in cancer: a novel frontier in antineoplastic therapy. Curr Med Chem 16: 66-93.

40. Varga Z, Hajdu P, Panyi G, Gaspar R, Krasznai Z (2007) Involvement of membrane channels in autoimmune disorders. Curr Pharm Des 13: 2456-2468.

41. Zheng W, Spencer RH, Kiss L (2004) High throughput assay technologies for ion channel drug discovery. Assay Drug Dev Technol 2: 543-552.

42. Seow D, Gauthier S (2007) Pharmacotherapy of Alzheimer disease. Can J Psychiatry 52: 620-629.

43. Banker G, Goslin K (1988) Developments in neuronal cell culture. Nature 336: 185-186.

44. Tzeng SF (2002) Neural progenitors isolated from newborn rat spinal cords differentiate into neurons and astroglia. J Biomed Sci 9: 10-16.

45. O'Connor SM, Stenger DA, Shaffer KM, Maric D, Barker JL, et al. (2000) Primary neural precursor cell expansion, differentiation and cytosolic Ca2+ response in three-dimensional collagen gel. Journal of Neuroscience Methods 102: 187-195.

46. Qu Y, Vadivelu S, Choi L, Liu S, Lu A, et al. (2003) Neurons derived from embryonic stem (ES) cells resemble normal neurons in their vulnerability to excitotoxic death. Exp Neurol 184: 326-336.

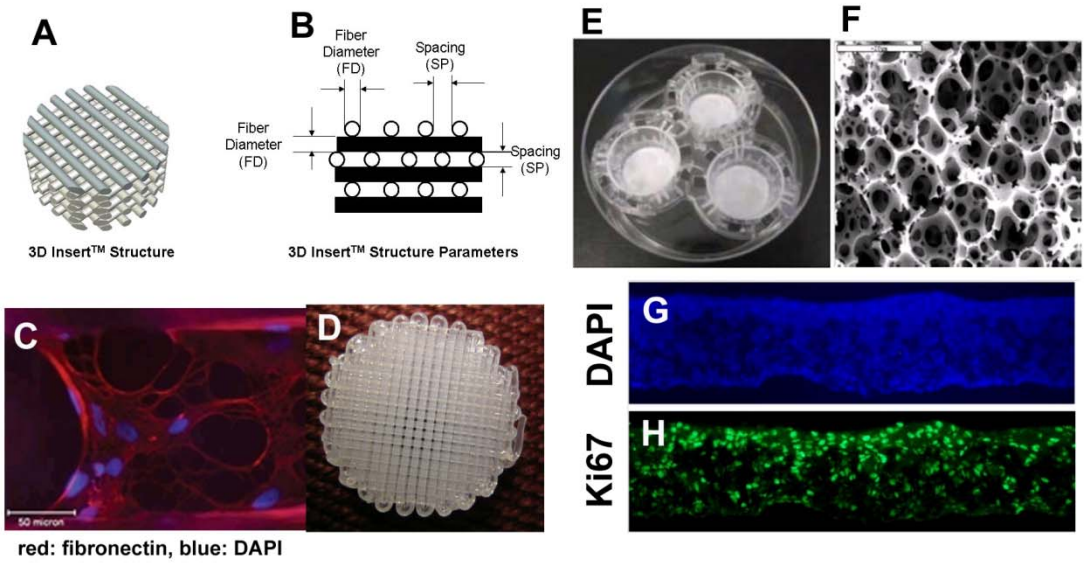

Figure 2. 1 Examples of commercially available 3D cell culture platforms with hard scaffolds.
(A-D) 3D PS insert™ by 3D biotek (www.3dbiotek.com): (A) 3D Insert™ structure, (B) structure parameters, (C) hMSC cells cultured in the scaffolds with fibronectin (red) and DAPT staining (blue) ; (E-F) Alvetex by Reinnervate (www.reinnervate.com): (E) the insert format of scaffolds sit in a 100 mm Petri-dish, (F) SEM images of the scaffold structure, (G) DAPI staining of the cells inside the scaffolds and (H) Ki67 staining of the proliferating cells inside the scaffolds.

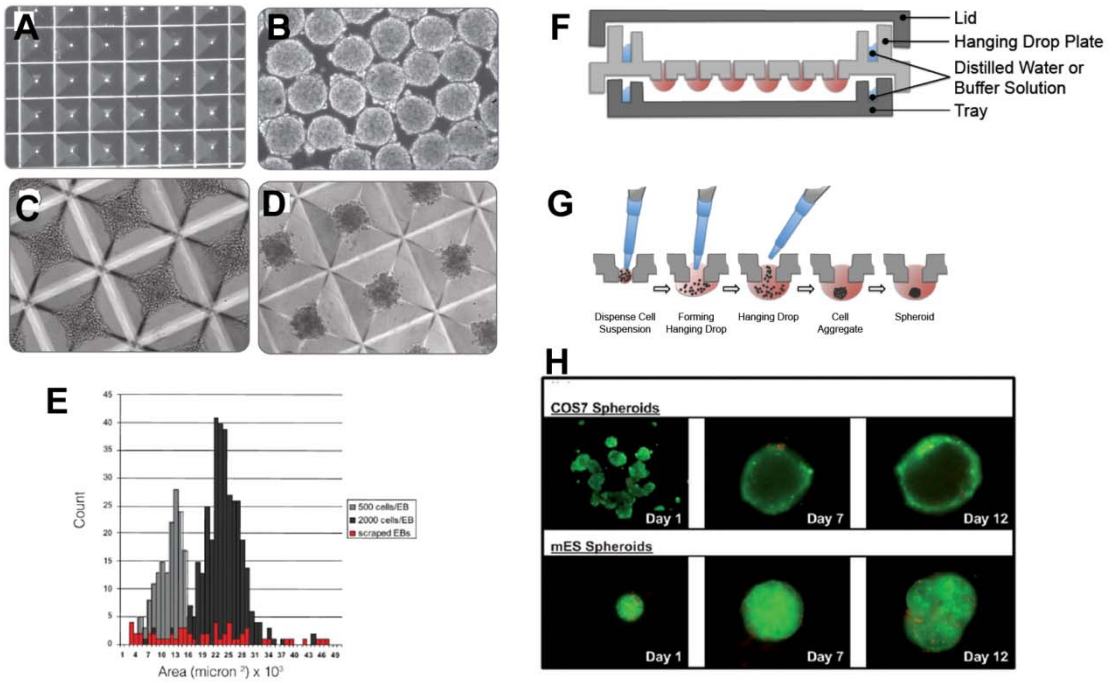

Figure 2. 2 Micro-patterning and scaffold free 3D cell culture examples.
(A-E) STEMCELLTechnologies AggreWell™ (http://www.stemcell.com): (A) AggreWell 400 plates with 400 µm diameter microwells. Photo taken at 40x magnification, (B) harvested embryoid bodies formed from AggreWell™ 400 with uniform size, (C) Even distribution of mESCs in AggreWell™ 400 after plating, (D) EB formation from mESCs in AggreWell™ 400 after 24 hours. (E) Size distribution resulted from different plating densities (light grey with 500 cells/EB and dark grey with 2000 cells/EB) compared with traditional scraping method (red); (F-H) Perfecta™ hanging drop plates by 3D Biomatrix (http://3dbiomatrix.com): (F) schematic illustration of Perfecta™ hanging drop plates, (G) schematic illustration of how to use Perfecta™ hanging drop plates, (H) spheroid formed from Perfecta™ hanging drop plates with COS7 cells and mES cells.

Table 2. 1 Commercially available 3D cell culture platform examples (part 1)

Company	Product name	Material type	Scaffold type	Microscopy	Mechanical property
Invitrogen	Affymatrix	Natural (alginate)	Structural (50-400 μm pores)	opague	medium
Sigma-Aldrich	HydroMatrix ™	Synthetic peptide	Biomimetic (nano scaled fibers)	transparent	N/A
3D Biotek	3D Insert™-PS Cell Culture Plates	Synthetic polystyrene	Structural (~200 μm pores)	opague	high
Glycosan	Extracel™ Hydrogel Kit	Natural	biomimetic	transparent	N/A
3D Biomatrix	Perfecta™ hanging drop plates	Synthetic polystyrene	Scaffolds free hanging drop	transparent	N/A
Insphero	N/A	N/A	Scaffolds free hanging drop	transparent	N/A
BellBrooks Labs	Iuvo platform	Natural (hydrogels)	biomimetic	transparent	N/A
CellASIC	Microfluidic Cell Array	Natural (hydrogels)	biomimetic	transparent	N/A
CELLnTEC	3D medium	Medium	N/A	N/A	N/A
Hamilton	Global Eukaryotic Microcarrier (GEM™)	Natural (Alginate core and ECM protein coating)	biomimetic	N/A	N/A
Hamilton	BioLevitator	N/A	N/A	N/A	N/A
Kuraray	Micro-Space Cell Culture	Resin	N/A	transparent	stiff
STEMCELL	AggreWell™	Synthetic	N/A	transparent	stiff
QGel	QGEL™ MT 3D MATRIX	Synthetic (4-arm Poly(ethylene) Glycol)	Biomimetic	transparent	soft
Reinnervate	Alvetex™	Synthetic polystyrene	Structural scaffolds	Opaque	stiff
Tissue Growth technology	DermiGen™	N/A	Bioreactor	N/A	N/A

Table 2.1 Commercially available 3D cell culture platform examples (part 2)

Company	Product name	Cell recovery	Ready to use	Storage	HTS	Price per plate	Note:
Invitrogen	Affymatrix	dissolving reagent	Yes	RT with dessicate	Yes 96 well	194	
Sigma-Aldrich	HydroMatrix™	centrifuge	No	-20 °C	Yes 96 well	180	
3D Biotek	3D Insert™-PS Cell Culture Plates	trypsin	Yes	RT	Yes 96 well	824	
Glycosan	Extracel™ Hydrogel Kit	Dissolving reagent	No	-20 °C	Yes 96 well	180	
3D Biomatrix	Perfecta™ hanging drop plates	Aspiration	Yes	RT	Yes 384 well only	26	
Insphero	N/A	Aspiration	Yes	RT	Yes 96 well	N/A	Provide microtissue in plates
BellBrooks Labs	Iuvo platform	N/A	No	-20 °C	Yes 96	210	Microfluidics
CellASIC	Microfluidic Cell Array	N/A	No	-20 °C	No	N/A	Microfluidics perfusion
CELLnTEC	3D medium	N/A	Yes	4 °C	No	N/A	Limited cell type, coupled with Millicell inserts
Hamilton	Global Eukaryotic Microcarrier (GEM™)	Trypsin and other enzyme	No	4 °C	Yes	~40	Carrier with magnetic core (BioLevitator system needed)
Hamilton	BioLevitator	N/A	N/A	N/A	N/A	N/A	Bioreactor
Kuraray	Micro-Space Cell Culture	Regular method	Yes	RT	Yes	N/A	Micro-pattern
STEMCELL	AggreWell™	Aspiration	Yes	RT	NO	N/A	For embryoid body formation
QGel	QGEL™ MT	N/A	No	-20 °C	NO	N/A	

	3D MATRIX						
Reinnervate	Alvetex™	N/A	Yes	RT	NO	N/A	
Tissue Growth technology	DermiGen™	Easy	N/A	N/A	N/A	N/A	

CHAPTER 3

THREE DIMENSIONAL NEURONAL CELL CULTURE MORE ACCURATELY MODEL VOLTAGE GATED CALCIUM CHANNEL FUNCTIONALITY IN FRESHELY DISSECTED NERVE TISSUE*

*Lai Y, Cheng K, and Kisaalita WS. Submitted to *PLoS one*, 11/09/2011.

3.1 Abstract

It has been demonstrated that neuronal cells cultured on traditional flat surfaces may exhibit exaggerated voltage gated calcium channel (VGCC) functionality. To gain a better understanding of this phenomenon, primary neuronal cells harvested from mice superior cervical ganglion (SCG) were cultured on two dimensional (2D) flat surfaces and in three dimensional (3D) synthetic poly-L-lactic acid (PLLA) and polystyrene (PS) polymer scaffolds. These 2D- and 3D-cultured cells were compared to cells in freshly dissected SCG tissues, with respect to intracellular calcium increase in response to high K^+ depolarization. The calcium increases were identical for 3D-cultured and freshly dissected, but significantly higher for 2D-cultured cells. This finding established the physiological relevance of 3D-cultured cells. To shed light on the mechanism behind the exaggerated 2D-cultured cells' functionality, transcriptase expression and related membrane protein distributions (caveolin-1) were obtained. Our results support the view that exaggerated VGCC functionality from 2D cultured SCG cells is possibly due to differences in membrane architecture, characterized by uniquely organized caveolar lipid rafts and the cytoskeleton. The practical implication of use of 3D-cultured cells in preclinical drug discovery studies is that such platforms would be more effective in eliminating false positive hits and as such improve the overall yield from screening campaigns.

Keywords: Superior cervical ganglion, Scaffold, 3D cell culture, Caveolin, L-type calcium channel, HTS

3.2 Introduction

A key goal in cell-based assay technology is to achieve cellular responses to external stimuli that are physiologically relevant to what happens *in vivo* as closely as possible. However, many whole-cell-based assays in use today rely on flat, two-dimensional (2D) glass or plastic substrates that may not produce results characteristic of *in vivo* conditions. Three dimensional (3D) substrates or scaffolds provide cells with *in vivo*-like topographical cues and thus enable cells to differentiate into specific phenotype and maintain specific functions that are usually impossible under 2D cell culture conditions [1,2,3]. Thus 3D cell-based assay systems are desirable in preclinical drug discovery applications

Various approaches and materials have been studied for creating three-dimensionality. Among them are microgravity bioreactors [4,5]**,** natural polymers especially collagen hydrogels [6,7,8], photopolymerized hydrogels [9], synthetic polymer scaffolds [10,11], self-assembling peptide scaffolds [12]**,** and micro/nano patterned substrates [13].

Synthetic polymer scaffolds offer several comparative advantages. First, in comparison to microgravity bioreactors and patterned substrates, polymer scaffolds are easier and faster to prepare and can be scaled down for incorporation into high throughput screening (HTS) systems. Second, in comparison to most hydrogels, polymer scaffolds offer less resistance to diffusion of nutrients and wastes to and from cells deeper in scaffold [7]. Third, in comparison to nanoscale pores and fibers associated with self-assembling peptide scaffolds, microscale pores in polymer scaffolds are large enough to host 3D multi-cellular aggregates or microtissues [14].

We have previously demonstrated that polymer based scaffolds can be integrated into HTS compatible platform for whole-cell-based assays [15,16,17]. Neural stem cells cultured in such polymer based scaffolds modeled *in vivo* surrogate (neural spheres) better than 2D cells in

terms of morphology, cellular growth profile, gene expression and voltage gated calcium channel (VGCC) function [15] – VGCC are emerging drug targets [18,19]. We extend our previous study herein and show that primary neuronal cells from mouse superior cervical ganglion (SCG) cultured in 3D polymer scaffolds model freshly dissected tissue with respect to VGCC function. Furthermore, our results suggest a role for membrane architecture in higher VGCC signal, in response to high K^+ depolarization observed in 2D cultures. Overall, our results support the view that 2D/3D cultured cells cytoskeleton/plasma membrane architecture differences are worthy of further exploration in efforts to better understand 3D cultured cells' better emulation of the *in vivo* function.

3.3 Materials and Methods

3.3.1 Ethics Statement

All the animals received the standard care in compliance with the Animal Welfare Act and the recommendation in the Guide for the Care and Use of Laboratory Animals of the National Institutes of Health. The protocol was approved by the Committee on the Ethics of Animal Experiments of the University of Georgia and was under the University of Georgia Animal Usage Proposal (Permit Number: A2009 3-048).

3.3.2 Scaffold fabrication

3D Scaffolds were fabricated by the gaseous salt leaching method [20] and have been previously described in detail [15]**.** Briefly, a highly viscous polymer solution was prepared by dissolving polymer particles in chloroform. Ammonium bicarbonate salt particles were added to the polymer solution and mixed thoroughly. Sieved ammonium bicarbonate particles in the range of 40-60 μm in diameter were used. Salt particles in this size range generated pores with an average diameter range of 60-100 μm. The salt:polymer ratio of 20:1 was chosen to achieve the

optimal balance between light transmission and mechanical strength. The paste mixture of polymer/salt/solvent was cast onto a glass Petri dish. After chloroform was partially evaporated under atmospheric pressure, the semi-solidified samples were immersed into boiling water until no gas bubbles were generated. The samples were vacuum-dried for 24 h and kept in desiccators until use. Before cell plating, the scaffolds were pre-wetted and sterilized in 70% ethanol under UV light, over night, and then rinsed with PBS three times. The scaffolds were coated with collagen by incubating in 0.1 mg/ml collagen solution for 2 h, followed by air drying at room temperature.

3.3.3 Scanning Electron Microscopy (SEM)

Cells in scaffolds were fixed with 2% glutaraldehyde in 0.1 M sodium cacodylate buffer (pH 7.2) for 1 h and then rinsed in cacodylate buffer three times (15 min each). This was followed by post-fixing with 1% OsO_4 in 0.1 M sodium cacodylate buffer for 1 h and rinsing in cacodylate buffer three times (5 min each). The samples were then dehydrated in 35, 50, 70, 80, 95 and 100% ethanol successively for 10 min each and dried in a SAMDRI-780A critical point drier (Tousimis Research Corporation, MD). Scaffolds were sputter-coated with gold for 60 s to achieve a thickness of about 15.3 nm. SEM images were captured with LEO 982 scanning electron microscope (LEO Electronenmikroskopie GmbH Korporation, Germany) with an acceleration voltage of 4 kV. A similar protocol was followed for scaffold samples without cells, with the exception that the preparation started with sputter coating.

3.3.4 SCG cell harvesting and plating

Neonatal mice (CD1) were used as the sources of SCG nerve cells. A mice SCG dissection protocol described elsewhere [21] was followed. All the animals received the standard care in compliance with the Animal Welfare Act and the recommendation in the Guide for the

Care and Use of Laboratory Animals of the National Institutes of Health. The protocol was approved by the Committee on the Ethics of Animal Experiments of the University of Georgia and was under the University of Georgia Animal Usage Proposal (Permit Number: A2009 3-048). After dissection, the ganglions were enzymatically digested in 1 mg/ml type IA collagenase for 1 hour. After gentle mechanical disruption with a Pasteur pipette, dissociated cells and cell chunks were plated into glass bottom Petri dishes (MatTek, MD) and polymer scaffolds, both of which were coated with 0.1 mg/ml type I collagen. On the average, cells from two ganglions were plated to one dish or scaffold. Cells were maintained in Eagle's Minimum Essential Medium supplemented with 2 mM L-Glutamine, 1 mM Sodium Bicarbonate, 10% FBS, and 50 ng/ml NGF. The cells were incubated at 37 °C in a 10% CO_2 humidified atmosphere. To prepare intact SCG tissue samples for staining, the outer sheath covering the freshly dissected ganglions was broken with fine forceps.

3.3.5 Live cell imaging and morphological studies

SCG cell morphology was observed by calcein acetoxymethyl ester (AM) (Biotium, Hayward, CA) staining. The non-fluorescent cell-permeant calcein AM is converted to non-permeable intensely fluorescent calcein by the intracellular esterase thus are widely utilized to stain living cells and their extensions [22]. Cells were washed with 2 mL PBS, three to five times (5 min each) then covered with sufficient amount of 2-μM calcein AM in PBS. After 30 min incubation at room temperature, the staining solution was replaced with fresh PBS, followed by aAnother 30 min incubation complete esterification of the intracellular calcein AM. Confocal images were obtained by 488 nm argon laser excitation and recorded through a 515 nm long Pass filter**.**

3.3.6 VGCC functionality characterization

Calcium imaging experiments were performed after 2-day and 7-day incubation for both the 2D and 3D cultured cell samples. To best represent the *in vivo* condition, intact SCG tissues were stained soon after the dissection, followed by the calcium imaging. The time between dissection and recording was approximately one hour. Intracellular calcium dynamics were recorded using the membrane permeable dye Calcium Green-1 AM coupled with confocal laser scanning microscopy. 2D cultured cells on the Petri dish were washed twice with HEPES buffered saline (HBS) and loaded with 5 μM dye in 1 ml of HBS containing 3% FBS and 0.02% Pluronic F-127. The Petri dishes were incubated at 37 °C for 30 min. After dye loading, cells were rinsed with HBS twice and returned to the incubator for another 30 min to allow complete dye de-esterification. A similar protocol was followed for 3D and intact SCG tissue samples. However, the dye concentration was increased to 10 μM to facilitate dye loading. Both the scaffold and intact SCG tissue were held in place by placing a small coverslip on top during the calcium imaging. Calcium Green-1 was excited with 488 nm argon laser and the fluorescence intensity was recorded through a 515 nm long Pass filter. Images were taken every 3 seconds. Cells were depolarized by adding 100 μl of high potassium buffer to a final concentration of 50 mM K^+ while imaging. The intracellular calcium dynamics were reflected by changes in intracellular Calcium Green-1 fluorescence intensity.

3.3.7 Microarray gene expression analysis

Total RNA was isolated from all samples using Qiagen RNeasy Kits (Qiagen,Valencia, CA) according to the manufacturer's standard protocol. The quantity of mRNA isolated from each sample was determined using the adsorption of each solution at 260 nm and 280 nm. The purity of each sample was monitored using the A260/A280 ratio. A ratio of 1.8-2.1 was

considered a “clean” sample and could be used in microarray experiments. Samples were kept on dry ice and sent to the Affymetrix Core Facility at the Medical College of Georgia (MCG) for Mouse Genome 430 2.0 array Expression Analysis (Affymetrix, Santa Clara, CA). The raw data has been deposited in MIAME compliant GEO database (Accession No. GSE30498). The expression value of each gene was obtained by Expression Console (Affymetrix) with the Robust Multichip Average (RMA) algorithm which consists of three steps: a background adjustment, quantile normalization and finally summarization. RMA was chosen because it is one of the most widely used algorithms and has been shown to be more sensitive than other methods. Genes within the scope of this study were manually picked. Student’s t tests and ANOVA tests were carried out to compare the expression differences between 2D, 3D and SCG tissue samples.

3.3.8 Immuno-fluorescence staining

Rabbit polyclonal Anti-Calcium channel L type DHPR alpha 2 subunit antibody (ab80990) and sheep polyclonal caveolin-1 antibody (ab81397) were purchased from Abcam (Cambridge, MA). Actin Cytoskeleton/Focal Adhesion Staining Kit was purchased from Millipore (Billerica, MA). Secondary antibodies (Alexa Fluor 488 chicken anti-rabbit and Alexa Fluor 488 donkey anti-sheep) were purchased from Invitrogen (Carlsbad, CA). Normal chicken serum was purchased from Zymed Laboratories, CA. For immuno-fluorescence staining, cells were rinsed once with phosphate-buffered saline (PBS), fixed with 4% paraformaldehye in PBS (30 min), washed with PBS, treated with 0.5% Triton X-100 (5 min) for membrane permeablization. To double stain L-type VGCC and caveolin-1, cells were washed with PBS, blocked with normal chicken serum (2% diluted with PBS/0.3% Tween-20) for 30 min at room temperature, washed with PBS (3 times, 5 min per wash), incubated overnight with primary antibodies (1:100), washed with PBS (3 times, 5 min per wash) followed by incubation for 1 h

with the secondary antibodies (1:500), washed with PBS (3 times, 5 min per wash), and then loaded with DAPI (1:5000) for 5 min at room temperature. To double stain vinculin with F-actin, TRITC-conjugated Phalloidin from Actin Cytoskeleton/Focal Adhesion Staining Kit was incubated together with secondary antibody for 1 h. After PBS wash, cells were ready for microscopy observation. Confocal imaging was performed with a Leica TCS SP2 microscope. Routine negative controls for staining were performed.

3.3.9 Statistical analysis

Neurite length, soma section area, soma section roundness and calcium response magnitude values were expressed as mean ± standard deviation (S.D.). The unpaired Student's t-test was used to compare the means of two samples. The *p* values are indicated in the text and decisions regarding significant difference were based on level of 0.05.

3.4 Results

3.4.1 SCG cell-scaffold interaction

SCG cells were found ideal for this study because of the ease with which freshly dissected ganglion tissue can be obtained to serve as a more realistic *in vivo* surrogate as opposed to neural spheres used in our previous study [15]. Also, we used the CD1 mouse strain as the source of SCG cells and tissue because this strain has been extensively used in toxicological and functional studies as an acceptable model for human medicine applications.

Mouse (SCG) cells were harvested and cultured on the 3D polymer scaffolds (made from poly-l-lactic-acid (PLLA) or polystyrene (PS)) and 2D substrates (glass or polystyrene) [11]. All 3D and 2D substrates were coated with 0.1 mg/ml Type I collagen from rat tail to rule out any differences from materials. The architecture of scaffolds generated from PLLA or PS were identical and had similar impact on cells (data not shown). However, while PLLA scaffolds are

suitable for *in vivo* studies that require scaffold biodegradation, PS scaffolds practically do not biodegrade and are only suitable for *in vitro* studies where degradation is not a concern. In this study, porous polymer scaffolds with equivalent average pore sizes of 60-100 μm in diameter were fabricated. This pore size range was empirically found to be ideal for mouse SCG cells, which are approximately 10 μm in diameter. Cell intrusion (deep penetration deep into pores) requires larger pores and pore openings, however, if too large, the pore would have no difference from the 2D situation and would make cell-matrix interaction identical to that found on flat surfaces [23]. The porosity of resulting scaffolds ranged between 88.4% and 95.6%, and the pores were inter-connected so that cells can travel between pores through channels and/or form neurites connections between two adjacent cell aggregates. As discussed in Cheng et al. [23], we used a polymer to salt ratio of 1: 20 to achieve the optimal light transmittance (80% in wet condition) while maintaining adequate mechanical strength, which is higher than the maximum possible force a typical fluid transfer workstation (e.g. FLEXstation, Molecular Devices, Sunnyvale, CA) could generate (0.11 mN). The detailed physical characteristics of those polymer scaffolds have been reported previously by Cheng et al. [23].

Cell viability and spatial distribution was examined by calcein AM live cell staining, coupled with confocal microscopy, on day 7 after plating. Figure 3.1a shows calcein stained SCG cells cultured on 2D flat surface. Figure 3. 1b shows the maximal projection of thirty images obtained by z-axis optical scanning and different colors were assigned according to the depth of the obtained image (color index shown as inset of Figure 3. 1b). Cells were viable with well developed neurites in both 2D and 3D cultured conditions. In 3D scaffolds SCG cells intruded as deep as 150 μm from the top of the scaffold, which further confirmed that the pores inside the scaffolds were interconnected and had formed open channels to allow cell migration in

all directions (Figure 3.1b). SEM was further used to study the morphology of polymer scaffolds and 3D cultured SCG cells. As shown in Figure 3. 1c, polymer (PLLA) scaffolds have interconnected holes that can host cell for growth and multicellular aggregates formation. SEM images also showed that cells formed multi-cellular clusters inside the pores of the scaffolds (Figure 3.1d) and had developed neurite connections between adjacent cells (Figure 3.1e).

3.4.2 3D cultured cells morphologically resemble cells from freshly dissected SCG tissue

Cell morphology was investigated with confocal images of calcein stained cells taken with higher magnification (60X) oil lens and quantitative cell morphology measurements were processed by SimplePCI 2000 software (Figure 3.2a-e). Calcein is a cytoplasmic marker which give a clear outline of intact cells thus can be utilized for cell morphological observation [22,24]. Detailed results are presented in Table 3.1. We used neurite density (the number of neurites per cell), neurite length, cell soma section area & roundness to characterize the cell morphology. Roundness, characterized by the circularity shape factor, calculated as: $4*Pi*area/perimeter^2$. Fig 2a and 2b are SCG cells cultured on 2D surfaces, two and seven days after plating, respectively, while Fig 2c and 2d are the same cells in 3D polymer scaffolds with same number of days in culture. As shown, on day 2 after plating, a few cells on 3D scaffolds had already developed short neurites and most cells were still round (Figure 3. 2c). Compared to the cells on 2D substrates (Figure 3. 2a), 3D cell neurite density was lower (0.7 vs. 2.4), and the neurites were shorter (10.9±3.2 μm vs. 38.9±17.7 μm, p=7.88e-7). In comparison to that on 2D substrates, cells on 3D scaffolds spread poorly with smaller cell soma section area (90.0±22.3 μm^2 v.s.149.8±59.3 μm^2, p=4.56e-6) and larger soma section roundness (0.81± 0.05 vs. 0.51±0.11, p=1.16e-15). In addition, a number of cells were found forming clusters which was not observed in 2D cells. On day 7 after plating, more neurites were observed among both 2D and 3D cells (Figure 3. 2b and

2d), with increased neurite lengths of 63.6±36.1 μm (p=5.75e-10) and 25.2±13.8 μm (p=0.001) respectively. The spreading condition of cells on 2D remained unchanged with comparable cell soma section area and roundness to the day 2 cells. However, the cells on 3D scaffolds were more spread with larger soma section area (144.5±56.9 μm^2, p=1.03e-4) and had lower roundness (0.64±0.15, p=7.89e-6). The significant morphological difference between 2D and 3D cells observed on day 2 still existed among day 7 cells.

Generally cells in 3D scaffolds developed shorter neurites and were less spread than the 2D cultured cells. The 3D cultured cell morphology more closely mimicked the cell morphology found in freshly dissected intact SCG tissue (Figure 3. 2i). The above differences between 2D versus 3D cultured cells suggested that polymer scaffolds can promotes cell attachment and differentiation that differs from what was observed with 2D substrates, which is consistent with conclusions from previous work [6,7,15,25].

3.4.3 VGCC functionality

Previous studies done by our group and others have shown differences in calcium currents between intact and dissociated adult mouse SCG cells [26], and difference in VGCC function between 2D and 3D cultured human neuroblastoma cells or differentiated neural progenitor cells in collagen hydrogels, cytodex microbead scaffolds and polymer scaffolds [6,7,15,25]**.** We reasoned that comparing VGCC functionality as reflected by calcium transient in response to high K^+ (50 mM) depolarization is a convenient first step in cornfirming 3D and *in vivo* similarities. The time course intracellular calcium concentration was recorded as fluorescence of the membrane permeable dye Calcium Green-1 AM with a confocal laser scanning microscope. Figure 3.2 (f-q) shows the typical time course changes in Calcium Green-1 AM fluorescence intensity under different conditions. Fig 2f, 2h and 2j are responsive cells upon

stimulation with high K^+ on 2D substrates (f), 3D scaffolds (h) and intact SCG tissue (j). A cell was considered responsive only when it showed an increase in fluorescence intensity of 15% or higher over the basal fluorescence intensity level. The magnitudes of the response from each cell were expressed as a peak fractional increase over basal fluorescence intensity (F-Fo)/Fo, where F is the peak fluorescence intensity and Fo is the basal fluorescence intensity. The percentage and magnitude of cellular VGCC responses to high K^+ depolarization within cells on 2D substrates, 3D scaffolds and intact SCG tissues are summarized in Figure 3. 3.

On day 2 after plating, 62.3% and 47.9% of cells on 2D substrates and 3D scaffolds respectively, were responsive to high K^+ HBS buffer. The 3D cultured cells' response magnitude was 0.26±0.08, which is much lower than the 2D cultured cells' response magnitude of 0.75±0.54 ($p=0.0012$). On day 7 after plating, the percentage of responsive 2D cultured cells increased to 100% as all the 28 cells measured had response to high K^+ buffer, with the response magnitude increasing to 0.84±0.32, although the difference was not statistically significant ($p=0.43$). The percentage of responsive cells on 3D scaffolds increased to 75.8% with the response magnitude increasing to 0.34±0.14 ($p=0.01$). As with results on day 2, the response magnitude of cells on 3D scaffolds on day 7 was still significantly lower than that of cells on 2D substrates ($p= 7.40e-7$). It was interesting to observe that both the response magnitudes of 3D cells on day 2 and day 7 were not significantly different from that of cells in intact SCG tissue, which was 0.30±0.11 from 25 responsive cells from a pool of 41 cells (p=0.88 and 0.80 respectively). Assuming that the cells in intact SCG tissue were not very different from cells *in vivo*, this observation provides evidence in support of the speculation that many cellular responses observed in 2D are probably exaggerations of *in vivo* function [27]. We are comfortable with the above assumption for several reasons. First, we made every effort to

minimize the time between dissection and recording (below 60 min) and we maintained the tissue under physiological conditions (HEPES Buffer Saline with 3% Fetal Bovine Serum). Second, our approach is similar to investigations that utilize brain slices [28] and other peripheral nerve tissues [20], where *in vivo* similarity is well accepted.

It is well known that there are different types of VGCCs which are structurally homologous [29,30]. Among those VGCCs, the dihydropyridine (DHP)-sensitive L-type channels and the currents caused by L-type VGCC have been thoroughly investigated and several related reviews have been published [31,32,33]. The high affinity of DHPs for the channels is a powerful test to differentiate L-type VGCC from non-L-type VGCC [34]. It has been shown that calcium transient induced by high potassium depolarization was mainly through L-type VGCC in neuronal cells [35,36,37]. We utilized a DPH class L-type VGCC blocker, Amlodipne besylate, to see if L-type VGCC was indeed the major player in our system. Amlodipne besylate is a well developed L-type calcium channel blocker that is marketed as an anti-hypertensive drug and for the treatment of angina. Amlodipne besylate has low cyto-toxicity; we have observed no cell death after treatment (5 μM for 90 minutes). Treated cells were depolarized with high K^+ buffer and intracellular calcium concentration changes were followed with Calcium-Green florescence. After treated with the inhibitor, no cells were observed to be responsive, with little or no fluorescence increase observed (Fig 2g, 2i and 2q), confirming that the calcium transient observed was indeed mainly due to L-type VGCC gating.

3.4.5 VGCC mRNA expression and protein localization

To explore what could possibly be the reason of the lower calcium transient in 3D cultured cells and tissue, we examined the L-type calcium channel mRNA expression level with microarray gene chips. VGCC are formed as a complex from several different subunits: α_1, $\alpha_2\delta$,

$\beta_{1\text{-}4}$, and $\gamma_{1\text{-}8}$. The α_1 subunit forms the ion conducting pore while the associated subunits have several functions including modulation of gating. α_1 subunit is also the major subunit that differentiates VGCC types. For L-type VGCC, there are four different α_1 subunits, i.e. $Ca_v1.1$ (*CACNA1S*), $Ca_v1.2$ (*CACNA1C*), $Ca_v1.3$ (*CACNA1D*) and $Ca_v1.4$ (*CACNA1F*). Surprisingly we did not observe significant differences between 2D and 3D cultured SCG cells for all four α_1 subunits (Figure 3. 4a). The mRNA levels for most of α_1 subunits from SCG did not differ from the cultured cell samples either, with only $Ca_v1.1$ (*CACNA1S*) slightly upregulated (significant at 0.05 level). Since L-type voltage gated calcium channel is composed of four different subunits, the expression of other subunits can be also very important in determining the expression of the whole channel. Thus we also examined the expression of $\alpha_2\delta$ (CACNA2D2), β (four family members $\beta1$ to $\beta4$ coded as CACNB1 to CACNB4) and γ subunits (eight members, $\gamma1$to $\gamma8$ coded as CACNG1 to CACNG8). Again, we did not observe any significant difference in mRNA expression for those subunits (Figure 3.4b).

Although mRNA expression level of all L-type VGCC subunits were not different between 2D and 3D cultured cells, this finding could not rule out the possibility that the VGCC functionality differences are due to channel expression difference. To study if the voltage gated channel protein had been translated from mRNA and how the proteins are localized, we stained the α_1 subunits of L-type VGCC (Figure 3.5a-c) with antibodies. We observed that L-type calcium channel has distinctive localization in 2D cultured cells when compare to 3D and tissue sample. In 2D cultured SCG cells, L-type calcium channels are clustered together, forming bright punctuated morphology (Figure 3.5a), while in 3D and tissue SCG cells, they are diffused all over the plasma membrane (Figure 3.5b&c), suggesting differences in calcium channel signaling platform architecture.

3.4.6 Cell membrane architecture

Ca^{2+} signaling proteins are known to be concentrated in lipid rafts/caveolar microdomains [38,39,40,41,42], which are dynamic flask shaped regions of cell membranes enriched with cholesterol and sphingolipid [43]. These microdomains appear to function as unique signal transduction platforms which tend to enrich certain signaling molecules while excluding others [43,44,45,46]. Since lipid raft can concentrate signaling related proteins and facilitate the interaction, they provide a favorable environment for a number of signaling transductions [46]. More importantly, Ca^{2+} signaling has been shown to be initiated from lipid raft microdomains [38], in which Ca^{2+} channels and their regulatory proteins are clustered for regulation of Ca^{2+} mediated cellular function [46,47,48,49,50]. To examine whether in 2D cultured SCG cells, L-type calcium channels are concentrated more in lipid raft area that can facilitate calcium signaling, we double stained the cells with caveolin-1 antibody and L-type VGCC (Fig 5a-f). Caveolin-1 is a caveolar protein and has been widely used as a caveolar lipid raft marker [51,52]. The colocalization of L-type calcium channel and caveolin-1 was demonstrated by superimpose L-type VGCC channel confocal images over caveolin-1 confocal images (Fig 5.g-i). The yellow color indicates the presence of both VGCC protein and caveolin-1. We observed that caveolin-1 spatial distribution was different between 2D and 3D cultures. In 2D cultured SCG cells, caveolin-1 had a punctuated distribution, while in 3D cultures and tissue it had a more diffused distribution. A similar differential protein spatial distribution pattern (punctuated versus diffused) between 2D and 3D samples has been observed with other proteins, e.g. focal adhesion kinase (FAK) [15,53]. Integrins stimulate the activation extracellular signal-regulated kinase (ERK) through multiple signal transduction pathways. For example, ERK can be activated through caveolin and several other moieties. Another interesting observation was

that caveolin-1 had a stronger signal at the edge of the microtissues formed in 3D scaffolds (Fig 5e). From Fig 5 g-i, almost all the red color in 2D samples are well superimposed with green, which indicating that almost all the VGCC proteins are located in caveolar lipid raft areas. However, in 3D and tissue samples some red color outside the green area is observable, indicating that some of the VGCC proteins are outside the caveolar lipid raft area. These results suggest that high calcium signals from 2D samples may result from VGCC proteins being well clustered in the lipid raft area in which they interact with other proteins that enhance their response to high K^+ depolarization.

We reasoned that if there were differences in cell membrane architecture, similar differences should be reflected in the cells' cytoskeleton organization [54], especially since many 3D cell culture studies have shown altered cytoskeletal protein distribution [53]. We used the immunostaining technique to study the distribution of the major cytoskeleton protein F-actin and its associated protein vinculin. From Figure 3.5j, 2D cultured SCG cells exhibited stretched bundle-shaped actin filaments while 3D cultured SCG and tissue SCG cells exhibited more short diffused actin filaments (Figure 3.5k&l), consistent with our reasoning.

3.5 Discussion

Scaffold curvature radius less than 100 μm compromises cell spreading and attachment along the bending direction and form the basis of contact guidance along the cylindrical substrata [25,55]. In our case, the pore curvature radius falls into the range to produce topographical effects. Another important feature is the inter-connected pores, which can host cell clusters formed by the cells seeded into the same pore. Cells in multi-cellular organizations significantly differ from cells on flat 2D surfaces [56].

In this study, we found that the cell morphology and VGCC function from cells in 3D scaffolds more closely modeled intact SCG tissues in comparison to cells on 2D surfaces. Similar 3D effects have been observed in other 3D cell culture studies. Wang and Good reported that culturing PC 12 neuron–like cells and SHSY-5Y neuroblastoma cells in a rotating bioreactor resulted in formations of cell clusters and inhibition of neural extensions [57]. Wu and others observed a similar phenomenon from SHSY-5Y cells cultured on Cytodex 3 mircobead scaffolds [25]. Furthermore, Webb and others found changes in extra-cellular matrix (ECM)-related gene expression consistent with decreasing cell migration and increasing tissue formation when fibroblast cells were transferred from 2D to 3D culture on porous Tecoflex-derived biomaterials [58], which is similar to the polymer scaffolds we used in this study.

Intracellular calcium transient in response to high potassium depolarization was identical between 3D cultured and intact SCG tissue cells, but significantly different between 3D and 2D cultured cells. The intracellular calcium transient caused by high potassium depolarization was almost fully blocked by L-type voltage gated channel blocker. Among all the types of VGCCs, L-type VGCCs are known to couple depolarization of the plasma membrane to a wide range of cellular responses [59]. Ca^{2+} entry via L-type VGCCs triggers activation of the Ryanodine Receptor Type 2 (RyR_2) in cardiac cells and initiates Ca^{2+}-induced Ca^{2+}-release [60], which greatly amplifies the cellular calcium transient required for effective initiation of contraction [59]. The similar association of L-type VGCCs and RyR_2 was also found in rat hippocampus neurons [61]. By blocking L-type VGCCs, we blocked the amplification of cellular calcium transient through Ca^{2+}-induced Ca^{2+}-release. In neuronal cells, L-type VGCCs were found mainly in cell bodies and proximal dendrites [62], while other types of VGCCs such as P type and N type are more concentrated in nerve terminals and dendrites. In our experiments, we focused our

observation on cell bodies only. This may be another reason we observed little or no cellular calcium transient after L-type VGCCs inhibition.

Although mRNA of L-type VGCC subunits were not differently expressed by 3D and 2D cultured cells, immunostaining of L-type VGCC shows that the distribution of VGCC were different between 3D and 2D cultured cells but similar between 3D cultured cells and tissue samples. L-type VGCCs class C alpha subunit (CaV1.2) and class D alpha subunit (CaV1.3) were both found to be concentrated at the cell bodies and proximal dendrites in rat hippocampus and cerebral cortex neurons [62]. These two classes of subunit were observed to have very different distribution patterns, with class D more diffused and class C punctuated. immunofluorescence staining of hippocampal sections of 2-month-old APP−/− and WT mice show that CaV1.2 has a more diffused distribution pattern [63]. We speculated that the different pattern of calcium channel distribution may be related with their functions. Our results provide evidence in support of the hypothesis that some cellular responses under traditional 2D environment are exaggerated [27].

There are no published studies specifically designed to shed light on the mechanisms behind the "2D exaggeration hypothesis." In terms of VGCC activity, the results presented here point to spatial channel distribution and more specifically punctuated distribution (2D) versus diffused (3D) pattern, which led us to suspect the presence of lipid rafts playing a role in exaggerating the 2D calcium signals. The parallel punctuated/diffuse distribution of caveolin-1 (caveolar lipid raft marker) was consistent with our speculation, pointing to fundamental differences in membrane architecture between 2D and 3D /tissue preparations.

From Fig 5 (e), a higher caveolin-1 protein signal was observed on the edge of microtissues formed in 3D scaffolds. Cells at the edge of the microtissue are typically in contact

with the polymer scaffold's rigid surface. It is well known that cells in contact with rigid surfaces tend to adapt to the microenvironment and exhibit a more rigid architecture, measured in terms of higher Young's modulus. One of the most abundant composition of caveolae lipid rafts are sphingolipids containing long, largely saturated acyl chains, which pack more tightly together [64,65]. Thus lipid raft generally are more compact and rigid. In *in vivo* situation, all cells are in contact with each other and have lower Young's modulus compared to 2D cells cultured on rigid surfaces. It is reasonable to suggest that 3D cultured cells model *in vivo* conditions better because, with the exception of cells on microtissue aggregate periphery in contact with rigid surfaces, the majority of cells inside the microtissue aggregate are in contact with neighboring soft cells as the case is *in vivo*.

Through use of freshly dissected SCG cells, we have shown that 3D cultured cells emulate the *in vivo* condition, with respect to VGCC function, better than 2D cultured cells. The explanation consistent with our findings is differences in membrane architecture. The practical issue that needs addressing is the meaning of our findings in the context of pre-clinical high throughput screening (HTS) of compounds with 2D versus 3D cell-based assays. In the design and validation of HTS assays, an assessment of the screening data, by measurements such as standard deviation (SD) or coefficient of variation (CV), is critical in determining whether an assay can identify hits with confidence. Zhang et al. [66] introduced the Z'-factor, a simple statistical dimensionless number that evaluates HTS assay quality with respect to identifying hits with a high degree of confidence.

$$Z' = 1 - [(3\sigma_{c+} + 3\sigma_{c-})/(|\mu_{c+} - \mu_{c-}|)]$$

Where σ_{c+} and σ_{c-} denote signal standard deviations of positive and negative controls, respectively, and μ_{c+} and μ_{c-} denote signal means of the positive and negative controls, respectively.

Use of Z'-factor is now an accepted industry standard. If the Z'-factor is sufficiently large (>0) at the defined conditions, then the assay can be used in HTS. Typically, a Z'-factor equal or greater than 0.5 characterizes a robust assay for HTS. We have recently used a calcium assay in a 2D/3D comparative study of the type of scaffolds used in this study and a few commercially available 3D plates. As expected, 2D plates exhibited statistically higher Z'-factor (0.79), but all the 3D plates, including one from our laboratory, supported robust assays with all the Z'-factors higher than 0.5 [67]. These results confirmed the expectation that in comparison to 2D, 3D assays are more likely to yield high σ_{c+} and lower μ_{c+} values, resulting in comparatively lower Z'-factors for 3D assays. If a physiologically more relevant 3D cell-based assay exhibit a lower Z'-factor, the physiologically less relevant 2D cell-based assay counterpart is more likely to yield false positive hits. Conversely, more physiologically relevant 3D cell-based assay would be more effective in eliminating false positive hits and as such improve the overall yield from drug screening campaigns. Given that many drugs achieve their efficacy by interacting with membrane-integrated ion channels or their associated receptor-ligand behavior [68], this result brings attention to the potential importance of introducing three dimensional cell-based assays in drug discovery programs.

This study constitutes the first step toward comparing 3D cultures to their *in vivo* counterparts within the cell-based assay HTS context. The results support the following conclusions.

1. Neonatal mouse SCG cells cultured in 3D PLLA or PS scaffolds more closely mimic the cells in intact SCG tissue than those cultures on 2D substrates with respect to high K+-mediated calcium transient.

2. The exaggerated VGCC function from 2D cultured SCG cells may partly be explained by differences in membrane architecture, characterized by uniquely organized caveolar lipid rafts and the cytoskeleton.

3.6 Acknowledgements

We thank Mr. Rahul Singh and Drs. Lina Wang and Dr. Charles Keith for technical assistance. This work was partly supported by NSF (0304340) and UGA Engineering Grants.

3.7 References

1. Mueller-Klieser W (1997) Three-dimensional cell cultures: from molecular mechanisms to clinical applications. Am J Physiol 273: C1109-1123.

2. Weaver VM, Petersen OW, Wang F, Larabell CA, Briand P, et al. (1997) Reversion of the malignant phenotype of human breast cells in three-dimensional culture and in vivo by integrin blocking antibodies. J Cell Biol 137: 231-245.

3. Abbott A (2003) Cell culture: biology's new dimension. Nature 424: 870-872.

4. Jessup JM, Goodwin TJ, Spaulding G (1993) Prospects for use of microgravity-based bioreactors to study three-dimensional host-tumor interactions in human neoplasia. J Cell Biochem 51: 290-300.

5. Lewis ML, Moriarity, D.M., and Campbell, P.S. (1993) Use of microgravity bioreactors for development of an in vitro rat salivary gland cell culture model. Journal Cellular Biochemistry 51: 265-273.

6. Desai A, Kisaalita WS, Keith C, Wu ZZ (2006) Human neuroblastoma (SH-SY5Y) cell culture and differentiation in 3-D collagen hydrogels for cell-based biosensing. Biosens Bioelectron 21: 1483-1492.

7. Mao C, Kisaalita WS (2004) Characterization of 3-D collagen hydrogels for functional cell-based biosensing. Biosens Bioelectron 19: 1075-1088.

8. O'Connor SM, Andreadis JD, Shaffer KM, Ma W, Pancrazio JJ, et al. (2000) Immobilization of neural cells in three-dimensional matrices for biosensor applications. Biosensors and Bioelectronics 14: 871-881.

9. Albrecht DR, Underhill GH, Wassermann TB, Sah RL, Bhatia SN (2006) Probing the role of multicellular organization in three-dimensional microenvironments. Nat Methods 3: 369-375.
10. Freed LE (1994) Biodegradable polymer scaffolds for tissue engineering. Nature Biotechnology 12: 689-693.

11. Mikos AG, Sarakinos G, Leite SM, Vacanti JP, Langer R (1993) Laminated three-dimensional biodegradable foams for use in tissue engineering. Biomaterials 14: 323-330.

12. Zhang S (2004) Beyond the Petri dish. Nat Biotechnol 22: 151-152.

13. Powers MJ, Domansky K, Kaazempur-Mofrad MR, Kalezi A, Capitano A, et al. (2002) A microfabricated array bioreactor for perfused 3D liver culture. Biotechnol Bioeng 78: 257-269.

14. Freyman TM, Yannas IV, Gibson LJ (2001) Cellular materials as porous scaffolds for tissue engineering. Progress in material science 46: 273-282.

15. Cheng K, Lai Y, Kisaalita WS (2008) Three-dimensional polymer scaffolds for high throughput cell-based assay systems. Biomaterials 29: 2802-2812.

16. Wang L, Kisaalita WS (2010) Characterization of micropatterned nanofibrous scaffolds for neural network activity readout for high-throughput screening. J Biomed Mater Res B Appl Biomater 94: 238-249.

17. Kisaalita WS (2009) 3-D Cell-Based Biosensors in Drug Discovery Programs: Taylor and Francis, 2009. 386 p.

18. Cosford ND, Meinke PT, Stauderman KA, Hess SD (2002) Recent advances in the modulation of voltage-gated ion channels for the treatment of epilepsy. Curr Drug Targets CNS Neurol Disord 1: 81-104.

19. Triggle DJ, Gopalakrishnan M, Rampe D, Zheng W (2006) Voltage-Gated Ion Channels as Drug Targets; Mannhold R, Kubinyi H, Folkers G, editors: Wiley-VCH, 2006. 479 p.

20. Nam YS, Yoon JJ, Park TG (2000) A novel fabrication method of macroporous biodegradable polymer scaffolds using gas foaming salt as a porogen additive. J Biomed Mater Res 53: 1-7.

21. Mains RE, Patterson PH (1973) Primary cultures of dissociated sympathetic neurons. I. Establishment of long-term growth in culture and studies of differentiated properties. J Cell Biol 59: 329-345.

22. Belletti S, Orlandini G, Vettori MV, Mutti A, Uggeri J, et al. (2002) Time course assessment of methylmercury effects on C6 glioma cells: submicromolar concentrations induce oxidative DNA damage and apoptosis. J Neurosci Res 70: 703-711.

23. Cheng K, Lai Y, Kisaalita WS (2008) Three-dimensional polymer scaffolds for high throughput cell-based assay systems. Biomaterials 29: 2802-2812.

24. Wu ZZ, Zhao Y, Kisaalita WS (2006) Interfacing SH-SY5Y human neuroblastoma cells with SU-8 microstructures. Colloids Surf B Biointerfaces 52: 14-21.
25. Wu ZZ, Zhao YP, Kisaalita WS (2006) A packed Cytodex microbead array for three-dimensional cell-based biosensing. Biosensors and Bioelectronics 22: 685-693.

26. Martinez-Pinna J, Lamas JA, Gallego R (2002) Calcium current components in intact and dissociated adult mouse sympathetic neurons. Brain Res 951: 227-236.

27. Cukierman E, Pankov R, Stevens DR, Yamada KM (2001) Taking cell-matrix adhesions to the third dimension. Science 294: 1708-1712.

28. Saino T, Satoh Y (2004) Application of real-time confocal laser scanning microscopy to observe living cells in tissue specimens. J Electron Microsc (Tokyo) 53: 49-56.

29. Dolphin AC (2006) A short history of voltage-gated calcium channels. Br J Pharmacol 147 Suppl 1: S56-62.

30. Yamakage M, Namiki A (2002) Calcium channels--basic aspects of their structure, function and gene encoding; anesthetic action on the channels--a review. Can J Anaesth 49: 151-164.

31. Dolphin AC (1999) L-type calcium channel modulation. Adv Second Messenger Phosphoprotein Res 33: 153-177.

32. Benitah JP, Alvarez JL, Gomez AM (2010) L-type Ca(2+) current in ventricular cardiomyocytes. J Mol Cell Cardiol 48: 26-36.

33. Lipscombe D, Helton TD, Xu W (2004) L-type calcium channels: the low down. J Neurophysiol 92: 2633-2641.

34. Ertel E, Godfraind T (2004) Calcium channel blockers and calcium channels. In: Godfraind T, editor. Calcium Channel Blockers: Birkhäuser, 2004. P26-28

35. Meier K, Knepel W, Schofl C (1988) Potassium depolarization elevates cytosolic free calcium concentration in rat anterior pituitary cells through 1,4-dihydropyridine-sensitive, omega-conotoxin-insensitive calcium channels. Endocrinology 122: 2764-2770.

36. Joshi DC, Singh M, Krishnamurthy K, Joshi PG, Joshi NB (2011) AMPA induced Ca(2+) influx in motor neurons occurs through voltage gated Ca(2+) channel and Ca(2+) permeable AMPA receptor. Neurochem Int. In Press

37. Shitaka Y, Matsuki N, Saito H, Katsuki H (1996) Basic fibroblast growth factor increases functional L-type Ca2+ channels in fetal rat hippocampal neurons: implications for neurite morphogenesis in vitro. J Neurosci 16: 6476-6489.

38. Lohn M, Furstenau M, Sagach V, Elger M, Schulze W, et al. (2000) Ignition of calcium sparks in arterial and cardiac muscle through caveolae. Circ Res 87: 1034-1039.

39. O'Connell KM, Martens JR, Tamkun MM (2004) Localization of ion channels to lipid Raft domains within the cardiovascular system. Trends Cardiovasc Med 14: 37-42.

40. Berridge MJ (2006) Calcium microdomains: organization and function. Cell Calcium 40: 405-412.

41. Taverna E, Saba E, Rowe J, Francolini M, Clementi F, et al. (2004) Role of lipid microdomains in P/Q-type calcium channel (Cav2.1) clustering and function in presynaptic membranes. J Biol Chem 279: 5127-5134.

42. Maguy A, Hebert TE, Nattel S (2006) Involvement of lipid rafts and caveolae in cardiac ion channel function. Cardiovasc Res 69: 798-807.

43. Calder PC, Yaqoob P (2007) Lipid rafts--composition, characterization, and controversies. J Nutr 137: 545-547.

44. Tsui-Pierchala BA, Encinas M, Milbrandt J, Johnson EM, Jr. (2002) Lipid rafts in neuronal signaling and function. Trends Neurosci 25: 412-417.

45. Leitinger B, Hogg N (2002) The involvement of lipid rafts in the regulation of integrin function. J Cell Sci 115: 963-972.

46. Pani B, Singh BB (2009) Lipid rafts/caveolae as microdomains of calcium signaling. Cell Calcium 45: 625-633.

47. Kiselyov K, Wang X, Shin DM, Zang W, Muallem S (2006) Calcium signaling complexes in microdomains of polarized secretory cells. Cell Calcium 40: 451-459.

48. Jacob SN, Choe CU, Uhlen P, DeGray B, Yeckel MF, et al. (2005) Signaling microdomains regulate inositol 1,4,5-trisphosphate-mediated intracellular calcium transients in cultured neurons. J Neurosci 25: 2853-2864.

49. Blackstone C, Sheng M (2002) Postsynaptic calcium signaling microdomains in neurons. Front Biosci 7: d872-885.

50. Blackstone C, Sheng M (1999) Protein targeting and calcium signaling microdomains in neuronal cells. Cell Calcium 26: 181-192.

51. Liu P, Rudick M, Anderson RG (2002) Multiple functions of caveolin-1. J Biol Chem 277: 41295-41298.

52. Volonte D, Galbiati F, Lisanti MP (1999) Visualization of caveolin-1, a caveolar marker protein, in living cells using green fluorescent protein (GFP) chimeras. The subcellular distribution of caveolin-1 is modulated by cell-cell contact. FEBS Lett 445: 431-439.

53. Schindler M, Ahmed I, Kamal J, Nur EKA, Grafe TH, et al. (2005) A synthetic nanofibrillar matrix promotes in vivo-like organization and morphogenesis for cells in culture. Biomaterials 26: 5624-5631.

54. Nakamura M, Sunagawa M, Kosugi T, Sperelakis N (2000) Actin filament disruption inhibits L-type Ca(2+) channel current in cultured vascular smooth muscle cells. Am J Physiol Cell Physiol 279: C480-487.

55. Dunn GA, Heath JP (1976) A new hypothesis of contact guidance in tissue cells. Exp Cell Res 101: 1-14.

56. Kunz-Schughart LA, Kreutz M, Knuechel R (1998) Multicellular spheroids: a three-dimensional in vitro culture system to study tumour biology. Int J Exp Pathol 79: 1-23.

57. Wang SS, Good TA (2001) Effect of culture in a rotating wall bioreactor on the physiology of differentiated neuron-like PC12 and SH-SY5Y cells. J Cell Biochem 83: 574-584.

58. Webb K, Li W, Hitchcock RW, Smeal RM, Gray SD, et al. (2003) Comparison of human fibroblast ECM-related gene expression on elastic three-dimensional substrates relative to two-dimensional films of the same material. Biomaterials 24: 4681-4690.

59. Catterall, W. A. 2011. "Voltage-gated calcium channels." Cold Spring Harb Perspect Biol 3(8): a003947.

60. Fabiato, A. 1983. "Calcium-induced release of calcium from the cardiac sarcoplasmic reticulum." Am J Physiol 245(1): C1-14.
61. Kim, S., Yun, H. M., Baik, J. H., Chung, K. C., Nah, S. Y. and Rhim, H. 2007. "Functional interaction of neuronal Cav1.3 L-type calcium channel with ryanodine receptor type 2 in the rat hippocampus." J Biol Chem 282(45): 32877-89.

62. Hell, J. W., Westenbroek, R. E., Warner, C., Ahlijanian, M. K., Prystay, W., Gilbert, M. M., Snutch, T. P. and Catterall, W. A. 1993. "Identification and differential subcellular localization of the neuronal class C and class D L-type calcium channel alpha 1 subunits." J Cell Biol 123(4): 949-62.

63. Yang, L., Wang, Z., Wang, B., Justice, N. J. and Zheng, H. 2009. "Amyloid precursor protein regulates Cav1.2 L-type calcium channel levels and function to influence GABAergic short-term plasticity." J Neurosci 29(50): 15660-8.

64. Cheng ZJ, Singh RD, Marks DL, Pagano RE (2006) Membrane microdomains, caveolae, and caveolar endocytosis of sphingolipids. Mol Membr Biol 23: 101-110.

65. Shu L, Lee L, Chang Y, Holzman LB, Edwards CA, et al. (2000) Caveolar structure and protein sorting are maintained in NIH 3T3 cells independent of glycosphingolipid depletion. Arch Biochem Biophys 373: 83-90.

66. Zhang JH, Chung TD, Oldenburg KR (1999) A Simple Statistical Parameter for Use in Evaluation and Validation of High Throughput Screening Assays. J Biomol Screen 4: 67-73.

67. Lai Y, Kisaalita W (submitted) Performance evaluation of 3D polystyrene 96-well plates with human stem cells and the calcium assay. Journal of Biomolecular Screening.

68. Denyer J, Worley, J., Cox, B., Allenby, G. and Banks, M. (1998) HTS approaches to voltage-gated ion channel drug discovery. Drug discovery today 3: 323-332.

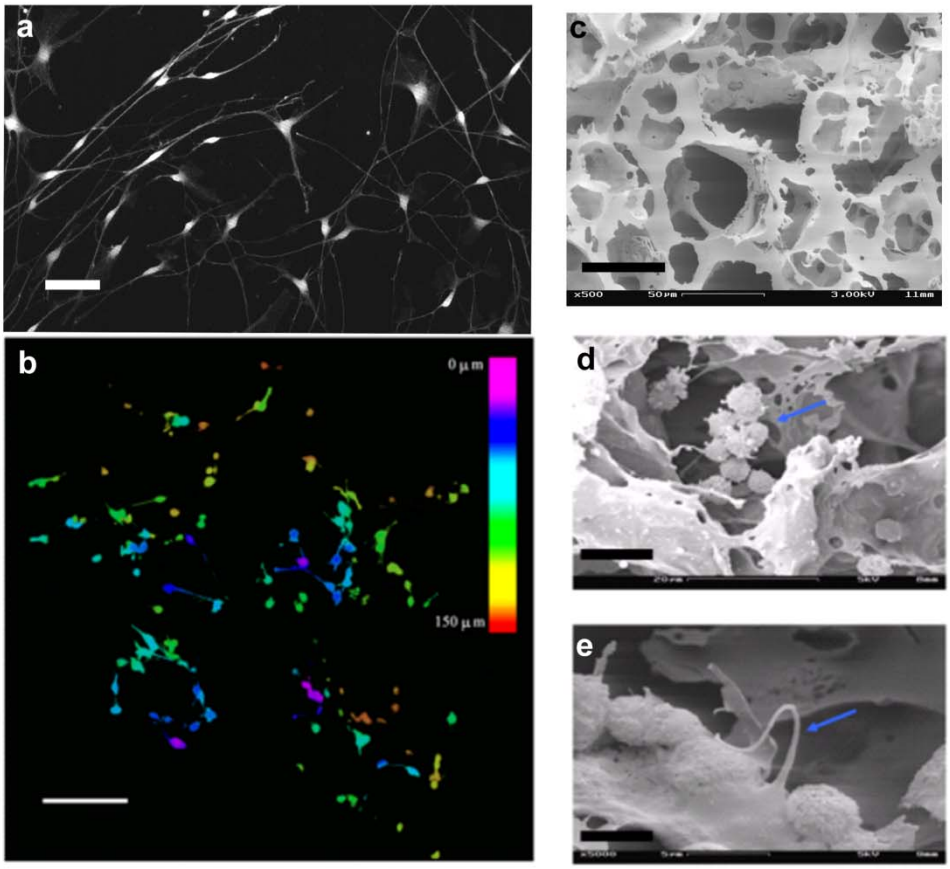

Figure 3. 1 Polymer (PLLA) scaffolds seeded with SCG cells.
(a) Confocal image with calcein stained SCG cells cultured on flat surfaces. (b) Confocal depth projection micrograph of a 20:1 PLLA polymer scaffold with 60-100 µm sized pores, seeded with SCG cells. Cells were stained with calcein and thirty Confocal images were taken in row along the z-axis after 7 days in culture. Maximum projected images were generated with different color corresponding to different depth from the polymer surface. As shown in the color bar, pink is closest to the surface and red is at 150 µm from the surface. (c) SEM image of polymer (PLLA) scaffold without cells. (c) SEM image of a SCG cell cluster (indicated by arrow) inside a pore on day 2 after plating. (e): SEM image showing a neurite (indicated by arrow) from one cell to another on day 7 after plating. Bars represent 50 µm in (a), 100 µm (b), 50 µm in (c), 10 µm in (d) and 5 µm in (e).

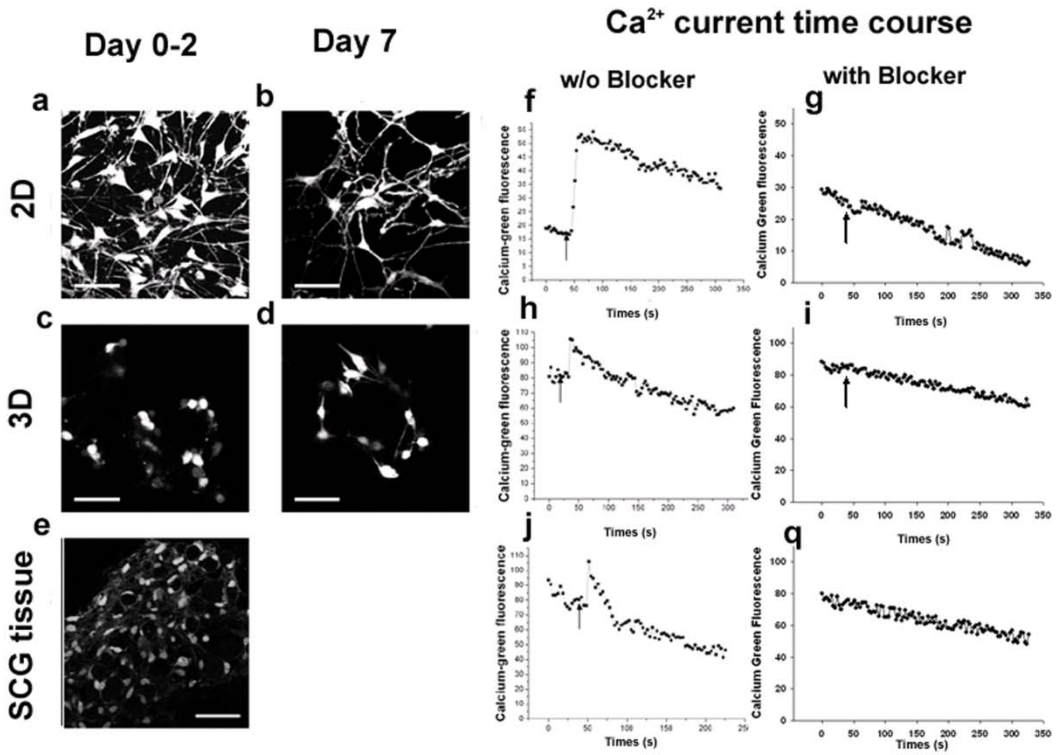

Figure 3. 2 Cell morphology and high K^+ depolarization induced intracellular calcium transient. Cell morphology was observed with a live cell indicator and cytoplasmic marker Calcein AM (a-e). Fluorescent images were captured by laser scanning confocal microscopy. (a) and (b) are confocal images of cells on 2D substrates on day 2 and day 7 after plating, respectively. (c) and (d) are volume rendered confocal depth projection images of cells on 3D PS scaffolds on day 2 and day 7 after plating, respectively. (e) is a volume rendered confocal image of the cells in a intact SCG tissue. Bars represent 50 μm in all these 5 images. High K^+ depolarization induced intracellular calcium changes were studied by Calcium Green, a calcium indicator (f-q). Intracellular calcium were reflected by Calcium Green's fluorescent intensities and recorded by Confocal microscopy every 3 seconds. In (f) and (h) show the typical calcium time course in response to high K^+ (50 mM) depolarization on 2D substrates and 3D scaffolds, respectively for day 2 cultures. (j) shows calcium time course from a typical responsive cell in an intact SCG tissue after dissection.(g), (i) and (q) are the typical calcium time course when calcium transient was suppressed by L-type calcium blocker from 2D, 3D and tissue samples, respectively. Arrows show the times points when high K^+ buffer was added. The general decreasing trend of fluorescence intensity was resulting from photo-bleaching during recording.

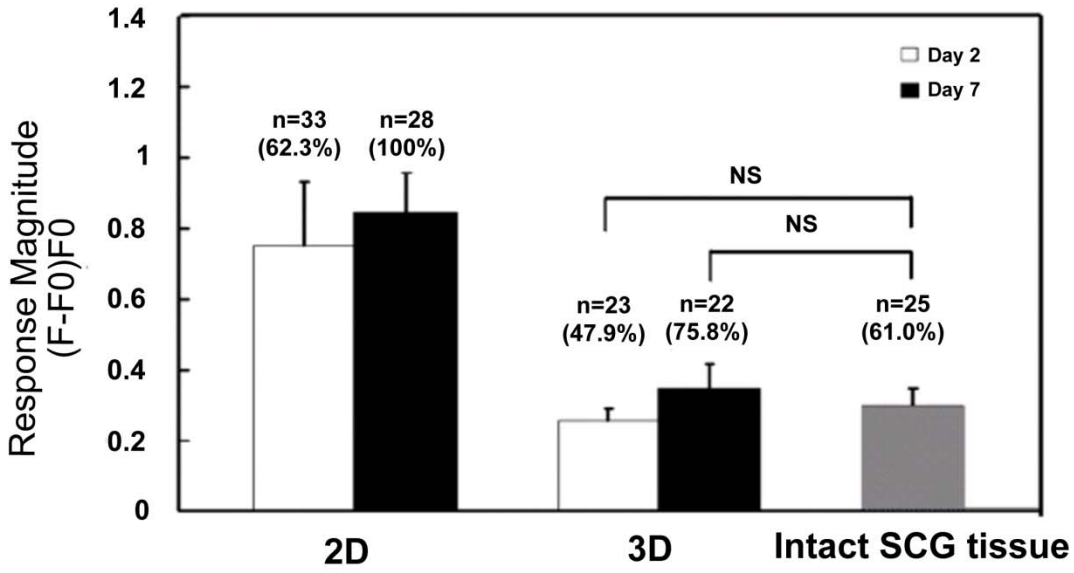

Figure 3. 3 Cellular VGCC functionality.
"NS" indicates that the means of the two samples compared are not significantly different with a level of $p>0.8$ by Student's t-test. "n" is the number of responsive cells. The percentage of responsive cells from the total cell pool is indicated in parenthesis. Error bars are the 95% confidence intervals.

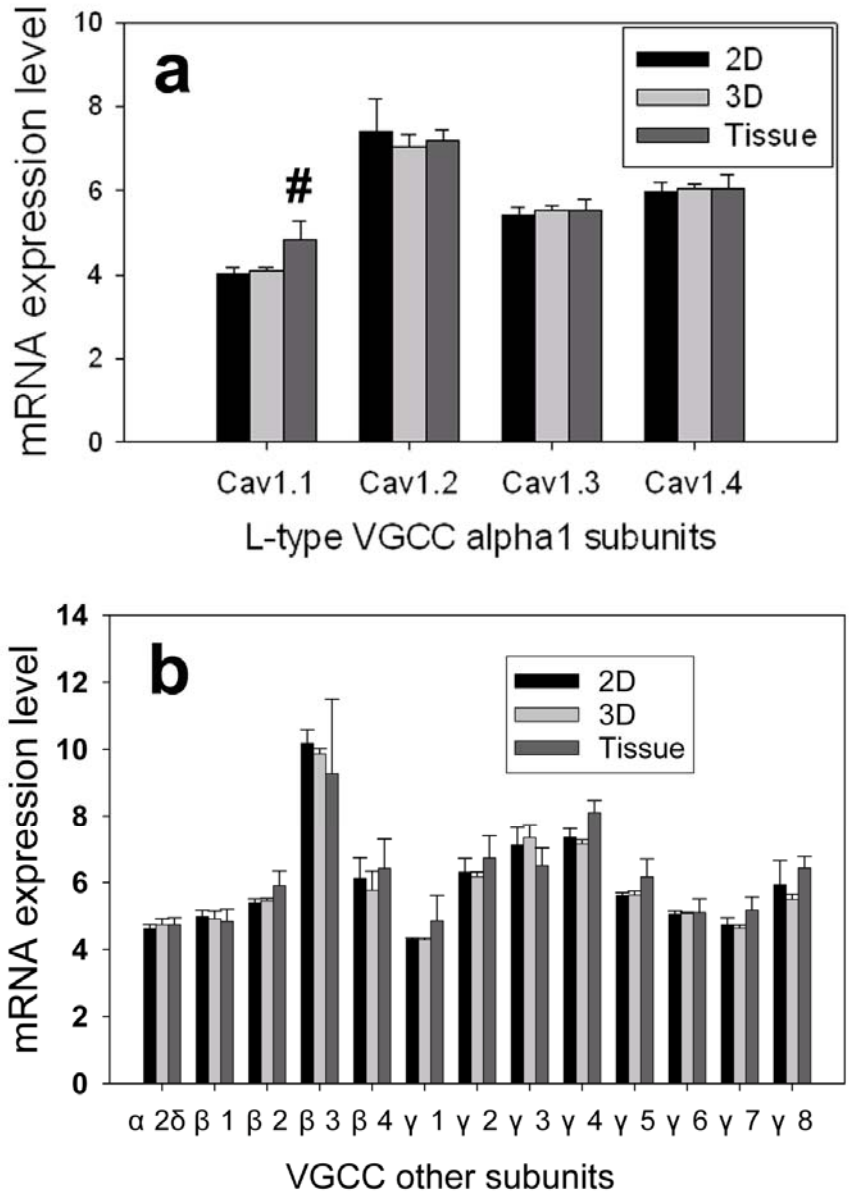

Figure 3. 4 Microarray gene analysis results.
Whole genome analysis was performed for SCG cells in 2D and 3D after 5 days in culture or in freshly dissected SCG tissue. Gene expression levels of L-type VGCC alpha 1 subunits (a) and other common subunits in VGCC (b) are presented here. The final gene expression levels were averaged from analysis of four biological replicates in each experimental condition (2D, 3D and tissue) (n=4). Error bars represent the standard deviation. # Indicates the mean of expression level from tissue sample was significantly different from that of 2D or 3D cultures with $p < 0.05$ by Student's t-test.

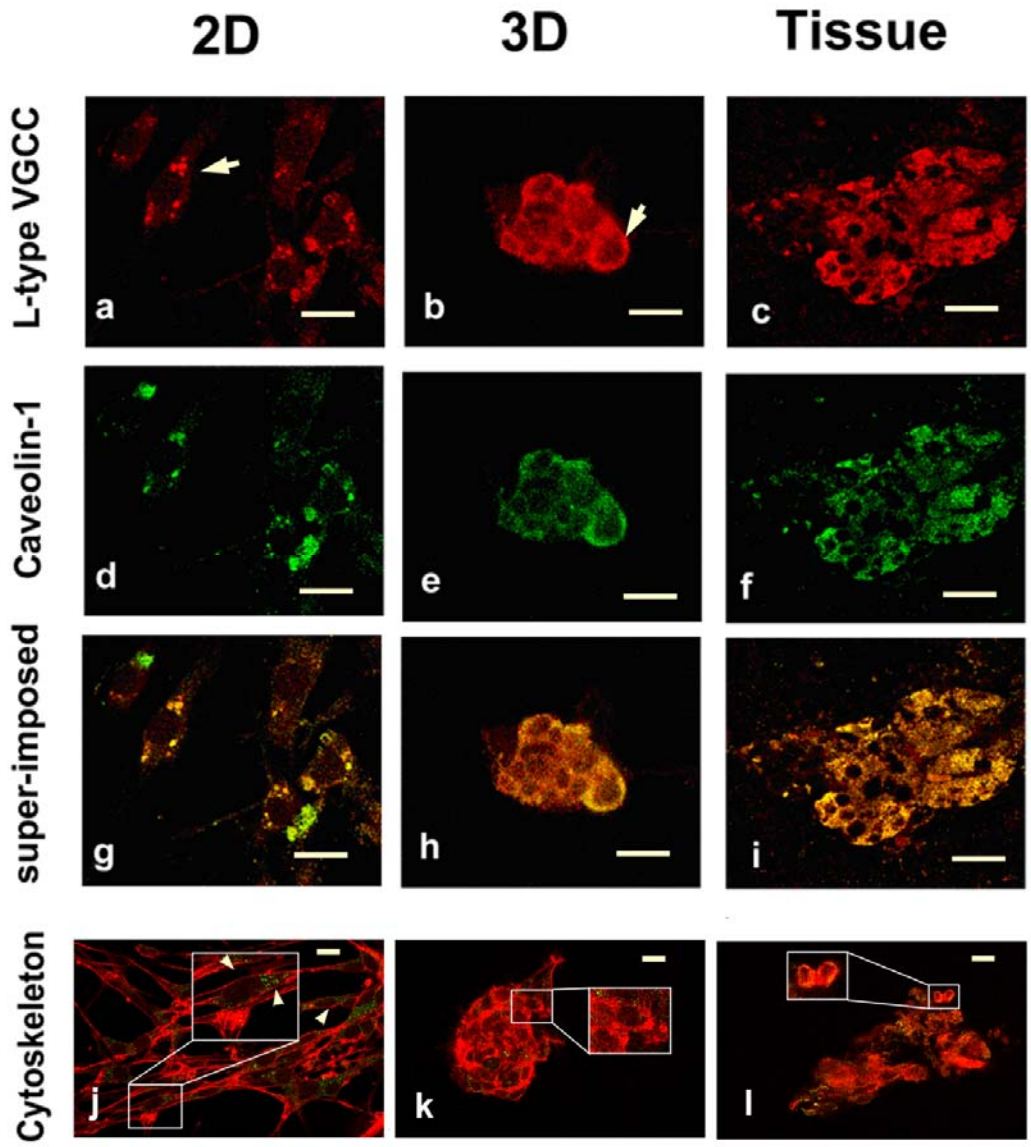

Figure 3. 5 L-type VGCC and caveolin-1 colocalization, and Cytoskeleton F-actin and vinculin protein expression.
(a) -(c) Confocal images of L-type calcium channel staining of SCG cells cultured on 2D surface (a), 3D scaffolds (b) and in freshly dissected SCG tissue (c). Arrows pointed to one cell. (d)-(f) Confocal images of caveolin-1 (caveolar protein) from SCG cells cultured on 2D surface (d), 3D scaffolds (e) and in freshly dissected SCG tissue (f). (g)-(i) are the super-imposed image of VGCC and caveolin-1 staining, yellow indicates that VGCC protein and caveolin-1 are colocalized. (j)-(l)Confocal images of F-actin (red) and vinculin (green) double stained SCG cells cultured on 2D surface (d), in 3D scaffolds (e) and in freshly dissected SCG tissue (f). Insets are digitally enlarged single cells. Arrowheads point to the long stretched actin filaments that were absent in 3D culture and tissue cells. Scale bars are 20 μm.

Table 3. 1 Cell morphology on 2D surfaces and in 3D substrates

2D surfaces				
	Neurite density	Neurite length	Soma section area	Soma section roundness
Day 2	121/50=2.4	38.9±17.7 μm (n=121)	149.8±59.3 μm^2 (n=50)	0.51±0.11 (n=50)
Day 7	88/11=8.0	63.6±36.1 μm (n=88)*	134.5±72.1 μm^2 (n=11)	0.54±0.11 (n=11)
3D substrates				
	Neurite density	Neurite length	Soma section area	Soma section roundness
Day 2	11/16=0.7	10.9±3.2 μm (n=11)$^{\#}$	90.0±22.3 μm^2 (n=16)$^{\#}$	0.81±0.05 (n=16)$^{\#}$
Day 7	60/14=4.3	25.2±13.8 μm (n=60)*$^{\#}$	144.5±56.9 μm^2 (n=14)*	0.64±0.15 (n=14)*$^{\#}$

*value was significantly different from that on the previous measuring data ($p<0.05$)
$^{\#}$value was significantly different from that for 2D

CHAPTER 4

NEURAL CELL 3D MICROTISSUE FORMATION IS MARKED BY CYTOKINES' UP-REGULATION*

*Lai Y, Asthana A, Cheng K, Kisaalita WS. 2011. *PLoS ONE* 6: e26821

4.1 Abstract

Cells cultured in three dimensional (3D) scaffolds as opposed to traditional two-dimensional (2D) substrates have been considered more physiologically relevant based on their superior ability to emulate the *in vivo* environment. Combined with stem cell technology, 3D cell cultures can provide a promising alternative for use in cell-based assays or biosensors in non-clinical drug discovery studies. To advance 3D culture technology, a case has been made for identifying and validating three-dimensionality biomarkers. With this goal in mind, we conducted a transcriptomic expression comparison among neural progenitor cells cultured on 2D substrates, 3D porous polystyrene scaffolds, and as 3D neurospheres (*in vivo* surrogate). Up-regulation of cytokines as a group in 3D and neurospheres was observed. A group of 13 cytokines were commonly up-regulated in cells cultured in polystyrene scaffolds and neurospheres, suggesting potential for any or a combination from this list to serve as three-dimensionality biomarkers. These results are supportive of further cytokine identification and validation studies with cells from non-neural tissue.

Keywords: Stem cell, Progenitor cell, mRNA, Scaffold, Biosensor, Cytokine

4.2 Introduction

Providing a 3D spatial microenvironment for cells to grow in, is the sole criterion that has traditionally been associated with three-dimensional cell culture. However, with recent advances in the field in the past decade, the meaning of 3D cell culture has been extended to providing the "total microenvironment" that supports the formation of microtissue that exhibits "complex" physiological relevance (CPR) or better emulation of the *in vivo* functionality in a manner not possible in 2D cultures [1]. Three main categories or microenvironment factors (MEFs) or "three-dimensions" from the literature include: 1) chemical or biochemical composition, 2) spatial (geometric 3D) and temporal dimensions, and 3) force and substrate physical properties [1]–[4]. However, there is still a lack of a quantifiable entity which can establish if the cellular response in a 3D culture is actually physiologically relevant and *in vivo*-like or just different from 2D. The identification and validation for this entity or a potential three-dimensionality biomarker is necessary due to three compelling reasons. First, apart from the concept of "three-dimensional matrix adhesion" originally proposed by Cukierman et al. [5] as a possible indication or "diagnosis" or marker for a culture state of three-dimensionality, the fields of tissue engineering and/or cell-based biosensors have not provided knowledge on the basis of which a consensus for three-dimensionality and the associated complex physiological relevance could be established. Because of this, claims of "physiologically more relevant" are readily made for cells cultured on any surface or scaffold that provides loosely defined 3D geometry, either at the nano- or micro- structure levels or their combinations, as long as the resulting cell phenotypes are different between the 2D and 3D geometries. Second, the concept of using combinatorial approaches to fabricate libraries of polymers or other material scaffolds [6], [7] for tissue engineering or cell-based drug discovery call for high throughput assay by which "hit

materials" can be quickly identified for further development. Cell-material interaction outcome can potentially guide the development of such assays or biosensors [8]. An interaction with a material which yields cells that emulate *in vivo* conditions would be most desirable. Three-dimensionality biomarkers would provide the intellectual basis for material discovery platform development. Third, in order to lower the costs associated with 3D platforms and make them more accessible for high throughput screening (HTS) applications, simplification of the platform without giving up the physiologically relevant behavior of the cells is necessary, as discussed in detail by Lai et al. [4].

Taken together, the subfield or field of 3D culture needs ubiquitous validated biomarkers. As a first step, in search for three-dimensionality biomarkers, we initiated a cytokine expression comparative transcriptomic study with neural progenitor (NP) cells grown on 2D flat surfaces, 3D polymeric scaffolds and as neurospheres (NS). NS were used as the *in vivo* surrogate, since they have been shown to emulate many *in vivo* functions that have not been possible in 2D cultures[9], [10]. Cytokines are involved in many crucial cell functions like innate and adaptive inflammatory host defenses, cell growth, differentiation, cell death, angiogenesis, and development and repair processes [11]. Based on the structural homologies of their receptors they can be broadly classified into families like Colony Stimulating Factors, Interleukins, Interferons, TGF (transforming growth factor) family, TNF (tumor necrosis factor) superfamily, PDGF (platelet-derived growth factor) family and Chemokines [11]. Although cytokines have been extensively studied in the field of immunology and oncology, tissue or cell-based biosensor engineers have paid little attention to these small proteins that have potential to revolutionize the field. The evidence for their existence in 3D cultures is compelling but they have not yet been looked at as candidates for potential 3D biomarkers. However, they were an ideal family to

explore for the search. The rationale behind their choice was based on the fact that, in a 3D microenvironment cells are surrounded by homotypic neighbors forming a loosely bound disorganized aggregate. When compared to *in vivo*, such a scenario exists only during avascular tumorogenesis or early stages of inflammatory wound healing and both these phenomenon are regulated by the same molecules – Cytokines [12]. So *in vitro*, the cells growing in 3D relate to any of those two models depending upon their type – malignant or primary, respectively, and therefore upregulation of their cytokine levels was physiologically relevant.

4.3 Materials and Methods

4.3.1 Materials and reagents

Neural progenitor cells were obtained from Regenerative Bioscience Center at University of Georgia as well as Millipore (ENStem-A^{TM}, Billerica, MA). Polystyrene, chloroform, ammonium bicarbonate were obtained from Sigma (St. Louis, MO). Neural basal media, penicillin/streptomycin, L-glutamine, recombinant human leukemia inhibitory factor (hLIF), basic fibroblast growth factor (bFGF), B-27 supplement and phosphate buffered saline (PBS) were obtained from Gibco (Gaithersburg, MD). RNeasy mini kit was obtained from Qiagen (Valencia, CA). Human Genome U133 plus 2.0 microarray chips were obtained from Affymetrix (Santa Clara, CA).

4.3.2 Scaffold fabrication and neural progenitor cell culture

The scaffold fabrication process in Cheng et al. [13] was followed. Briefly, a viscous polymer solution was prepared by dissolving polystyrene (PS) in chloroform. Sieved ammonium bicarbonate particles in the range of 40–60 μm were added to the polymer solution and mixed thoroughly. These particles generated larger scaffold pore sizes from 60–100 μm, probably due to particle agglomeration. The paste mixture of polymer/salt/solvent was cast into the wells of a

standard glass cell culture vessel. The optimal polymer/salt/solvent ratio of 1:20:5 (w/w/v) as determined in Cheng et al. [13] was used to generate the paste mixture. Casting was followed by chloroform evaporation, vacuum drying, and baking at 80°C overnight. Before use for cell culture, the scaffolds were sterilized by immersing in 70% alcohol overnight. PS scaffolds offer advantages of low cost, transparency for optical detection, and/or compatibility with existing instrumentation platforms in High Throughput Screening (HTS) applications.

Human neural stem cells or neural progenitors (NP) were maintained in neural basal media (Invitrogen, PA) supplemented with penicillin/streptomycin, L-glutamine, recombinant human leukemia inhibitory factor (hLIF), bFGF and B-27, at 37°C in a 5% CO2 humidified incubator. Medium was half changed every 48 hours. For differentiation, cells were allowed to grow until 90% confluent, after which they were exposed to differentiation medium which was half changed every 24 hours. The composition of differentiation medium was similar to the subculture medium described above with the exception of bFGF. For subculturing, 90% confluent cells were aspirated by pipetting and the subculture ratio was typically 1:2 to 1:3. Before cell seeding, both the 3D scaffolds and 2D substrates were coated with poly-ornithine and laminin to rule out any differences that may be caused by the polymer material itself. Neurospheres (NS) were formed by plating cells into non-coated dishes with shaking. Dishes without coating and shaking prevented NP cells from attaching to the surface and encourage them to attach to each other and form spheroid structures. The cell seeding density was 50,000 cells/cm2 for both 2D and 3D cultures.

4.3.3 Microarray gene expression analysis

Total RNA was isolated from all samples using Qiagen RNeasy Kits (Qiagen, Valencia, CA) according to the manufacturer's standard protocol. The quantity of mRNA isolated from

each sample was determined using absorption at 260 and 280 nm. The purity of each sample was monitored using the A260/A280 ratio as well as housekeeping genes. A ratio of 1.8–2.1 was considered a "clean" sample and could be used in microarray experiments. Samples were sent to Affymetrix Core facility at Medical College of Georgia (MCG) for Human Whole Genome U133 plus 2.0 GeneChip Expression Analysis (Affymetrix, Santa Clara, CA). The expression data is publicly available on the GEO site as Series GSE13715.

The expression value of each gene was obtained by Expression Console (Affymetrix) with the RMA (Robust Multiple-array Average) algorithm. RMA is an algorithm widely applied to create expression values for Affymetrix data. The raw intensity values from Affymetrix genechips are background corrected, log2 transformed and then quartile normalized before a linear model was fit to obtain an expression measure for each probe set.

4.3.4 Statistical analysis

Linear discriminant analysis (LDA) with cross-validation was fulfilled by SAS DISCRIM procedure. Student t-test was used to compare the mean expression from two conditions (2D vs. 3D and 2D vs. NS) with significance level of 0.05. To determine whether cytokines as a group were significantly regulated by culture condition (i.e., 2D, 3D and NS), the permutation t-test method [14] was utilized.

4.4 Results

The development of stem cell-based, HTS compatible, *in vivo* tissue-emulating biosensor platform requires a substrate or scaffold that is not only easy to fabricate but also provides stem cells with a 3D micro environment. For this purpose, 3D porous scaffolds were prepared from polystyrene (PS), a polymer material that has been widely applied in fabricating cell culture vessels. The physical and chemical properties of the scaffolds used in this study have been

described by Cheng et al. [13]. Mouse superior cervical ganglion (SCG) and NP cells cultured in these scaffolds, and NP cells cultured as neurospheres (spheroids) have exhibited similar responses as freshly dissected SCG tissue in terms of voltage gated calcium channel and resting membrane potential, while 2D cultured cells exhibited significantly higher responses[13]. Based on Tuj staining (neuronal marker) the neural progenitor cells in scaffolds and neurospheres differentiated into nerve cells [15]. Additionally, spheroids have successfully emulated *in vivo* drug resistance [9], providing rationale for use of the neurospheres as an *in vivo* surrogate.

4.4.1 Quality of transcript expressions

Five experimental groups, with four biological replicates each, were chosen for this study. The five experimental groups were: 1) NP cells before differentiation induction cultured on 2D culture vessel (B2D), 2) NP cells before differentiation in 3D scaffolds (B3D), 3) one week culture of NP cells after differentiation induction on 2D surfaces (A2D), 4) one week culture of NP cells after differentiation in 3D scaffolds (A3D), and 5) neurospheres (NS). In order to minimize the cell passage and other environmental effects on cells, the samples were generated in 2D–3D paired manner, which means at least one 2D and one 3D sample were generated at the same time and from the same batch of cells. Intensity results of the transcripts were examined and normalized to exclude background signals and reported in arbitrary units using RMA (Robust Multiple-array Average) algorithm. RMA is an algorithm widely applied to create expression values for Affymetrix genechip data. The raw intensity values from Affymetrix genechips were first background corrected, log2 transformed and then quartile normalized. The final expression measure was obtained by fitting a linear model for each probe set on each array.

Before we analyze the expression data, quality control tests were performed. No array results were accepted if the correlation coefficient (R^2 value) between replicates was less than

0.95. Overall, samples exhibited good correlations with each other. Differentiation status and culture vessel difference didn't affect the overall gene expression pattern (Figure 4.1, top). We also examined the overall pattern of gene expression based on signal intensity box-plot (Figure 4.1, bottom). As is the case in box-plot data presentations, the lowest bar represents the observed sample minimum, the base of the box represents the lower quartile while the top represents the upper quartile, the bar inside the box represents the median, and the top bar represents the highest sample observation. The box-plot displays differences between populations without making any assumptions of the underlying statistical distribution. With the exception of a few samples, most of the five values represented in all the data sets (Figure 4.1, bottom), are in agreement. The third sample from B3D group (B3D_3) exhibited a very distinctive distribution of the expression value in which it had the lowest sample maximum and the smallest "distance" between upper quartile and lower quartile and had a very low correlation with other samples grown under similar conditions, as shown in Figure 4.1 (top). In order for array data to be accepted for analysis, the overall gene expression pattern has to be similar with no wide divergence between samples. Large variations indicate either hybridization errors or problems with the quality of the RNA used. For this reason B3D_3 was excluded from further analysis. Also, the third sample from A3D group had overall low expression values and a noticeable shift in intensity histogram (data not shown). It had a low correlation coefficient with sample grown under similar condition (Figure 4.1, top) and was also excluded from further analysis.

4.4.2 Cytokines' transcript and culture classification

The focus on cytokines in this study was based on previous proteomic and transcriptomic evidences from other 3D culture studies indicating that cytokines' expression levels are altered by culture conditions [16]–[19]. The list of cytokines analyzed was obtained from the

Immunology Database and Analysis Portal (ImmPort) (https://www.immport.org/immportWeb/queryref/geneListSummary.do). There were a total of 681 probesets found in our microarray corresponding to the list of human cytokines. The permutation method was used to determine whether cytokines as a group was significantly regulated by culture conditions (i.e. 2D and 3D). Although we reduced the number of probesets to be analyzed from the genechip total of 54000 to 681, by focusing only on cytokines, the number of variables (transcript expression level in our case) still greatly exceeded the number of samples. Permutation testing is superior to standard tools for estimating statistical significance for multiple hypotheses testing due to its ability to empirically determine whether the observed class distinction could be obtained by chance. Briefly, the assay samples were re-iteratively reassigned randomly to the classification label (2D, 3D or NS). This process was done by randomly sampling function from R console's base package. After each reiteration, a list of *p* values were calculated measuring the significance of newly designated culture condition label for each probesets (2D vs. 3D or 2D vs. NS). After 1000 permutations, summary statistics (we used the median *p* value) with the permuted class distinction were generated and compared to those obtained in the experimental data [14], [20]. Results showed that cytokines as a group was significant when comparing 2D with 3D or NS (at a significance level of 0.05).

Next, we used linear discriminant analysis (LDA) to test if cytokine transcriptomic expressions can form a good criterion to separate 2D samples from 3D samples. LDA is a multivariate statistical technique commonly used to build a linear prescriptive or descriptive model which can characterize or classify each observation into two or more groups. LDA is also commonly used as a dimension reduction method for further classification analysis. Compared to

cluster analysis such as Principle Component Analysis (PCA), LDA requires prior knowledge of the classes, which fitted our purpose of study.

The LDA results are presented in Table 4.1. As shown cytokines successfully classified 2D from 3D samples with acceptable low error counts. After-differentiation had a lower error rate in comparison to before-differentiation condition. This indicated that if 3D biomarker cytokines do exist, they may be culture time dependent. As pointed out by Lai et al. [4], under such circumstances biomarking with a profile as opposed to an end- point measurement would be the most practical and would increase the robustness of the biomarker. NS exhibited 0 error classification count, suggesting that it was more different from all other culture conditions.

In Table 4.2 we list 16 cytokines selected by stepwise discriminant analysis with a cut off *p*-value of 0.01. With these 16 cytokines, the classification of 2D, 3D and NS is achieved with 0 error rate after cross-validation. Ten of these cytokines are commonly up-regulated in both 3D and NS culture conditions (however not statistically significant). Two are down-regulated both in 3D and NS. Although statistically these cytokines can discriminate 2D from 3D effectively, they are not as a group necessarily the best candidates for 3D biomarkers. This is because, the multivariate nature of the data makes the transcript expression levels correlated with each other, which means each of the variables (cytokine transcript expression levels in our case) can be represented by a group of other variables. Other cytokines may have the same or similar statistical power of these 16 cytokines to discriminate 2D from 3D, with better biological meanings. For this reason, cytokines significantly up-regulated in 3D and NS culture conditions were examined in detail.

4.4.3 Cytokines up-regulated in 3D and NS

In Tables S1 and S2 (Appendix A), we present cytokine significantly up-regulated ($p \leq 0.05$) in 3D and NS cultures. Forty and ninety-one probesets were up-regulated in 3D and NS culture conditions, respectively. The higher number in NS cultures is possibly due to inability to control the size of neurospheres. Many NS were observed to be larger than the 3D structure pore sizes (e.g., three times the maximum pore size of 100 μm)[13]. With large NS, the core of the cellular aggregate may experience hypoxia to the extent that genes not observed in 3D are up-regulated. Evidence in support of this comes from MIP-2 gene (inflammatory protein-2) induced by hypoxia [21] that was also found to be up-regulated in NS but not in 3D conditions in our study. Table 4.3 lists 13 genes (ANGTL7/CDT6, ARMET/MANF, BMP8B/OP2, CCL13/MCP-4, FGF5, GHRL, IL-11, IL-1B/IL-1F2, NOV/IBP-9, PDGFB, STC1, TGFA, and VEGF-A), whose transcripts were up-regulated in both 3D and NS culture conditions, and examples of their functions. We particularly focused on these genes in the following physiologic function discussion because they were less likely to be up-regulated because of conditions like hypoxia that may be present in NS but absent in 3D conditions.

4.5 Discussion

Consistent with our results, up-regulation of cytokines in 3D cultures compared to 2D has been reported by several transcriptomic studies using cells from the four main tissue types (nerve, muscle, connective, and epithelial) cultured in a wide variety of platforms. For example, Klapperich and Bertozzi [19] showed that seven cytokines (IL-8, CXCL1, CXCL2, CXCL3, CXCL5, VEGF, LIF) were up-regulated in human fetal lung fibroblasts (IMR-90) cultured in a collagen–glycosaminoglycan (collagen/GAG) 3D mesh when compared to 2D surfaces. Also, up-regulation of six cytokines (CXCL1- 3, IL-8, MIP-3a, Angiopoetin like4) by a melanoma cell

line (NA8) cultured on poly-2-hydroxyethyl methacrylate (polyHEMA) plates was reported by Ghosh at al. [18]. Transcriptomic findings such as those in the above examples have been further substantiated by studies at the protein level. For example, Enzerink et al. [16] have reported induction of chemokine (CCL2-5, CXCL1-3, CXCL8) secretion due to clustering of cells in five different fibroblast cell lines cultured in agarose. Also, Fischbach et al. [17] cultured tumor cells (oral squamous cell carsinoma) in a 2D and 3D RGD-alginate system and reported a dramatic enhancement of IL-8 levels in 3D. Another study by the same group showed that when the same cells were grown in Matrigel (lrBM) there was up-regulation of cytokines when compared to 2D. This observation is of particular importance as cells grown on Matrigel have already been shown to produce an outcome similar to *in vivo*, like the formation of mammary gland acinus and milk-like secretion into lumen [22] proving that Matrigel can provide all the relevant microenvironmental factors. This suggests that the up-regulation of cytokines in 3D compared to 2D is not a random differential response but is pertinent as a similar response is elicited when a proven physiologically relevant microenvironmental platform is provided.

We have used the themes of tumorogenesis, inflammation and development as shown in Table 4.3 to closely examine the13 up-regulated transcripts in both 3D and NS culture conditions; cells in a 3D culture *in vitro* relate to *in vivo* phenomenon like avascular tumor progression, early stages of inflammatory wound healing or embryonic development depending upon their type- malignant, primary or stem [4]. As these conditions are regulated by autocrine and paracrine cytokine signaling *in vivo*, the up-regulation of cytokines in 3D culture is physiologically relevant.

Angiogenesis is recurrent function among the genes listed in Table 4.3, which is not surprising. As already mentioned, as a microtissue grows beyond a certain size, nutrient and

oxygen depletion become limiting factors leading to the inhibition of cell proliferation and initiation of angiogenic signaling. Oxygen concentration in 3D tissues depends on the balance between oxygen delivery and consumption. *In vivo*, this balance is tightly regulated by evenly distributed capillary networks but *in vitro* homotypic 3D microtissues lack vasculature and therefore develop a hypoxic core as their size increases. This event leads to the cells producing chemical signals (cytokines) for angiogenesis and is quite similar to the response occurring in normal hypoxic tissues where balanced signaling cascades lead to vascular remodeling and angioadaptation until the tissue oxygen concentration is back within its normal range[23]. The up-regulation of VEGF-A and other genes with angiogenic function like ANGPTL7/CDT6, FGF5, NOV/IBP-9, and TGFA is pointing to a functional class of cytokines with great potential as three-dimensionality biomarkers.

The above genes may play other roles besides being factors involved with hypoxia induced angiogenesis. For example, VEGF-A has been shown to regulate neuronal development, survival, neurite growth and it also possesses gliotrophic properties. Also, it's up-regulation is not limited to neuronal cells; it has been shown to be up-regulated in 3D cultures of a variety of cell and tissue types including human fetal lung fibroblasts [19], oral squamous cell carcinoma, glioblastoma, breast cancer [17], neonatal rat cardiomyocytes and neonatal mouse cardiomyocytes [24]. This up-regulation in a non-cell type specific manner in 3D cultures of VEGF-A, and probably other members of the class, lends credibility to the notion of ubiquity of these potential biomarkers in different cells derived from different tissue types.

Another recurrent gene function theme in Table 4.3 is terminal differentiation, a process by which cells commit to being part of a particular tissue or organ and perform a particular function. Terminal differentiation is preceded by inhibition of proliferation and cell cycle arrest.

This exerts endoplasmic reticulum stress on the cell, but anti-apoptotic factors like Bcl-2 protect the cell from apoptosis and commit it to differentiation. In 3D, much like in organs *in vivo*, there is a spatial constraint on the microtissue, exerted by the defined pore size of the scaffold, which prevents them from proliferating freely, maintaining them in a quiescent state. Evidence in support of this comes from the fact that cells grown in 3D have shown lower proliferation rates than their 2D counterparts and higher expression of cyclin dependent kinase inhibitors (CDI) p21 [25]. Also integrin mediated adhesion to the ECM leads to activation of Bcl-2 family of genes and makes the 3D cells more resistant to apoptosis[26]. Such conditions are favorable for the cell to undergo terminal differentiation and this can be clearly seen by up-regulation in a number of differentiation and survival factor in 3D and NS compared to 2D, like PDGFB and STC1. Neural progenitor cells cultured in 3D have been shown to differentiate and produce a heterogeneous population consisting of neurons, astrocytes and oligodendrocytes [27]. Such cultures essentially behave as a coculture where cells are in symbiotic relationship with each other and might produce factors that can modulate the functions of the other cell types. This has been confirmed by intermediate filament glial fibrillary acidic protein (GFAP), a marker for astrocytic differentiation that was up-regulated in 3D and NS compared to 2D cultures (data not shown). It is a well known fact that astrocytes play a trophic role in supporting neurons. Factors secreted by astrocytes generally belong to the FGF, TGF and EGF families that play an important role in early neurogenesis[28]. Members of these families act as potent mitogens for multipotential neural progenitors and have been implicated in the regulation of several aspects of neurogenesis. Therefore up-regulation of members of these cytokine families in 3D and NS in this study is not surprising. The identification and validation of a few cytokines as three-

dimensionality biomarkers that are ubiquitous among cells from different tissue types needs to be done.

Overall, cytokines gene expression results in this study support the notion that 3D cultured cells in various formats are different from their 2D counterparts. Furthermore, up-regulated cytokines' transcripts, independent of culture format, have been identified; this group of 13 cytokines commonly up-regulated in cells cultured in polystyrene scaffolds and neurospheres are suggesting potential for any or a combination from this list to serve as three-dimensionality biomarkers. These results are supportive of further cytokine identification and *in vitro*/*in vivo* validation studies with cells from non-neural tissue.

4.6 Acknowledgements

The authors thank Dr. Lina Wang and Drs. Andrew Sornborger and Paul Schliekelman for technical assistance. This work was supported by an NSF grant (0304340) and a UGA Engineering Grant.

4.7 References

1. Kisaalita WS (2010) 3D cell-based biosensors in drug discovery programs: Microtissue engineering for high throughput screening. Boca Raton: CRC Press. 77 p.

2. Green JA, Yamada KM (2007) Three-dimensional microenvironments moderate fibroblast signaling responses. Adv Drug Deliv Rev 59: 1293-1298.

3. Griffith LG, Swartz MA (2006) Capturing complex 2D tissue physiology in vitro. Nat Rev Mol Biol 7: 211-224.

4. Lai Y, Asthana A, Kisaalita WS (2011) Biomarkers for simplifying HTS 3D cell culture platforms for drug discovery: the case for cytokines. Drug Discov Today 16(7/8): 293-297.

5. Cukierman E, Pankov R, Stevens DR, Yamada KM (2001) Taking cell-matrix adhesions to the third dimension. Science 294(5547): 1708-1712.

6. Simon CG Jr, Stephens JS, Dorsey SM, Becker ML (2007) Fabrication of combinatorial polymer scaffold libraries. Rev Sci Instrum 78(7): 2755-2761.

7. Yang Y, Bolikal D, Becker ML, Kohn J., Zeiger, DN et al. (2008) Combinatorial polymer scaffold libraries for screening cell-biomaterial interactions in 3D. Advanced Materials 20(11): 2037-2043.

8. Yang Y, Dorsey SM, Becker ML, Lin-Gibson S, Schumacher GE et al. (2008) X-ray imaging optimization of 3D tissue engineering scaffolds via combinatorial fabrication methods. Biomaterials 29(12): 1901-1911.

9. Yamada KM, Cukierman E (2007) Modeling tissue morphogenesis and cancer in 3D. Cell 130(4): 601-610.

10. Kato-Negishi M, Tsuda Y, Onoe H, Takeuchi S (2010) A neurospheroid network-stamping method for neural transplantation to the brain. Biometarials 31: 8939-8945.

11. Oppenheim JJ (2001) Cytokines: past, present, and future. Int J Hematol 74(1): 3-8.

12. Coussens LM, Werb Z (2002) Inflammation and cancer. Nature 420(6917): 860-867.

13. Cheng K, Lai Y, Kisaalita WS (2008). Three-dimensional polymer scaffolds for high throughput cell-based assay systems. Biomaterials 29(18): 2802-2812.

14. Good PI (2005) Permutation, parametric and bootstrap tests of hypotheses, 3rd ed. New York: Springer. P 128.

15. Wu ZZ, Kisaalita WS, Wang L, Zachman AL, Zhao Y et al. (2010) Effects of topography on the functional development of human neural progenitor cells. Biotechnol Bioeng 106(4): 649-659.

16. Enzerink A, Salmenpera P, Kankuri E, Vaheri A (2009) Clustering of fibroblasts induces proinflammatory chemokine secretion promoting leukocyte migration. Mol Immunol 46(8-9): 1787-1795.

17. Fischbach C, Kong HJ, Hsiong SX, Evangelista MB, Yuen W et al. (2009) Cancer cell angiogenic capability is regulated by 3D culture and integrin engagement. Proc Natl Acad Sci U S A 106(2): 399-404.

18. Ghosh S, Spagnoli GC, Martin I, Ploegert S, Demougin P et al. (2005) Three-dimensional culture of melanoma cells profoundly affects gene expression profile: a high density oligonucleotide array study. J Cell Physiol 204(2): 522-531.

19. Klapperich CM, Bertozzi CR (2004) Global gene expression of cells attached to a tissue engineering scaffold. Biomaterials 25(25): 5631-5641.

20. Cheok MH, Yang W, Pui CH, Downing JR, Cheng C et al. (2003) Treatment-specific changes in gene expression discriminate in vivo drug response in human leukemia cells. Nat Genet 34(1): 85-90.

21. Zampetaki A, Mitsialis SA, Pfeilschifter J, Kourembanas S (2004) Hypoxia induces macrophage inflammatory protein-2 (MIP-2) gene expression in murine macrophages via NF-kappaB: the prominent role of p42/ p44 and PI3 kinase pathways. FASEB J 18(10): 1090-1092.

22. Weaver VM, Petersen OW, Wang F, Larabell CA, Briand P et al. (1997) Reversion of the malignant phenotype of human breast cells in three-dimensional culture and in vivo by integrin blocking antibodies. J Cell Biol 137(1): 231-245.

23. Pries AR, Reglin B, Secomb TW (2001) Structural adaptation of microvascular networks: functional roles of adaptive responses. Am J Physiol Heart Circ Physiol 281(3): H1015-H1025.

24. Kelm JM, Ehler E, Nielsen LK, Schlatter S, Perriard JC et al. (2004) Design of artificial myocardial microtissues. Tissue Eng 10(1-2): 201-214.

25. Birgersdotter A, Sandberg R, Ernberg I (2005) Gene expression perturbation in vitro--a growing case for three-dimensional (3D) culture systems. Semin Cancer Biol 15(5): 405-412.

26. Frisch SM, Ruoslahti E (1997) Integrins and anoikis. Curr Opin Cell Biol 9(5): 701-706.

27. Watanabe K, Nakamura M, Okano H, Toyama Y (2007) Establishment of three-dimensional culture of neural stem/progenitor cells in collagen Type-1 Gel. Restor Neurol Neurosci 25(2): 109-117.

28. Kuhn HG, Winkler J, Kempermann G, Thal LJ, Gage FH (1997) Epidermal growth factor and fibroblast growth factor-2 have different effects on neural progenitors in the adult rat brain. J Neurosci 17(15): 5820-5829.

29. Peek R, Kammerer RA, Frank S, Otte-Holler I, Westphal JR (2002) The angiopoietin-like factor cornea-derived transcript 6 is a putative morphogen for human cornea. J Biol Chem 277(1): 686-693.

30. Apostolou A, Shen Y, Liang Y, Luo J, Fang S. (2008) Armet, a UPR-upregulated protein, inhibits cell proliferation and ER stress-induced cell death. Exp Cell Res 314(13): 2454-2467.

31.Yu YQ, Liu LC, Wang FC, Liang Y, Cha DQ et al. (2010) Induction profile of MANF/ARMET by cerebral ischemia and its implication for neuron protection. J Cereb Blood Flow Metab 30(1):79-91.

32. Lindholm P, Peranen J, Andressoo JO, Kalkkinen N, Kokaia Z et al. (2008) MANF is widely expressed in mammalian tissues and differently regulated after ischemic and epileptic insults in rodent brain. Mol Cell Neurosci 39(3):356-371.

33. Allerstorfer S, Sonvilla G, Fischer H, Spiegl-Kreinecker S, Gauglhofer C et al. (2008) FGF5 as an oncogenic factor in human glioblastoma multiforme: autocrine and paracrine activities. Oncogene 27(30):4180-4190.

34. Lindholm D, Harikka J, da Penha Berzaghi M, Castren E, Tzimagiorgis G et al. (1994) Fibroblast growth factor-5 promotes differentiation of cultured rat septal cholinergic and raphe serotonergic neurons: comparison with the effects of neurotrophins. Eur J Neurosci 6: 244-252.

35. Reuss B, Hertel M, Werner S, Unsicker K (2000) Fibroblast growth factors-5 and -9 distinctly regulate expression and function of the gap junction protein connexin43 in cultured astroglial cells from different brain regions. Glia 30(3): 231-241.

36. Volante M, Rosas R, Ceppi P, Rapa I, Cassoni P et al. (2009) Obestatin in human neuroendocrine tissues and tumours: expression and effect on tumour growth. J Pathol 218(4): 58-466.

37. Ito Y, Yamamoto M, Li M, Mitsuma N, Tanaka F et al. (2000) Temporal expression of mRNAs for neuropoietic cytokines, interleukin-11 (IL-11), oncostatin M (OSM), cardiotrophin-1 (CT-1) and their receptors (IL-11Ralpha and OSMRbeta) in peripheral nerve injury. Neurochem Res 25(8):1113-1118.

38. Yanagisawa M, Nakashima K, Arakawa H, Ikenaka K, Yoshida K et al. (2000) Astrocyte differentiation of fetal neuroepithelial cells by interleukin-11 via activation of a common cytokine signal transducer, gp130, and a transcription factor, STAT3. J Neurochem 74(4): 1498-1504.

39. Mehler MF, Rozental R, Dougherty M, Spray DC, Kessler JA (1993) Cytokine regulation of neuronal differentiation of hippocampal progenitor cells. Nature 362(6415): 62-65.

40. Nagashima G, Suzuki R, Asai J, Fujimoto T (2002) Immunohistochemical analysis of reactive astrocytes around glioblastoma: an immunohistochemical study of postmortem glioblastoma cases. Clin Neurol Neurosurg 104(2): 125-131.

41. Sharief MK (1998) Cytokines in multiple sclerosis: pro-inflammation or pro-remyelination? Mult Scler 4(3): 169-173.

42. Merrill JE, Benveniste EN (1996) Cytokines in inflammatory brain lesions: helpful and harmful. Trends Neurosci 19(8): 331-338.

43. Planque N, Perbal B (2003) A structural approach to the role of CCN (CYR61/CTGF/NOV) proteins in tumourigenesis. Cancer Cell Int 3(1): 15.

44. Kubota S, Takigawa M. (2007) CCN family proteins and angiogenesis: from embryo to adulthood. Angiogenesis 10(1): 1-11.

45. Lin CG, Chen CC, Leu SJ, Grzeszkiewicz TM, Lau LF (2005) Integrin-dependent functions of the angiogenic inducer NOV (CCN3): implication in wound healing. J Biol Chem 280(9): 8229-8237.

46. Perbal B. (2001) NOV (nephroblastoma overexpressed) and the CCN family of genes: structural and functional issues. Mol Pathol 54(2):57-79.

47. Chevalier G, Yeger H, Martinerie C, Laurent M, Alami J et al. (1998) novH: differential expression in developing kidney and Wilm's tumors. Am J Pathol 152(6): 1563-1575.

48. Calzolari F, Appolloni I, Tutucci E, Caviglia S, Terrile M et al. (2008) Tumor progression and oncogene addiction in a PDGF-B-induced model of gliomagenesis. Neoplasia 10(12): 1373-1382.

49. Sjoborg M, Pietz K, Ahgren A, Yamada N, Lindvall O et al. (1998) Expression of platelet-derived growth factor after intrastriatal ibotenic acid injury. Exp Brain Res 119(2): 245-250.

50. Williams BP, Park JK, Alberta JA, Muhlebach SG, Hwang GY et al. (1997) A PDGF-regulated immediate early gene response initiates neuronal differentiation in ventricular zone progenitor cells. Neuron 18(4): 553-562.

51. Nakao N, Brundin P, Funa K, Lindvall O, Odin P. (1994) Platelet-derived growth factor exerts trophic effects on rat striatal DARPP-32-containing neurons in culture. Exp Brain Res 101(2): 291-296.

52. Koide Y, Sasaki T. (2006) Stanniocalcin-1 (STC-1) as a molecular marker for human cancer. Rinsho Byori 54(3): 213-220.

53. Zhang K, Lindsberg PJ, Tatlisumak T, Kaste M, Olsen HS et al. (2000) Stanniocalcin: A molecular guard of neurons during cerebral ischemia. Proc Natl Acad Sci U S A 97(7): 3637-3642.

54. Serlachius M, Zhang KZ, Andersson LC (2004) Stanniocalcin in terminally differentiated mammalian cells. Peptides 25(10): 1657-1662.

55. Dunn IF, Heese O, Black PM (2000) Growth factors in glioma angiogenesis: FGFs, PDGF, EGF, and TGFs. J Neurooncol 50(1-2): 121-137.

56. Junier MP. (2000) What role(s) for TGFalpha in the central nervous system? Prog Neurobiol 62(5): 443-473.

57. Plate KH, Breier G, Weich HA, Mennel HD, Risau W. (1994) Vascular endothelial growth factor and glioma angiogenesis: coordinate induction of VEGF receptors, distribution of VEGF protein and possible in vivo regulatory mechanisms. Int J Cancer 59(4): 520-529.

58. Zagzag D, Lukyanov Y, Lan L, Ali MA, Esencay M et al. (2006) Hypoxia-inducible factor 1 and VEGF upregulate CXCR4 in glioblastoma: implications for angiogenesis and glioma cell invasion. Lab Invest 86(12): 1221-1232.

59. Nag S, Takahashi JL, Kilty DW (1997) Role of vascular endothelial growth factor in blood-brain barrier breakdown and angiogenesis in brain trauma. J Neuropath Exp Neurol 56(8): 912-921.

60. Krum JM, Rosenstein JM (1998) VEGF mRNA and its receptor flt-1 are expressed in reactive astrocytes following neural grafting and tumor cell implantation in the adult CNS. Exp Neurol 154(1): 57-65.

61. Rosenstein JM, Krum JM (2004) New roles for VEGF in nervous tissue--beyond blood vessels. Exp Neurol 187(2): 246-253.

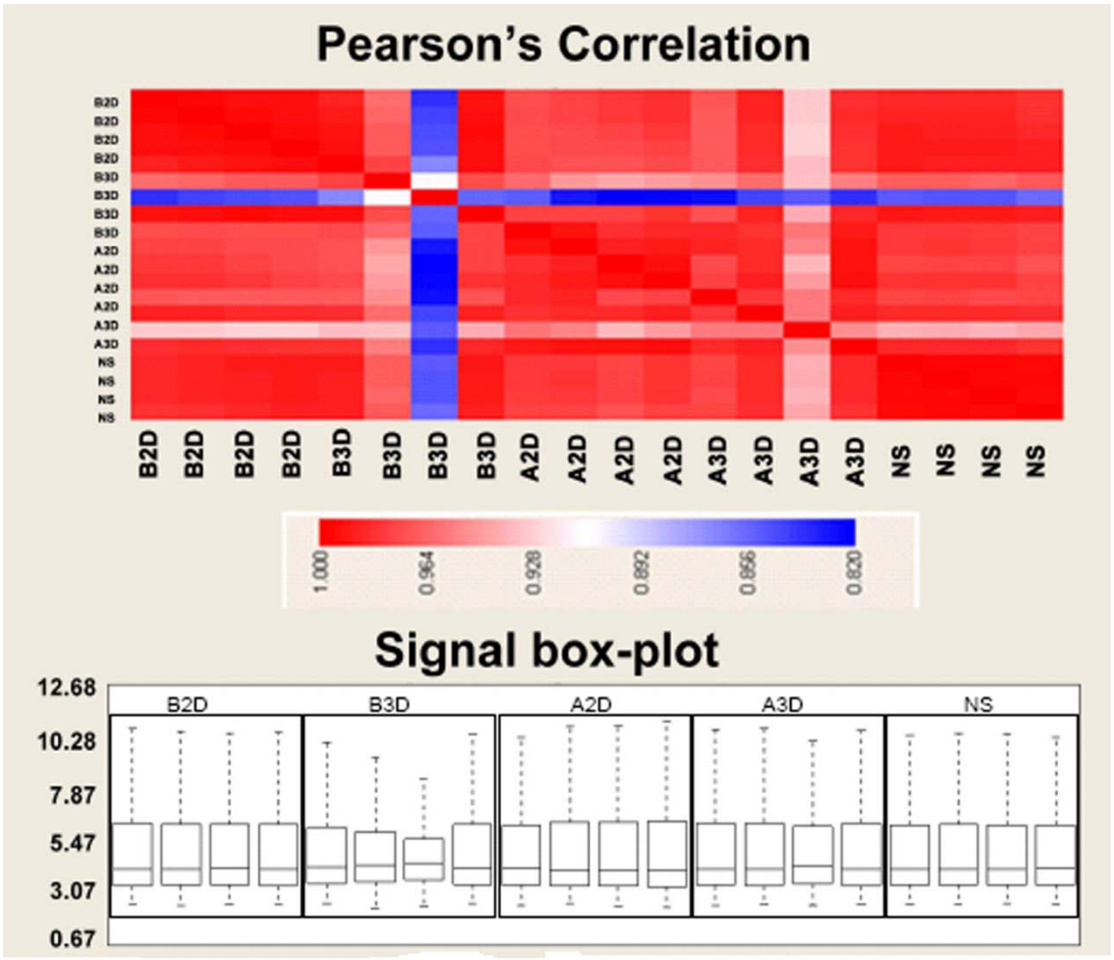

Figure 4. 1 Quality control of Microarray data**.**

The quality of the microarray data was accessed by Pearson's correlation of the samples and the overall distribution of the mRNA expression. The upper panel shows the Pearson's correlation for each pair of the samples. B2D indicate the samples from "Before differentiation, 2D culture condition", A2D "After differentiation, 2D culture", B3D "Before differentiation, 3D culture", A3D "After differentiation, 3D culture", and NS "Neurospheres". Pearson's correlation coefficient is a widely used similarity measure for gene expression data. It measures the similarity between two profiles by calculating the linear relationship of the distributions of the two corresponding random variables. The Pearson's correlation value is indicated the color bar color scale (values close to 1 indicate good correlation). The lower panel shows the box-plot of each sample. The box shows the range of the middle 50% with a line in the center for the median value. Additional lines indicate the overall range of the data.

Table 4. 1 Classification of samples by linear discrimination analysis after cross-validation with 681 cytokine probesets.

From	Number of samples classified to					Total	Error
	2D		3D				
2D	7		1			8	12.5%
3D	2		8			10	20%
Total	9		9			18	16.25%
From	Number of samples classified to					Total	Error
	A2D	A3D	B2D	B3D	NS		
A2D	4	0	0	0	0	4	0
A3D	1	2	0	0	0	3	33.33%
B2D	0	0	3	1	0	4	25%
B3D	0	0	2	1	0	3	66.67%
NS	0	0	0	0	4	4	0
Total	5	2	5	2	4	18	25%

Table 4. 2 Most influential genes in LDA Classification by stepwise selection ($p<0.01$).

Symbol	Title	P value	Up regulated in:
GREM2	gremlin 2, cysteine knot superfamily, homolog (Xenopus laevis)	<.0001	
STC1	stanniocalcin 1	<.0001	3D and NS
GDF3	growth differentiation factor 3	0.0003	3D and NS
IFNA4	interferon, alpha 4	0.0008	3D and NS
NRG1	neuregulin 1	0.006	
INSL5	insulin-like 5 peptide	0.007	3D and NS
GHRL	Ghrelin/obestatin preprohormone	0.0012	3D and NS
LIF	leukemia inhibitory factor (cholinergic differentiation factor)	0.0059	NS
PPBPL2	pro-platelet basic protein-like 2	0.0017	3D and NS
FASLG	Fas ligand (TNF superfamily, member 6)	0.0041	3D and NS
CCL28	chemokine (C-C motif) ligand 28	<.0001	3D
FGF22	fibroblast growth factor 22	0.0016	NS
UCN3	urocortin 3 (stresscopin)	<.0001	3D and NS
CXCL2	Chemokine (C-X-C motif) ligand 2	0.0032	3D and NS
IFNA7	interferon, alpha 7	<.0001	3D and NS
EDN3	endothelin 3	0.005	3D

Table 4. 3 Cytokines up-regulated in both 3D and neurospheres with role examples in cells of nerve tissue origin.

Title	Symbol	Tumorogenesis	Inflammation	Development
angiopoietin-like 7/ cornea-derived transcript 6	ANGPTL7/ CDT6	Reduces tumor growth & acts as a negative regulator of angiogenesis in corneal cells [29].		Maintenance of corneal avascularity [29].
arginine-rich, mutated in early stage tumors/ mesencephalic astrocyte-derived neurotrophic factor	ARMET/ MANF	Inhibits tumor cell proliferation under hypoxia induced ER stress & protects tumor cells from ER stress-induced death [30].	Protects neurons from ER stress. Promotes neuron proliferation & prevents apoptosis during neuro-degeneration [31]	Expressed in developing nigro-striatal system at P1 & P10, suggesting a role in development of midbrain dopaminergic neurons [32].
Bone morphogenetic protein 8b (osteogenic protein 2)	BMP8B			
chemokine (C-C motif) ligand 13	CCL13			
fibroblast growth factor 5	FGF5	Oncogenic activities in astrocytic tumours by promoting growth, survival and migration & supporting neoangiogenesis [33].		Regulates neuron differentiation, survival [34], as well as astroglial properties [35].
Ghrelin/obestatin preprohormone	GHRL	Regulates tumor proliferation [36].		
interleukin 11	IL11			Neuropoietic effect on neurons [37]. Astrocyte [38] & neuronal differentiation [39].
interleukin 1,	IL1B	Expressed by glial	Pro-inflammatory	Inducer of

beta		cells around a tumor that are involved in immune reactions against the tumor & the damage caused by it [40].	causes neural damage after CNS injury by inducing nitric oxide, free radicals & neurotoxins. Induces astrocytes to produce GFs that affect survival & proliferation of oligodendrocytes [41].	remyelination [42].
nephroblastoma overexpressed gene	NOV	Associated with tumorogenesis, tumor differentiation, metastasis [43] & angiogenesis [44].	Regulates angiogenesis and fibroblast functions during wound healing [45].	Expressed in early stages (E3) neuroepithelium and later stage (E3–E7) neural tube [46]. Detected highly in human neuronal cells and axons [47]. Embryonic vascular development [44].
platelet-derived growth factor beta polypeptide (simian sarcoma viral (v-sis) oncogene homolog)	PDGFB	Induces the formation & progression of gliomas in neural progenitor cells. Required to overcome cell-cell contact inhibition and confers *in vivo* infiltrating potential to tumor cells [48].	Released by astrocytes and neurons after injury. Important for neuroprotection and repair in connection with neural disease and injury [49].	Neuronal development and diffentiation of undifferentiated NE cells directly to neurons [50]. Increases survival and neurite outgrowth of fetal striatal neurons [51].
stanniocalcin 1	STC1	Marker of human cancer. Regulates tumor size, proliferation & micrometastases	Protects neurons from oxidative & hypoxic stress [53].	Regulates terminal differentiation of neural cells [54].

		[52].		
transforming growth factor, alpha	TGFA	Mitogenic for glioma cell lines. Participates in angiogenesis of glioma by inducing expression of VEGF [55].		Regulates neural progenitors proliferation/cell fate choice, neuronal survival/differentiation, astrocytic reactivity & has neurotrophic effects on neurons [56].
vascular endothelial growth factor A	VEGFA	Induces angiogenesis, promotes cell migration & invasion potential of glioma cells [57,58].	Role in blood-brain barrier (BBB) breakdown and angiogenesis after brain injury [59]. Astrocytes in the perilesional area express VEGF-A early after injury [60].	Shows angiogenic, blood–brain barrier permeabilizing, neurotrophic, gliotrophic, and anti-apoptotic actions. [61].

CHAPTER 5

PERFORMANCE EVALUATION OF 3D POLYSTYRENE 96-WELL PLATES WITH HUMAN NEURAL STEM CELLS IN A CALCIUM ASSAY*

*Lai Y and Kisaalita WS. To be submitted to *Journal of Laboratory Automation*

5.1 Abstract

In this study, we have generated a HTS compatible 3D cell culture platform by chemically welding polystyrene scaffolds into standard 2D polystyrene 96-well plates. The variability of scaffolds was minimized by introducing automation into the fabrication process. The fabricated 3D cell culture plates were compared with several commercially available 3D cell culture platforms with light and SEM microscopy. Voltage gated calcium channel functionality was used to access the Z'-factors of all plates including a 2D standard plate control. We found that with No-Wash (NW) fluo-4 calcium assay and neural progenitor cells, all plates display acceptable Z'-factors for use in HTS. Our plates have several advantages, such as versatility, economical and are ready-to-use off the shelf. These characteristics are especially desired in pre-clinical drug discovery applications.

Keywords: 3D cell culture, Scaffold, HTS, Voltage gated calcium channel, HTS, Progenitor cell, Cell based assay, Drug discovery

5.2 Introduction

Traditionally, flat surface two dimensional (2D) based cell cultures are widely used in pre-clinical drug discovery studies. However, recent studies have shown that three dimensional (3D) cell cultures provide more physiologically relevant results and should be the preferred choice to be implemented in high throughput screening (HTS) platforms. Currently, there are several commercially available, "ready-to-use" 3D cell culture systems for HTS. A fraction of these systems are based on natural or synthetic structures designed to provide some elements found in *in vivo* extracellular matrix (ECM) [1]. Examples include Extracel™ and HyStem™ hyaluronic acid-based hydrogels from Glycosan BioSystems, HydroMatrix™ Peptide Hydrogel, and MaxGel™ Human ECM both marketed by Sigma-Aldrich. Another fraction is comprised of structures that purely provide 3D microspaces. Examples include Micro-Space Cell Culture plate from Kuraray, 3D Insert™ from 3D Biotek, and Algimatrix from Invitrogen. Also, there are a few systems that are scaffold free, where other conditions (e.g. gravity) are provided that promote the formation of microtissues without a need for scaffolding. The most well known example is the recently introduces Perfecta^{TM} 3D hanging drop plates marketed by 3D Biomatrix^{TM}

In comparison to standard polystyrene 2D multiwall plates, 3D plates can cost between 5- and 165-fold. At the same time, there is relentless pursuit to lower the screening cost per compound in the drug discovery HTS labs. In response to this need, we developed a patent-pending process to convert a standard 2D polystyrene plate into 3D plates, by chemically welding polystyrene scaffolds into standard 96-well plates [2]. A similar idea has been independently developed by Knight et al [3] and is being marketed as Alvetex ®; however no HTS compatible products have been provided. The first prototype in our lab revealed

unacceptable well-to-well variability and we have addressed this problem by using an automated fluid handling robot Biomek NP for key operations in the fabrication process. In this paper we have evaluated the performance of the polystyrene plates with a high K^+ voltage gated calcium channel (VGGC) gating assay in neural stem cells and we have compared the performance to 2D plate equivalent as well as a few commercially available plates. While the results show a lower Z'-factor in comparison to 2D, the porous polystyrene 3D plate performance is comparable to the more expensive plates included in the study.

5.3 Materials and Methods

5.3.1 Materials and reagents

Neural progenitor cells were obtained from Regenerative Bioscience Center at University of Georgia as well as Millipore (ENStem-A™, Billerica, MA). Polystyrene, chloroform, ammonium bicarbonate, glutaraldehyde, and sodium cacodylate buffer were obtained from Sigma (St. Louis, MO). Neural basal medium, penicillin/streptomycin, L-glutamine, recombinant human leukemia inhibitory factor (hLIF), basic fibroblast growth factor (bFGF), B-27 supplement and phosphate buffered saline (PBS) were obtained from Gibco (Gaithersburg, MD). Fluo-4 No-Wash (NW) calcium assay kit and Algimatrix cell culture plates were obtained from Invitrogen (Carlsbad, CA). Celltreat 3D Insert™-PS Cell Culture Plates were purchased from Chemglass Life Science (Vineland N.J). Extracel™ Hydrogel Kit was obtained from Glycosan (Alameda, CA).

5.3.2 Neural progenitor cell culture

Human neural stem cells or neural progenitors (NP) were maintained as described in Cheng et al. [2]. The growth medium for NP cell was neural basal medium (Invitrogen, PA) supplemented with penicillin/streptomycin, L-glutamine, recombinant human leukemia

inhibitory factor (hLIF), bFGF and B-27. Medium was half changed every 48 hours. For subculturing, 90% confluent cells were aspirated by pipetting and the subculture ratio was typically 1:2 to 1:3. Before cell seeding, both the 3D polystyrene scaffolds (ours and 3D Insert™-PS Cell Culture Plates) and 2D 96 well plates were coated with poly-ornithine and laminin to promote better cell adhesion. The subculture of NP cells in Algimatrix and Extracel™ Hydrogel was done according to manufacturer's instruction. Where no specific seeding density was required by the manufacturer, we seeded the plate at 10000 cells per well.

5.3.3 Multi-well plate fabrication with Biomek NP

The scaffold fabrication process is illustrated in Figure 5.1. Briefly, a viscous polymer solution was prepared by dissolving polystyrene (PS) in chloroform. Sieved ammonium bicarbonate particles in the range of 40-60 μm were added to the polymer solution and mixed thoroughly. The paste mixture of polymer/salt/solvent was poured into a reservoir suitable for robotics. The reservoir was immediately covered to minimize the evaporation of chloroform. The cover has 96 holes for easy access by the Biomek NP controlled pipet tips. Since ammonium bicarbonate particles tend to sink to the bottom of the reservoir, the mixture solution was pipetted up and down three times before transferring to plates in order to improve the uniformity. 15 to 30 μl of the mixture was transferred to each well of the 96-well plates and the plates were shaken at 200 RPM for 20 seconds both counter-clockwise and clockwise to ensure even distribution of the mixture. The plates were then left to air dry. The above procedures were carried out by Beckman coulter's robotics Biomek NP to improve efficiency and consistency. After chloroform was completely evaporated under atmospheric condition as well as byvacuum drying overnight, the plates were immersed into 37 °C water for overnight. Not only ammonium bicarbonate is easily dissolved in water, at temperatures above 36 °C, but it decomposed to ammonia, carbon dioxide,

and water, creating porous polymer scaffolds. After fabrication, the scaffolds were subjected to oxygen plasma treatment with PLASMOD^{TM} oxygen plasma system for 60 seconds to increase the hydrophilicity of the material.

5.3.4 No-Wash (NW) calcium assay

10 mL NW fluo-4 dye loading solution was prepared immediately before each experiment according to manufacturer's protocol. The growth medium in the plates was removed and 100 µl of the dye loading solution was quickly but carefully added into each well. The plates were then incubated for 45 minutes at 37 °C in a standard incubator. The fluorescence signals were monitored and recorded on the FlexStation (Molecular Device, Sunnyvale, CA) every 3 seconds with excitation wavelength of 485 nm and emission wavelength of 538 nm. High potassium buffer was added to the plates at 34 seconds and the calcium transient signals were recorded for 100 seconds.

The Z'-factor is calculated using the formula:

$$Z' = 1 - \frac{3(SD_p + SD_n)}{(S_p - S_n)}$$

Where Sp is the signal recorded upon addition of high potassium buffer, and Sn is the signal using normal buffer which serves as negative control. Eight replicates were generated for each of these signals. A "response magnitude" was calculated as (F-F0) /F0, where F is the peak value upon addition of high potassium buffer and F0 is the basal signal. For negative control group, we choose the maximum fluorescence as F after buffer addition to calculate the response magnitude.

5.3.5 SEM imaging

Cells in scaffolds were fixed with 2% glutaraldehyde in 0.1 M sodium cacodylate buffer (pH 7.2) for 1 h and then rinsed in cacodylate buffer three times (15 min each). The samples

were then dehydrated in 35, 50, 70, 80, 95 and 100% ethanol successively for 10 min each and dried in a SAMDRI-780A critical point drier (Tousimis Research Corporation, MD). Scaffolds were sputter-coated with gold for 60 s to achieve a thickness of about 15.3 nm. SEM images were captured with LEO 982 scanning electron microscope (LEO Electronenmikroskopie GmbH Korporation, Germany) with an acceleration voltage of 4 kV.

5.4 Results

5.4.1 Fabrication and characterization.

The fabrication process of 96-well plates was modified from Cheng et al. [2]. Beckman coulter robotic liquid handler Biomek NP was used to implemented automation into the fabrication process. Before application, Biomek NP was calibrated according to manufacturer's instruction to ensure the best accuracy and precision. The fabrication process is illustrated in Figure 5.1 (A). The process can be divided into two parts: 1) carried out by robotic liquid handler Biomek NP and 2) carried out manually outside Biomek NP. We first prepare a viscous polystyrene polymer solution by dissolving polystyrene in chloroform with ammonium bicarbonate particles. The ammonium bicarbonate particles were sieved to include only the sizes range from 40 μm to 60 μm. The paste mixture was poured into a Biomek NP compatible reservoir (Axygen, Union City, Ca) so that 96 pipette tips can transfer the liquid from this reservoir simultaneously. 96 well openings (5 mm in diameter) were drilled on the cover of the reservoir so that the evaporation of chloroform can be minimized without blocking the openings for easy access of the pipette tips. 15-30 μl of the mixture was transferred to each of the well by the liquid handler and immediately followed by shaking with low speed to evenly spread the viscous mixture. The plates were covered to control the evaporation of the chloroform so it slightly dissolved the surface of the polystyrene in the plates to firmly fix the scaffolds to the

polystyrene plates. After chloroform was completely evaporated, the plates were collected and immerse into 37 ^{o}C water to ensure complete removal of the salt particles. The baking process described in Cheng et al. [2] was omitted for the 96 well plates since the adhesive used to glue the glass to the plates was sensitive to heat. The plates were sterilized by exposing to UV light in a biohazard laminar flow hood for overnight. While automation improved the consistence of the plates fabricated as expected, in some wells, the scaffold was not well aligned with the bottom glass. Such wells were excluded from the follow up studies. Further process improvement are needed to eliminate such wells from the plates. However the plates are versatile as it is possible to change physical properties such as porosity, thickness and light transmittance by altering the composition of the starting mixture, the amount of liquid and even the material itself. In the following study we used salt/polymer weight of 15/1 (wt/wt) and 20 µl mixture for each well which has been well tested in our previous studies [2]. Please note that the properties can be tailored for other cells.

5.4.2 Morphology of different 3D 96-well plates.

The neural progenitor (NP) cells used in this study are derived from human embryonic stem cells and are feeder-free. These cells have been shown to be good cell model to study the human neuronal cell functions [4,5]. To test whether our plates are suitable for HTS and whether they are comparable to the commercially available plates, we cultured NP cells on traditional 2D plates, our PS porous 3D plates as well as three commercially available plates (Algimatrix, 3D Insert^{TM}-PS Cell Culture Plates, and Extracel™ Hydrogel Kit). Figure 5.2 (A-E) shows the light microscopy images of NP cells cultured on 2D plates and in 3D plates. It is clear that 2D cultured cells can be viewed individually by light microscopy easily, while in all the 3D plates, it is somewhat difficult to observe the detailed structures of single cells. In Figure 5.2 (D&E), cell

spheroids (identified by arrows) formed in the 3D culture vessels are visible. Due to the fact that these spheroids are at different height, we were not able to take one picture with all the spheroids in focus. For the Algimatrix, since there were a lot of bubbles released by the scaffolds after cell seeding, we were not able to see the spheroids very clearly either. According to the manufacturer's manual, the bubbles disappear after several days of culturing. But for short term culturing as in our study, the bubbles can be a problem for observation.

Our porous scaffolds and the 3D Insert^{TM}-PS Cell Culture Plates were both not spheroid based and the structure of the cells was further investigated by SEM as shown in Figure 5.3 (A-I). Figure 5.3 (A-D) are NP cells on our porous scaffolds that have been cultured for three days. A, B and C are top views with different magnification. D is the side view showing cells that penetrated deep into the scaffolds. The cells did not form spheroids directly in our scaffolds. Instead they scattered in the scaffolds with rounder shape and short neurites. After a longer period of culturing (e.g., 10 days), the cells formed spheroids in the cavities of the scaffolds (Figure 5.3. E & F). For the 3D Insert^{TM}-PS Cell Culture Plates, without coating of ECM proteins (e.g., laminin in our case), NP cells formed spheroids and loosely floated in the culture medium (data not shown) and were easily washed away by pipetting. Thus we coated the scaffolds with polyorithine and lamine as we did for the 2D polystyrene dishes. As shown in Figure 5.3 (G-I), NP cells attached to the polystyrene fibers and most of the cells had a flatten shape just as they were on 2D surfaces.

5.4.3 NW calcium assay

We chose the calcium assay for this study, because ion channels have emerged as an attractive drug discovery target class for modern drug discovery [6,7,8]. Ion channels have been discovered to be associated with neuronal signal transduction, muscle contraction, T-cell

activation, cell proliferation, apoptosis and other important cellular functions. Recent ion channel studies have expanded from targets for CNS and cardiovascular disorder to targets for other diseases such as cancer [9] and immune disorders [10]. Unlike some enzyme and receptor targets which can be screened with high throughput biochemical assays, ion channels rely heavily on cell-based assay for both primary and secondary screening [11]. Thus the development of efficient, physiologically more relevant, HTS compatible cell-based assay is essential for ion channel targeted drug discovery.

The cells were loaded with a membrane permeable dye NW Fluo-4 which has been specially designed for HTS application, with no wash steps. However, it still requires the complete removal of the culture medium. The intracellular calcium concentration was monitored by the fluorescence intensity changes with FLEXstation microplate reader for 100 seconds. At 34 seconds, a buffer with or without high potassium was added by the automatic liquid transferring function of the FLEXstation. Typical time course fluorescence intensity changes are shown in Figure 5.4. We observed that cells on 2D surface have relatively higher peaks after the addition of high potassium than all the 3D plates tested. The cells cultured in 3D Insert^{TM}-PS Cell Culture Plates had relative higher peaks compared to the cells cultured on other 3D plates. The rest had comparable peak values. The Z'-factor values calculated are listed in Table 5.1. Again, 2D plates have a much better Z'-factor than all the 3D plates. Our porous scaffolds yielded similar Z'-factor values as invitrogen's Algimatrix and glyconsan's Extracel™ Hydrogel.

5.5 Discussion

Although the necessity to use a more complex *in vitro* model (e.g., 3D cultured cells) for drug discovery has been demonstrated in the recent decades, it is not easy to implement the 3D cell cultures in real HTS applications. The Z'-factor, after being developed by Zhang et al. in

1999 [12], has become a popular tool in HTS assay development for comparison and evaluation of the quality of assays. A useful HTS assay should have a Z'-factor score between 0.5-1.0. As observed in our study, 2D plates have an excellent Z'-factor of 0.790 which is close to the reported NW Fluo-4 calcium assay's Z'-factor (0.842 with jurkat cells and 0.827 with HEK293 cells) by Invitrogen (http://www.invitrogen.com/site/us/en/home/Products-and-Services/Applications/Drug-Discovery/Target-and-Lead-Identification-and-Validation/g-protein_coupled_html/cell-based-second-messenger-assays/fluo-4-am-fluo-4-nw-calcium-indicators.html, last accessed on Oct. 7th, 2011). The differences between our 2D assay's Z'-factor and the company's reported ones may result from the use of different cells, stimulant drugs and instrument. All the 3D plates have a lower but acceptable Z'-factors, with 3D Insert™-PS Cell Culture Plates having the highest score of 0.671. As shown in the material and method part, in order to get a higher Z'-factor, the assay should have an overall low well to well variability (to lower the standard deviation) and high difference between positive and negative response magnitudes (to increase the (Sp-Sn)). As shown in Table 5.1, all assays have small standard deviation and near zero negative control's response magnitude, which indicated that the main difference of Z'-factor is a result from the positive response magnitude. We have previously reported that 2D cells have exaggerated VGCC calcium transient signal when compared to 3D cells [2]. Exaggerated VGCC calcium transient signal generates high positive response magnitude which may be the reason why 2D has a better Z'-factor compared to all the 3D plates. The exaggerated cellular responses may then place a high confidence in the assay as reflected by its high Z'-factor which may not be warranted from *in vivo* physiology context.

Among the four 3D plates, Insert™-PS Cell Culture Plates have a better Z'-factor of 0.671 and a high average positive response magnitude. As shown in Figure 5.3 (G-I), the cells

cultured on Insert™-PS Cell Culture Plates attached to the surface of polystyrene fibers and had a morphology similar to 2D cultured cells. The reason for the better Z'-factor score for Insert™-PS Cell Culture Plates may result from the fact that the cells on this scaffolds are actually a mixture of 2D and 3D cells. Claimed to be 3D cell culture, the 3D Insert™-PS plates were not so 3D after coating with ECM proteins. According to the manual for this product, the plates are normally used without coating. However, as the application of stem cells in drug discovery grows, it's relatively difficult to use a culture vessel without introducing the ECM proteins. Stem cells are much more difficult to adhere to non-coated surfaces and they would more likely stick to each other and float in the medium as opposed to stay in the openings of the scaffolds, especially when forces were applied to them such as in washing steps or buffer changing steps. We observed floating cell spheroids around the 3D insert when no coating was introduced. When the plates were coated with laminin, a lot of cells attached to the fibers and formed flat morphology just as they were grown on 2D flat surfaces. There may be spheroids entrapped in between fibers since we observed increased cell spheroids numbers around the insert after medium change. But after so many wash steps required in SEM sample preparation, we were not able to observe the spheroids in SEM pictures.

Our scaffolds generated similar Z'-factors as Algimatrix by Invitrogen and Extracel™ Hydrogel by Glycosan. However, our porous scaffold plate offers several advantages over the others. The key feature comparisons of the tested plates are summarized in Table 5.2. First, our porous plates are versatile. We can adjust the parameter (e.g., pore size, porosity and etc) easily during fabrication to tailor to different applications. We can use the plates with or without coating of ECM proteins, which makes introducing 3D chemical cues on surface easy. We can also seed one plate partially and still be able to use the rest of the plate later. Algimatrix plates

are very sensitive to moisture. If moisture is introduced before cell seeding, the morphology of the scaffold will change and cell seeding will be more difficult. Thus Algimatrix plates cannot be coated with ECM proteins and the whole plate has to be used in one time. Second, our plate is easy to store and transport. Since the main component of our plates is polystyrene, just as the regular 2D plates. They can be treated as those polystyrene 2D plates and stored at room temperature. The other plates more or less require some special treatment during storage and transportation, e.g., Algimatrix plates have to be packaged with desiccant and Extracel hydrogel requires low temperature. Last but not the least, our plates are very economical. With the major raw material being polystyrene, sodium bicarbonate and chloroform, the cost to produce our plates can be kept to the minimum.

In conclusion, cells cultured on 2D surfaces have exaggerated calcium signals compare to those in 3D culture systems. It may be better to use the more physiologically relevant 3D culture based assay to more effectively eliminate false positive hits and improve the overall yield from drug screening campaigns. Compared to the tested commercial available 3D plates, our plate has similar Z'-factor with several advantages: 1) the properties of the scaffolds can be easily adjusted in the product fabrication process; 2) it is versatile to introduce ECM coating in the system; 3) it is relatively more economical; and 4) it is easier to store and is ready-to-use off the shelf.

5.6 References

1. Murugan R, Ramakrishna S (2006) Nano-featured scaffolds for tissue engineering: a review of spinning methodologies. Tissue Eng 12: 435-447.

2. Cheng K, Lai Y, Kisaalita WS (2008) Three-dimensional polymer scaffolds for high throughput cell-based assay systems. Biomaterials 29: 2802-2812.

3. Knight E, Murray B, Carnachan R, Przyborski S (2011) Alvetex(R): polystyrene scaffold technology for routine three dimensional cell culture. Methods Mol Biol 695: 323-340.

4. Dhara SK, Hasneen K, Machacek DW, Boyd NL, Rao RR, et al. (2008) Human neural progenitor cells derived from embryonic stem cells in feeder-free cultures. Differentiation 76: 454-464.

5. Breier JM, Gassmann K, Kayser R, Stegeman H, De Groot D, et al. (2010) Neural progenitor cells as models for high-throughput screens of developmental neurotoxicity: state of the science. Neurotoxicol Teratol 32: 4-15.

6. Mathie A (2010) Ion channels as novel therapeutic targets in the treatment of pain. J Pharm Pharmacol 62: 1089-1095.

7. Macphee C (2004) New advances in drug discovery. Expert Opin Investig Drugs 13: 1213-1215.

8. Molokanova E, Savchenko A (2008) Bright future of optical assays for ion channel drug discovery. Drug Discov Today 13: 14-22.

9. Arcangeli A, Crociani O, Lastraioli E, Masi A, Pillozzi S, et al. (2009) Targeting ion channels in cancer: a novel frontier in antineoplastic therapy. Curr Med Chem 16: 66-93.

10. Varga Z, Hajdu P, Panyi G, Gaspar R, Krasznai Z (2007) Involvement of membrane channels in autoimmune disorders. Curr Pharm Des 13: 2456-2468.

11. Zheng W, Spencer RH, Kiss L (2004) High throughput assay technologies for ion channel drug discovery. Assay Drug Dev Technol 2: 543-552.

12. Zhang JH, Chung TD, Oldenburg KR (1999) A Simple Statistical Parameter for Use in Evaluation and Validation of High Throughput Screening Assays. J Biomol Screen 4: 67-73.

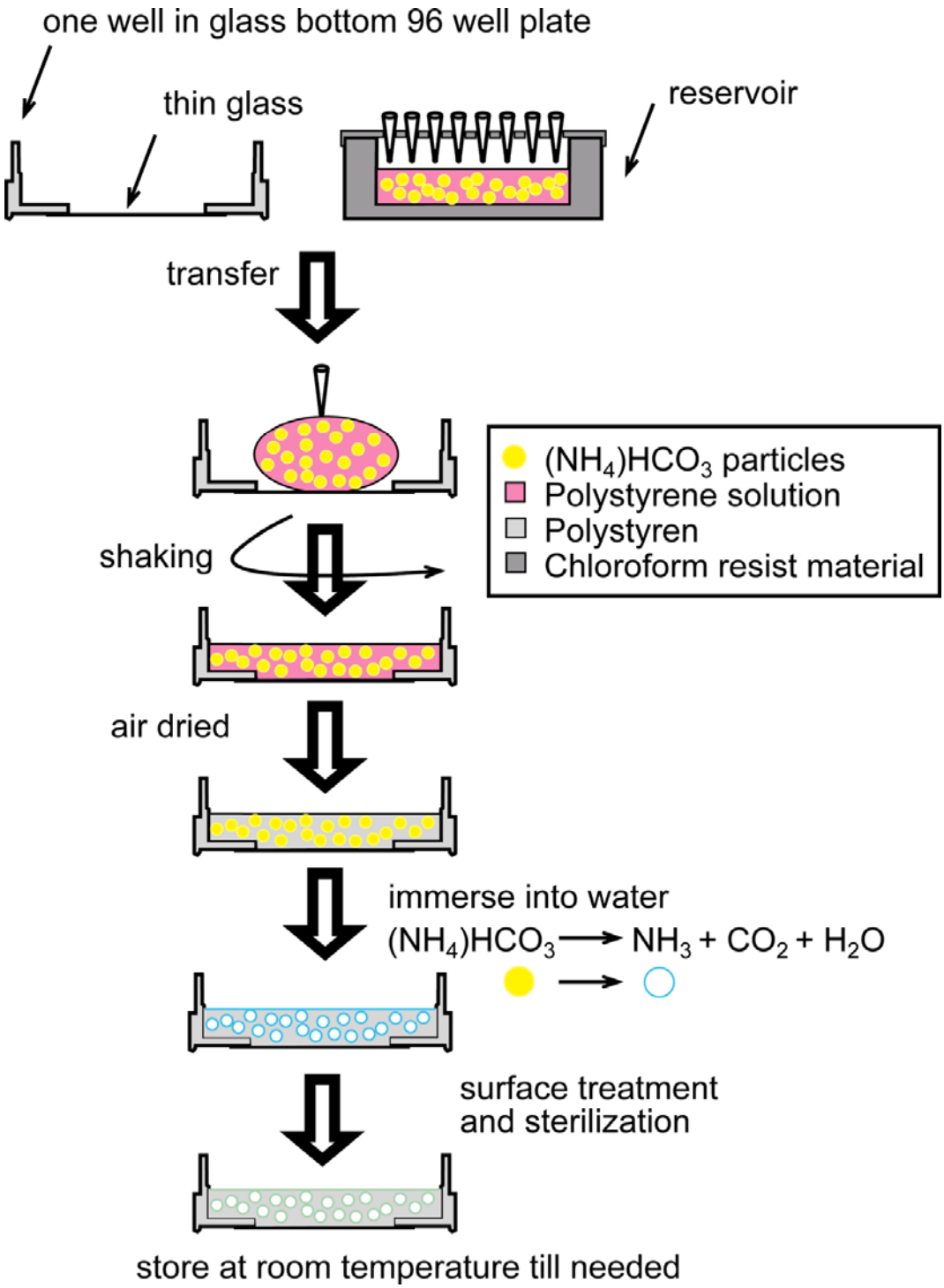

Figure 5. 1 Fabrication of polystyrene 3D porous scaffold 96 well plates.
Key procedures up till air dried are done with automation.

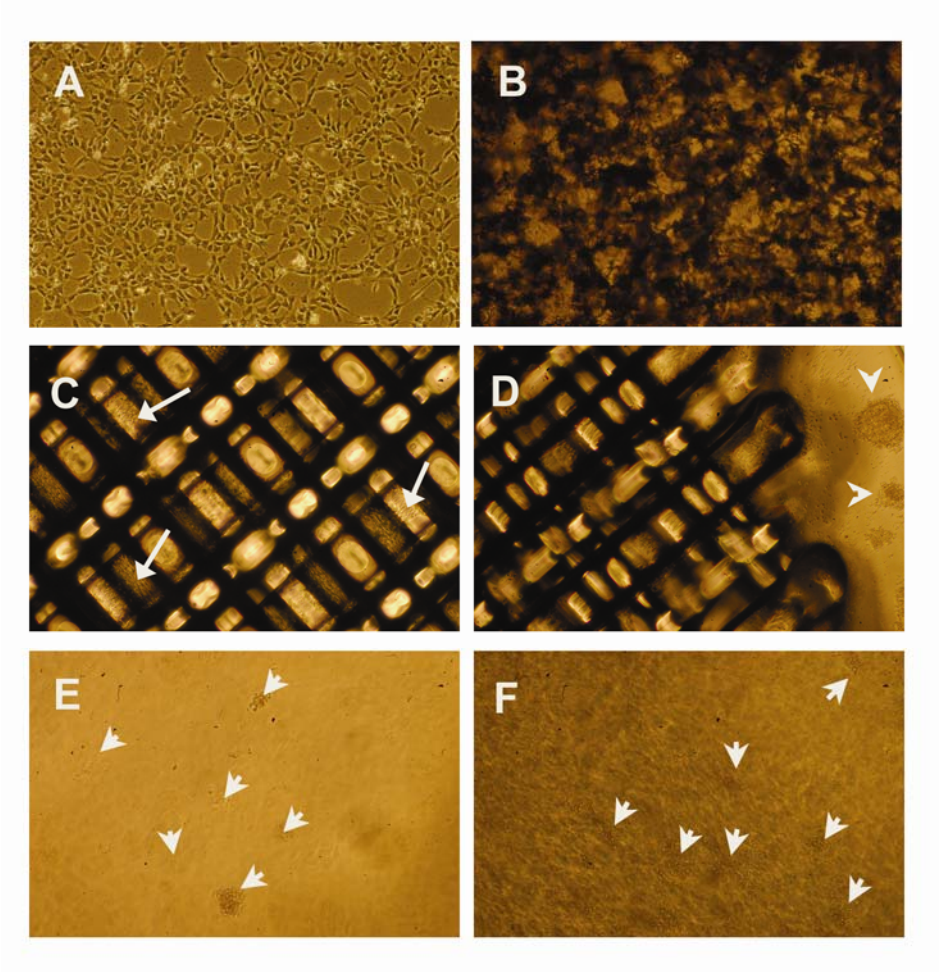

Figure 5. 2 Light microscopy of NP cells cultured in different condition.
(A) NP cells cultured on 2D flat surfaces. (B) polystyrene porous scaffold-based 3D plates, (C-D) Celltreat 3D Insert™-PS Cell Culture Plates, arrow in C pointed to visible cells, arrowhead in D pointed to floating cell clusters outside the scaffold (E) Extracel™ Hydrogel (F) Invitrogen Algimatrix; arrows in E and F pointed to cell spheroids (some are out of focus due cells on different height)

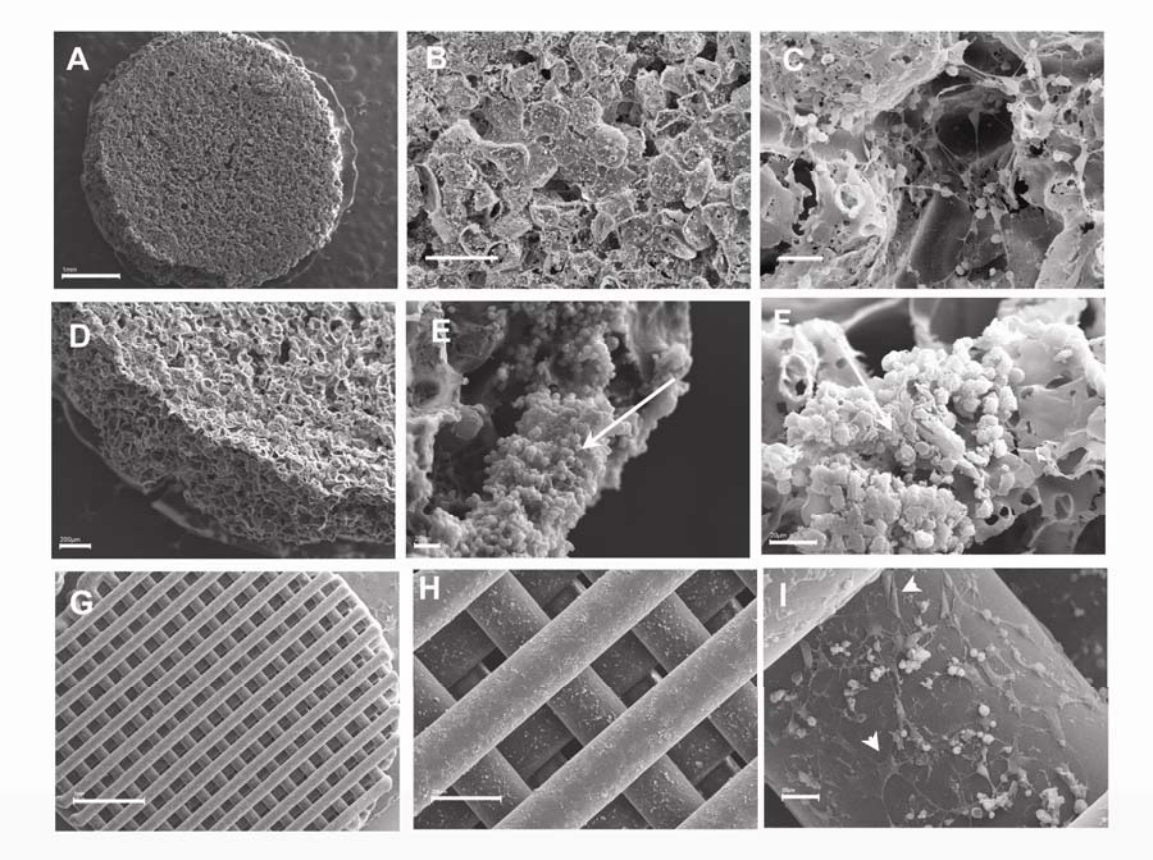

Figure 5. 3 SEM images of selected 3D 96-well plates.
(A-C) are top view of SEM images of the porous polystyrene scaffolds with different magnification, the scaffolds were coated with polyorithine and laminin; (D) the same scaffolds viewed from side. (E)-(F) showing cluster of cells (pointed by arrows) inside the scaffolds after elongated culturing time (7 days). (G-I) are SEM pictures of Celltreat 3D Insert^{TM}-PS scaffolds with different magnification. Scale bars represent 1 mm in (A) and (G), 200 μm in (B), (D) & (H), and 20 μm in rest of figures.

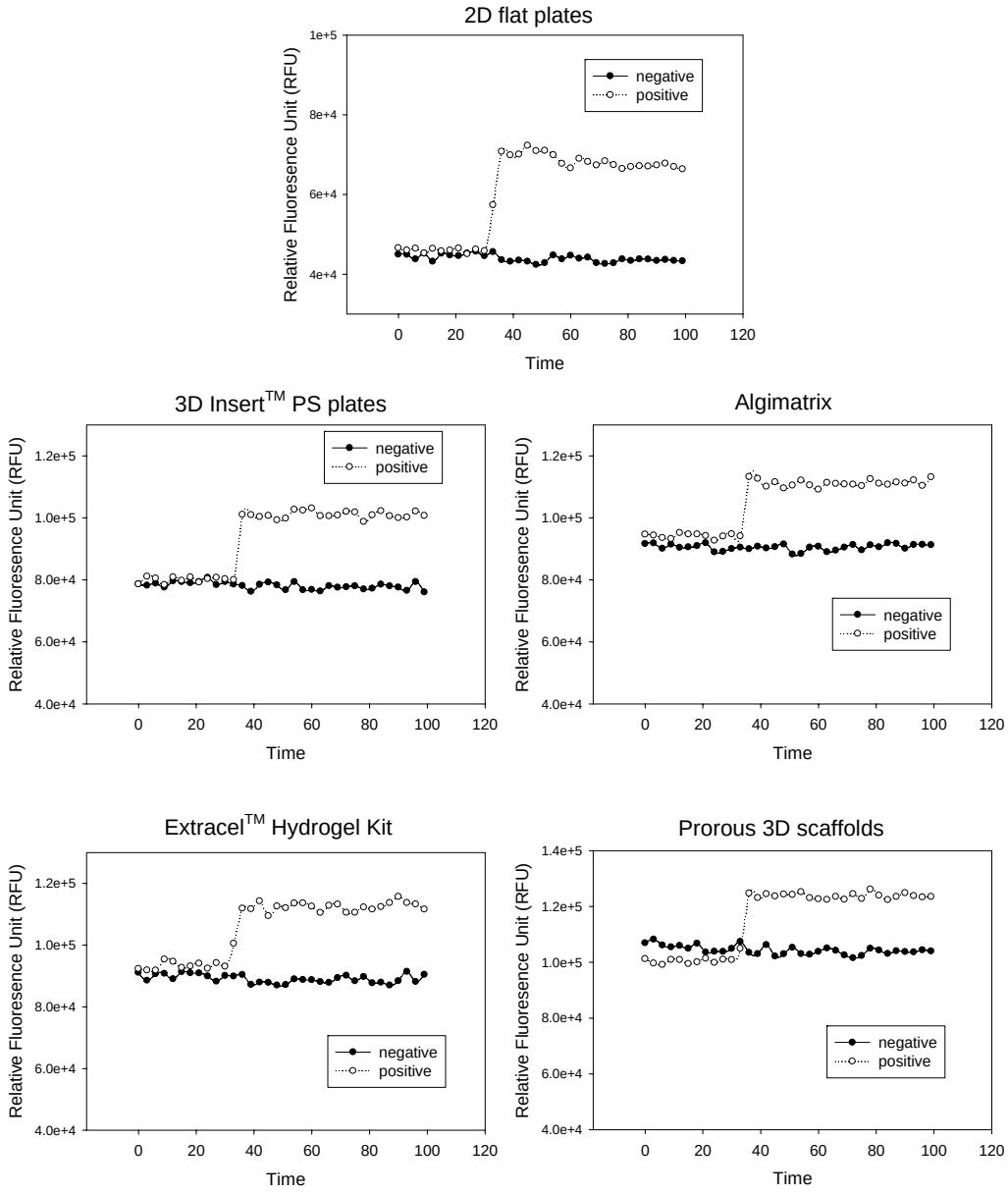

Figure 5. 4 Representative NW Fluo-4 fluorescence time-course measured by Flexstation for different plates.

Table 5. 1 Z'-factors for NW calcium assay

Type	2D	Porous	Fibrous	Algimatrix	Glycosan
Z'-factor	0.790	0.516	0.671	0.522	0.548
Mean signal (F-Fo)/Fo	0.587	0.253	0.359	0.198	0.271
SD	0.032	0.035	0.031	0.021	0.031

Z'-factors were calculated from 8 replicates.

Table 5. 2 Feature comparisons of the tested 3D cell culture platforms

Attributes	Porous PS scaffolds	3D Insert™-PS Cell Culture Plates	Algimatrix	Extracel™ Hydrogel Kit
Company	N/A	3D Biotek	Invitrogen	Glycosan
Material	Polystyrene synthetic	Polystyrene synthetic	Alginate natural	Hydrogel natural
Pore size	Flexible: 40-60 μm 60-100 μm 100-150 μm	~200 μm	50-400 μm	N/A
Fiber diameter	N/A	~150 μm	N/A	N/A
Mechanical	High	High	Med	Low
Ready-to-use	Yes	Yes	Yes	No*
Microscopy	Opaque	Opaque	Opaque	Transparent
Cell recovery	Trypsin	Trypsin	Dissolving reagent	Dissolving reagent
Scaffold removal	Hard	Easy	Easy	Hard
Storage	RT	RT	RT with desiccate	Freezer
Price	N/A	$824/for 96 wells	$194/plate (96 well plate)	$180/enough for one 96 well plate

*Although claimed to be ready-to-use by the merchandiser, we classified it as not ready-to-use because mixing and transferring steps are required.

CHAPTER 6

SUMMARY AND CONCLUSIONS

6.1 Summary and Conclusions

This dissertation targeted at promoting 3D cell culture platforms for neuronal cells in pre-clinical drug discovery application by 1) providing better evidence for 3D cultured neuronal cell's *in vivo* emulation, 2) attempting to generate three dimensionality markers for better 3D culture platform definition, and 3) developing a HTS compatible 3D cell culture platforms with reduced cost.

Utilizing freshly dissected superior cervical ganglion as *in vivo* surrogate, we successfully demonstrated that Neonatal mouse SCG cells cultured in 3D PLLA or PS scaffolds have better physiological relevance than the cells cultured on 2D substrates with respect to high K+-mediated calcium transient. The exaggerated VGCC function from 2D cultured SCG cells may partly be explained by differences in membrane architecture, characterized by uniquely organized caveolar lipid rafts and the cytoskeleton.

The comparative transcriptomic data obtained by us revealed that the 3D cultured cells in various formats are different from their 2D counterparts in terms of gene expression. Furthermore, up-regulated cytokines' transcripts, independent of culture format, have been identified; a group of 13 cytokines commonly up-regulated in cells cultured in polystyrene scaffolds and neurospheres have potential to provide one or a combination to serve as three-dimensionality biomarkers. These results are supportive of further cytokine identification and *in vitro*/*in vivo* validation studies with cells from non-neural tissue.

Utilizing automation and robotics, we have successfully fabricated HTS compatible 3D cell culture formats as the first step for our 3D cell culture platforms to be adopted by pre-clinical drug discovery industry. Compared to the tested commercially available 3D plates, our plate has similar Z'-factor for NW fluo-4 calcium assay stimulated by high potassium depolarization, suggesting acceptable HTS compatibility. Our 3D cell culture plates have the following advantages comparing to the tested commercially available products: First, the properties of the scaffolds can be easily adjusted in the fabrication process. Second, it is very easy to coat the plates with ECM proteins for added complexity and enhanced cell attachment. Third, the simple fabrication, storage and transportation make the plates relatively more economical. Fourth, the plates are true ready-to-use without further preparation needed.

6.2 Limitation and future studies

The *in vivo* emulation property of our cell model was verified with VGCC functionality only. This is a convenient first step toward to the *in vivo* emulation property verification. However, more comprehensive verification may be needed to expand the applications of our polymer 3D cell culture platform.

The finding that cytokines are generally up-regulated in 3D cultured cells is obtained through comparative transcriptomic. Whether and how effective the up-regulated mRNAs can be translated to proteins need to be tested. Also, the comparative transcriptomic experiments were carried at a specific age of the cell cultures. As discussed in Chapter 2 and 4, the cytokine expression can fluctuate during culturing, a time course protein expression profile may be necessary to establish effective three dimensionality biomarkers.

The automation fabrication of 3D cell culture plates is limited to 96-well plates only. The mixture of polystyrene, chloroform and salt particles are very viscous. If handled at very low

volume (e.g., for the use in 384-well plates), the mixture's quantity will not be precise enough to produce acceptable plates. The number of plates can be generated in a single run is also limited due to chloroform's volatility. For our experiments, we only generated several plates at a single run so the evaporation of chloroform didn't affect the property of the plates. If intended for industrial production, the evaporation speed of chloroform should be monitored to ensure the quality of the products.

APPENDIX A

SUPPLEMENTARY DATA

Table S 1. Significantly up-regulated genes in 3D

Title	Symbol	*P*-value	Affymetrics Probeset ID
angiopoietin-like 7	ANGPTL7	0.034	206423_at
Apelin, AGTRL1 ligand	APLN	0.034	244166_at
arginine-rich, mutated in early stage tumors	ARMET	0.0096	202655_at
bone morphogenetic protein 1	BMP1	0.017	202701_at
bone morphogenetic protein 1	BMP1	0.0029	205574_x_at
bone morphogenetic protein 1	BMP1	0.037	207595_s_at
Bone morphogenetic protein 6	BMP6	0.041	241141_at
Bone morphogenetic protein 8b (osteogenic protein 2)	BMP8B	0.034	235275_at
calcitonin/calcitonin-related polypeptide, alpha	CALCA	0.0049	210727_at
cholecystokinin	CCK	0.0093	205827_at
chemokine (C-C motif) ligand 13	CCL13	0.030	216714_at
cerberus 1, cysteine knot superfamily, homolog (Xenopus laevis)	CER1	0.021	221378_at
connective tissue growth factor	CTGF	0.040	209101_at
Chemokine (C-X-C motif) ligand 2	CXCL2	0.021	1569203_at
cysteine-rich, angiogenic inducer, 61	CYR61	0.016	210764_s_at
fibroblast growth factor 5	FGF5	0.017	208378_x_at
fibroblast growth factor 7 (keratinocyte growth factor)	FGF7	0.049	205782_at
Ghrelin/obestatin preprohormone	GHRL	0.0080	237647_at
gremlin 1, cysteine knot superfamily, homolog (Xenopus laevis)	GREM1	0.041	218469_at
interleukin 10	IL10	0.0019	207433_at
interleukin 11	IL11	0.012	206926_s_at
interleukin 12B (natural killer cell stimulatory factor 2, cytotoxic lymphocyte maturation factor 2, p40)	IL12B	0.0030	207901_at

interleukin 18 (interferon-gamma-inducing factor)	IL18	0.030	206295_at
interleukin 1, beta	IL1B	0.039	39402_at
interleukin 1 family, member 8 (eta)	IL1F8	0.029	231755_at
interleukin 21	IL21	0.0092	221271_at
Interleukin 23, alpha subunit p19 /// (1.3) mRNA for T-cell receptor beta chain /// T-cell receptor rearranged beta-chain V-region (V-D-J) mRNA, clone ph15	IL23A	0.042	234865_at
interleukin 3 (colony-stimulating factor, multiple)	IL3	0.011	207906_at
Interleukin 8	IL8	0.039	217193_x_at
left-right determination factor 1	LEFTY1	0.041	206268_at
Latent transforming growth factor beta binding protein 3	LTBP3	0.0049	237144_at
Pre-B-cell colony enhancing factor 1	PBEF1	0.018	243296_at
nephroblastoma overexpressed gene	NOV	0.035	214321_at
platelet-derived growth factor beta polypeptide (simian sarcoma viral (v-sis) oncogene homolog)	PDGFB	0.0089	216061_x_at
stanniocalcin 1	STC1	0.011	204597_x_at
transforming growth factor, alpha	TGFA	0.00083	205016_at
tumor necrosis factor (ligand) superfamily, member 10	TNFSF10	0.0019	202688_at
vascular endothelial growth factor A	VEGFA	0.013	210513_s_at

Table S 2. Significantly up-regulated genes in neurospheres.

Title	Symbol	*P*-value	Affymetrics Probeset ID
Adrenomedullin	ADM	1E-06	202912_at
Adrenomedullin 2	ADM2	0.016	220538_at
Angiopoietin-like 7	ANGPTL7	0.054	206423_at
arginine-rich, mutated in early stage tumors	ARMET	0.0002	202655_at
bone morphogenetic protein 5	BMP5	3E-05	205431_s_at
Bone morphogenetic protein 8b (osteogenic protein 2)	BMP8B	0.050	235275_at
chromosome 19 open reading frame 10	C19orf10	0.0002	216483_s_at
chromosome 19 open reading frame 10	C19orf10	0.001	221739_at
complement component 5	C5	0.002	205500_at
chemokine (C-C motif) ligand 13	CCL13	0.040	216714_at
chemokine (C-C motif) ligand 23	CCL23	0.040	210548_at
CD320 molecule	CD320	0.037	218529_at
chemokine-like factor	CKLF	0.0005	219161_s_at
chemokine-like factor	CKLF	0.049	221058_s_at
C-type lectin domain family 11, member A	CLEC11A	0.002	211709_s_at
CKLF-like MARVEL transmembrane domain containing 3	CMTM3	0.018	1555705_a_at
CKLF-like MARVEL transmembrane domain containing 3	CMTM3	0.004	224733_at
CKLF-like MARVEL transmembrane domain containing 6	CMTM6	0.034	217947_at
CKLF-like MARVEL transmembrane domain containing 6	CMTM6	0.009	223047_at
CKLF-like MARVEL transmembrane domain containing 7	CMTM7	0.0003	226017_at
chemokine (C-X-C motif) ligand 10	CXCL10	0.013	204533_at
Chemokine (C-X-C motif) ligand 2	CXCL2	0.033	230101_at
defensin, beta 4 /// defensin, beta 4, pseudogene	DEFB4 /// DEFB4P	0.020	207356_at
epidermal growth factor (beta-urogastrone)	EGF	0.006	206254_at

family with sequence similarity 3, member C	FAM3C	0.014	240062_at
fibroblast growth factor 11	FGF11	0.0002	227271_at
Fibroblast growth factor 14	FGF14	0.0006	230231_at
Fibroblast growth factor 14	FGF14	0.024	230288_at
fibroblast growth factor 20	FGF20	0.039	220394_at
fibroblast growth factor 22	FGF22	0.048	221315_s_at
fibroblast growth factor 5	FGF5	0.022	208378_x_at
fibroblast growth factor 6	FGF6	0.040	208417_at
galanin	GAL	0.007	207466_at
galanin	GAL	0.005	214240_at
growth differentiation factor 10	GDF10	0.003	206159_at
growth differentiation factor 15	GDF15	0.003	221577_x_at
glial cell derived neurotrophic factor	GDNF	0.025	230090_at
Ghrelin/obestatin preprohormone	GHRL	0.019	237647_at
glia maturation factor, gamma	GMFG	0.004	204220_at
interferon, alpha 14	IFNA14	0.021	208182_x_at
interferon, alpha 16	IFNA16	0.025	208448_x_at
interferon, alpha 17	IFNA17	0.018	211405_x_at
interferon, alpha 21	IFNA21	0.012	211145_x_at
Interleukin 11	IL11	0.034	206926_s_at
interleukin 19	IL19	0.034	220745_at
interleukin 1, beta	IL1B	0.048	39402_at
inhibin, beta E	INHBE	0.005	210587_at
jagged 2	JAG2	0.004	209784_s_at
jagged 2	JAG2	6E-05	32137_at
midkine (neurite growth-promoting factor 2)	MDK	0.0005	209035_at
macrophage migration inhibitory factor (glycosylation-inhibiting factor)	MIF	0.0002	217871_s_at
pre-B-cell colony enhancing factor 1	PBEF1	0.0001	1555167_s_at
pre-B-cell colony enhancing factor 1	PBEF1	2E-05	217738_at
pre-B-cell colony enhancing factor 1	PBEF1	4E-06	217739_s_at
nephroblastoma overexpressed gene	NOV	0.027	214321_at
nephroblastoma overexpressed gene	NOV	0.0008	204501_at
neuropeptide Y	NPY	0.017	206001_at
nudix (nucleoside diphosphate linked moiety X)-type motif 6	NUDT6	0.004	220183_s_at

nudix (nucleoside diphosphate linked moiety X)-type motif 6	NUDT6	0.0008	230329_s_at
osteoglycin	OGN	0.038	218730_s_at
platelet-derived growth factor beta polypeptide (simian sarcoma viral (v-sis) oncogene homolog)	PDGFB	0.036	216061_x_at
platelet-derived growth factor beta polypeptide (simian sarcoma viral (v-sis) oncogene homolog)	PDGFB	0.043	204200_s_at
platelet derived growth factor D	PDGFD	1.98E-07	219304_s_at
platelet derived growth factor D	PDGFD	0.002	222860_s_at
prokineticin 1	PROK1	0.022	229124_at
pleiotrophin (heparin binding growth factor 8, neurite growth-promoting factor 1)	PTN	0.010	208408_at
pleiotrophin (heparin binding growth factor 8, neurite growth-promoting factor 1)	PTN	0.001	209465_x_at
pleiotrophin (heparin binding growth factor 8, neurite growth-promoting factor 1)	PTN	0.008	209466_x_at
pleiotrophin (heparin binding growth factor 8, neurite growth-promoting factor 1)	PTN	0.018	211737_x_at
relaxin 2	RLN2	0.008	214519_s_at
small inducible cytokine subfamily E, member 1 (endothelial monocyte-activating)	SCYE1	0.005	202541_at
small inducible cytokine subfamily E, member 1 (endothelial monocyte-activating)	SCYE1	5.11E-07	202542_s_at
small inducible cytokine subfamily E, member 1 (endothelial monocyte-activating)	SCYE1	0.0007	227605_at
sema domain, immunoglobulin domain (Ig), short basic domain, secreted, (semaphorin) 3C	SEMA3C	0.005	203788_s_at
sema domain, immunoglobulin domain (Ig), short basic domain,	SEMA3C	0.0005	203789_s_at

secreted, (semaphorin) 3C			
stanniocalcin 1	STC1	1E-05	204597_x_at
stanniocalcin 1	STC1	0.0256	204595_s_at
stanniocalcin 1	STC1	1E-07	204596_s_at
Stanniocalcin 1	STC1	7E-05	230746_s_at
stanniocalcin 2	STC2	0.0006	203438_at
stanniocalcin 2	STC2	0.001	203439_s_at
transforming growth factor, alpha	TGFA	0.005	205016_at
thrombopoietin (myeloproliferative leukemia virus oncogene ligand, megakaryocyte growth and development factor)	THPO	0.040	211831_s_at
tumor necrosis factor receptor superfamily, member 11b (osteoprotegerin)	TNFRSF11B	0.019	204933_s_at
tumor necrosis factor (ligand) superfamily, member 9	TNFSF9	0.007	206907_at
taxilin alpha	TXLNA	0.042	1561358_at
urotensin 2 domain containing	UTS2D	0.047	243175_at
vascular endothelial growth factor A	VEGFA	3E-07	210513_s_at
vascular endothelial growth factor A	VEGFA	0.002	210512_s_at
vascular endothelial growth factor A	VEGFA	0.011	211527_x_at
vascular endothelial growth factor A	VEGFA	0.0006	212171_x_at
VGF nerve growth factor inducible	VGF	0.003	205586_x_at

APPENDIX B

OTHER PUBLICATIONS

THREE-DIMENSIONAL POLYMER SCAFFOLDS FOR HIGH THROUGHPUT CELL-BASED ASSAY SYSTEMS*

Abstract

Many whole cell-based assays in use today rely on flat, two-dimensional (2D) glass or plastic substrates that may not produce results characteristic of in vivo conditions. In this study, a three-dimensional (3D) cell-based assay platform was established by integrating 3D synthetic polymer scaffolds with standard cell culture dishes and multi-well plates. This technology can be used to feasibly modify any traditional 2D cell-based assay vessels for 3D cell-based assay with currently used high throughput screening (HTS) systems. We examined neural stem (NS) cells' growth profile, morphology, cell–matrix interaction, gene expression and voltage gated calcium channel (VGCC) functionality of this novel 3D assay platform. Our results showed that unlike the NS cells cultured on traditional 2D planar surfaces, cells in 3D scaffolds are more physiologically relevant with respect to in vivo characteristics exhibited by in-vivo surrogates such as neural spheres. This new biomimetic cell-based assay platform may provide a broadly applicable 3D cell-based system for use in drug discovery programs and other research fields.

Keywords: Biomimetic material; ECM; Cell culture; Scaffold; Stem cell

* Cheng K, Lai Y, Kisaalita WS. 2008. *Biomaterials* 29: 2802-2812.

TAKING CELL CULTURE IN DRUG DISCOVERY TO THE THIRD DIMENSION - A PATENT REVIEW*

Abstract

In comparison to two-dimensional (2D), three-dimensional (3D) cell culture systems are believed to more closely emulate in vivo conditions, and thus are becoming popular models for screening in drug discovery and other studies related to human diseases. The rising importance of 3D cell cultures is reflected in the four-fold increase of related publications between 1996 and 2006. This paper reviews US patents issued that underpin the practical utilization of 3D cell culture systems. Patents are grouped according to the materials used including synthetic and natural polymer, inorganic/nonmetallic materials, and specialized medium. While earlier applications of 3D cell culture systems relied heavily on their ability to prolong cell growth and promote cell propagation, recent applications mainly focus on in vivo emulation attributes. In all cases the 3D claims are based on morphology, which may not be sufficient. Genomic and cellular functional assays to substantiate these claims are needed.

* Lai Y, Wang L, Cheng K, Kisaalita WS. 2008. *Recent Patents on Biomedical Engineering* 1: 103-115

BIOMARKERS FOR SIMPLIFYING HTS 3D CELL CULTURE PLATFORMS FOR DRUG DISCOVERY: THE CASE FOR CYTOKINES*

Abstract

In this review, we discuss the microenvironmental cues that modulate the status of cells to yield physiologically more relevant three-dimensional (3D) cell-based high throughput drug screening (HTS) platforms for drug discovery. Evidence is provided to support the view that simplifying 3D cell culture platforms for HTS applications calls for identifying and validating ubiquitous three-dimensionality biomarkers. Published results from avascular tumorigenesis and early stages of inflammatory wound healing, where cells transition from a two-dimensional (2D) to 3D microenvironment, conclusively report regulation by cytokines, providing the physiological basis for focusing on cytokines as potential three-dimensionality biomarkers. We discuss additional support for cytokines that comes from numerous 2D and 3D comparative transcriptomic and proteomic studies, which generally report upregulation of cytokines in 3D compared with 2D culture counterparts.

*Lai Y, Asthana A, Kisaalita WS. 2011. *Drug Discovery Today* 16: 293-297